IMAGE BASED SYSTEM FOR THE QUALIFICATION OF SKIN ERYTHEMA

Bachelor Thesis

Trabajo Fin de Grado

Biomedical Engineering

Author: Irene Cumplido Mayoral

Supervisor: Juan José Vaquero López

Leganés, June 2015

Author: **Irene Cumplido Mayoral**

Supervisor: **Juan José Vaquero López**

Title: **Image based system for the qualification of skin erythema**

TRIBUNAL

President: Pascau Gonzalez Garzón, Javier

Secretary: Contreras Lallana, Pedro

Vocal: Larcher Laguzzi, Fernando

The public defense of this Bachelor Thesis took place on the 4th of July 2015 in Leganés in the campus of the *Escuela Politécnica Superior* of the *Universidad Carlos III de Madrid.*

Acknowledgements

I would like to express my gratitude to all the people that have supported, guided, and helped me over this period of my Bachelor Thesis development.

To my supervisor Juan José Vaquero, for giving me the opportunity to work on this project, for his advice and assistance.

To Dr. José Manuel Zubeldia, for supporting this project and offering his help when needed.

To Carlos Sanchez, for making me enjoy everyday at the lab while helping me whenever I was lost.

To my friends and family. To Alba and my parents, for all their patient and support. I would not have achieved this without you.

Abstract

Skin allergy tests are the main procedure for diagnosing IgE-mediated reactions; which are commonly known as allergy. These reactions are produced by an overreaction of the immune system to substances that get in contact with the body, called allergens.

From the skin allergy tests, the most commonly performed procedures are the skin prick tests (SPTs), which are based on introducing a small drop of allergen within the epidermis. If an allergic reaction occurs, histamine is released, causing local blood vessels to dilate, and thus, increasing the concentration of RBCs. Consequently, the local skin region becomes red in appearance, which is known as erythema. In addition, another symptom of this reaction is the increase in venules' permeability, which produces a leakage of plasma (mainly composed by water). Then, extracellular fluid accumulates and a wheal appears. The dimensions of this wheal are used to determine if an specific allergen provokes a hypersensitivity reaction or not.

This diagnostic method is based on visual appearance, which is subjected to user-dependency. There is not an standardized way for measuring the wheal diameter, nor the erythematous area dimensions.

Therefore, the objective of this work is to implement an image based system for performing an automatic diagnosis for hypersensitivity reactions. To achieve this, skin optical properties and light propagation within tissue are studied. Besides, for this purpose, absorbance and scattering coefficients for hemoglobin (contained in erythema) and water (contained in edema) are used for determining the illumination setup of the system. The specified wavelengths enhance visual appearance of erythema's and edema's light reflectance. From these values, absorption maps are built, which are then used to quantify both chromophore's concentrations.

The implementation of this system would mean an standardization for allergy tests diagnosis, as well as a cost reduction in experts training.

Contents

List of Figures

1. Introduction

Allergic reactions are overreactions of the immune system to substances that come in contact with different parts of the body; such as skin; eyes; nose; the respiratory tract; or the gastrointestinal tract. These substances are called allergens and most people's immune systems do not recognise them as harmful. In people who are not allergic, they stimulate the secretion of a specific type of antibodies (proteins used by the immune system to detect harmful species) which normally circulate within the blood (IgG). In allergic people, on the contrary, allergens cause the secretion of a different type of antibodies (IgE), which attach to mast cells and stimulate the release of the chemicals that produce allergy symptoms.[1]

Allergic diseases are highly common and have increased worldwide in the last years with greatest complexity, particularly in children. According to the World Allergy Organization, approximately 10% to 30% of the world population is affected by respiratory allergies [2]. In addition, around 40% to 50% of school children are suffering from higher sensitivities. The reasons of these increasing rates are unknown, which makes prevention of this disease difficult. To solve this issue, research and development of new approaches for its diagnosis and management are been boosted. [2]

While most of these allergic reactions take place within seconds or minutes after the exposure to the allergen (immediate reaction), some reactions occur after several hours (late-phase reaction). The range of symptoms originated from both of them can go from mild to severe and, even, being life-threatening. The late ones are generally associated with anaphylaxis or anaphylactic shock. [3]

Different types of allergies are recognised depending on the body part where the reaction takes place, which can be limited to a small area, or may affect the entire body. Because of this, distinctive classifications for the detected symptoms are made:

- *Respiratory allergies*: they affect the respiratory tract and are divided into allergic rhinitis and asthma. Allergic rhinitis, which can also be called rhinoconjunctivitis, is diagnosed for a group of symptoms affecting the nose. These reactions cause coughing, itchy nose, wheezing, shortness of breath, sinus problems, and also red, itching and watery eyes. It can evolve to asthma.
- *Skin allergy (dermatitis)*: which causes inflammation and rash of the skin and can be classified into atopic dermatitis (eczema) and contact dermatitis.
- *Other allergies*: which stand for food and drug allergies and insect venom. They cause different types of reactions that can be related to anaphylaxis.

Even though allergies can not generally be prevented, allergic reactions can. Avoiding contact with the specific allergens can highly improve the conditions of the patient's life, as well as taking medication to counteract possible reactions or even making use of allergy injection therapy to minimize the symptoms [2]. The first step to carry out these strategies is diagnosing the disease.

1.1. Motivation

Human hypersensitivity diseases can be diagnosed by a wide range of different modalities. Since their implantation, the most important diagnostic methods have consisted of in vivo skin tests for IgE-mediated hypersensitivities. On the other hand, advances over the years in immunologic diagnostic technology have increased the significance of in vitro tests for IgE- and cell-mediated immunity in terms of diagnostic tools. These tests include lymphocyte functional assays and identification of specific cellular components such as transcription markers; protein products; or cell surface differentiation markers. However, a larger cost effectiveness and a biggest reliability,

make the in vivo testing techniques to be the preferred diagnostic method chosen for IgE-mediated diseases. [4]

In vivo cutaneous tests were developed and introduced in the s.XIX. In 1865, Dr Charles Beckley performed the potentially first skin tests. But it was not until the 1770s when the technique was definitely introduced as a diagnostic method. Since then and until today, small modifications have been applied to this initial procedure, which confirms clinical sensitivity to allergens. According to the different protocols followed, skin tests are divided into three different methods; intra-epidermic reactions (prick/ puncture tests); intra-dermo-reactions; and epi-cutaneous reactions. [5]

The motivation of this project is to develop a device for demonstrating immediate IgE-mediated allergic reactions, based on the performance of skin prick tests (SPTs). This test is based on the percutaneous injection of a small quantity of substance that is suspected to cause allergic reactions (taking into account the clinical history of the patient). If there is a positive result against the substance, blood flow is increased in the area, causing erythema (redness of skin), and a edema due to swelling. The visual changes of skin color and vertical displacement are manually measured, as the size of these areas are the parameters used to indicate the result of the diagnosis [5]. Therefore, visual observation plays an important role in allergy and dermatology, favoring the use of digital imaging and of automatic diagnostic tools in these areas.

Taking into account that the test's performance is based on manual measurements, it is generally time consuming and inaccurate. This is because its reliability depends on; the skill of the tester, as a good training is required to ensure proper interpretation and efficacy of the results; the test instrument used; the color of the tested skin, as darker skins are more difficult to diagnose; the skin reactivity; potency and composition of test reagents; and the day when the test was taken [4]. Moreover, this visual measurement is user-dependent and highly subjective, there is not an standardized established way of diagnosing allergy accurately.

Due to the lack of reliability of the actual procedure and the boost of digital imaging, the motivation of this project is to improve the diagnostic method followed for hypersensitivity reactions by the use of image analysis. This would improve the cost

efficiency of the procedure; in terms of time; experts training; and interpretation standardization.

1.2. Objectives

The general objective of this work is to develop an image based system for qualifying and quantifying erythema, which means redness of the skin, as well as edema detection. This system is going to be applied to skin allergy tests (whose visual symptoms are the above described); so as to check the reliability of the developed method by diagnosing allergy in humans.

The specific objective is to visually qualify and quantify physiological changes that take place under the skin when erythema is observed. For this, biomedical optics are used; illuminating the region of interest with specific light wavelengths may improve image detection of the skin features that appear in allergy reactions. In this case, the wavelength peaks are chosen based on the accumulation of water and the increase of blood flow that occurs at local regions during these reactions. Finally, image processing is carried out based on those incident wavelengths, analyzing the images on their corresponding spectrum and obtaining a quantification of the described parameters (blood and water), so as to perform a comparison between the manual and the automatic diagnosis.

In summary, images from the SPTs, performed on the user's forearm, will be taken using a charged-coupled device (CCD) sensor camera. The illumination chosen will be useful for the detection of physiological changes, using an efficient photographic set-up. In addition, light distribution will be also studied using a tissue mimicking skin. At the end, image processing will be used to diagnose allergic reactions in an automated manner.

In order to achieve these objectives, the following activities have been defined::

1. Designing and developing a photographic set-up for carrying the experiments; hence, the allergy diagnosis.
    - Choice of radiation light wavelength; 565 nm (visible light) and 940 nm (near- inferred light (NIR)).
    - Choice of camera quantum efficiency.
2. Studying the physiological properties of skin by means of skin optics; spectral absorbance of blood and water.
3. Digital automatization of diagnosis. Comparing the results obtained: manual diagnosis Vs automatic diagnosis.

2. Background

2.1. Skin Structure

The skin is in charged of separating the internal environment of the body from the external one, being the largest organ of the body. As seen in **Fig.1**, it is composed of three layers; two cutaneous layers, epidermis and dermis; and a subcutaneous one. These are composed of different structures and account for different functions. As a consequence of this structural distinction, light is propagated in a different manner in each of them.

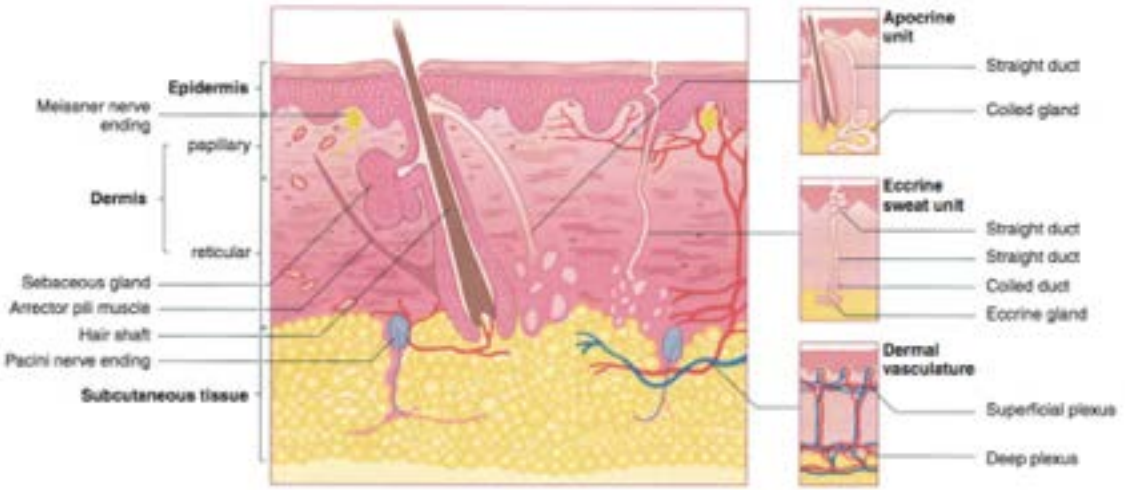

Fig. 1: Cross-sectional schematic diagram of skin. Extracted from [6]

2.1.1. Epidermis

The epidermis is the outermost layer of the skin. It is mainly composed by keratinocytes forming the external epithelium. These cells contain keratin filaments, a type of intermediate filaments. Epithelia do not have blood vessels or arteries, lymphatic vessels or nerves, thus, it depends on connective tissue for nutrition, oxygenation and innervation. Its thickness varies according to the volume of water contained and its

location on the body. However, in average, it expands over a depth of 0.2 mm [7]. Even though keratinocytes predominate, melanocytes can also be found. These cells carry melanin, which is a high light-absorbing pigment produced by melanosomes. Depending on its chemical structure, two different types can be found; eumelanin and pheomelanin.

The epidermis is divided into five sublayers, which are (from outermost to innermost); stratum corneum; stratum lucidum; stratum granulosum; stratum spinosum; and stratum basale. In this last layer, keratinocytes are produced, which then move upward to the outer surface.

2.1.2. Dermis

The dermis is the layer beneath the epidermis. It is much thicker, usually from 1 to 4 mm [7] and it conforms the connective tissue that supports the epidermis. Opposite to epithelia tissue, it carries blood and lymphatic vessels and nerves. In addition, cells are immersed in the extracellular matrix (ECM). The majority of found cells are; [6]

- Fibroblasts; connective tissue cells that secrete collagen and elastin.
- Macrophages; scavenger cells that phagocyte invading organisms and dead cells.
- Mast cells; cells that produce histamine and other chemicals to trigger inflammation.
- Plasma cells; fundamental cells for the immune system, which synthesize antibodies.
- Adipose cells; cells that store energy in the form of fat.
- Leukocytes or white blood cells; cells that play an important role in the inflammatory response and defend agains infections.

The dermis is classified into two layers; the papillary layer (upper), made of loosely connected tissue and containing most os the mentioned cells; and the reticular layer (inner), which contains aggregates of collagen fibers aligned parallel to the skin surface. [7]

2.1.3. Subcutaneous layer

The subcutaneous layer is an elastic layer composed mainly by adipocytes whose role is to absorb shocks for blood vessels and nerves. Because of this, it is not classified as another skin layer. [7]

2.2. Hypersensitivity Reactions: Allergy

2.2.1. The Immune System

The function of the immune system is to maintain homeostasis in the body by fighting harmful agents. Therefore, the ability of the body to guard it against damage through its defenses is called immunity. Two types of immunity are found; innate and adaptive.

Innate immunity is nonspecific, which means that it does not involve a specific recognition of the agent. Moreover, it is a type of general defense present at birth that includes two lines of protection. The first line refers to the physical and chemical barriers of the body (skin and mucous membranes) and the second line of defense involves the action of different cells and processes (natural killer cells, inflammation, fever and antimicrobial substances). [8]

Adaptive immunity, on the contrary, is specific and involves the recognition of the substance once it has beaten the innate defense. Substances that provoke immune responses are called antigens, which means antibody generators [9]. Adaptive immunity is characterized by; specificity for antigens detection; and memory for the previously encountered ones. Lymphocytes, a type of white blood cell (WBC), are in charged of this property and are divided into T lymphocytes (T cells) and B lymphocytes (B cells). The immune system’s response in the presence of an antigen is then based either on the

action of B cells, by synthesizing and secreting antibodies, or the action of T cells, by evolving into effector cells. [8][9]

A time flow representation of the elements involved in body defense can be seen in **Fig. 2.** Adaptive immunity processes usually take more than one day to react when the body encounters an antigen for the first time, due to the small number of lymphocytes with the necessary antigen receptors. However, due to the memory property, copies of that antigen are spread throughout the body after that first encounter, making the immediate reaction possible in the following attacks.

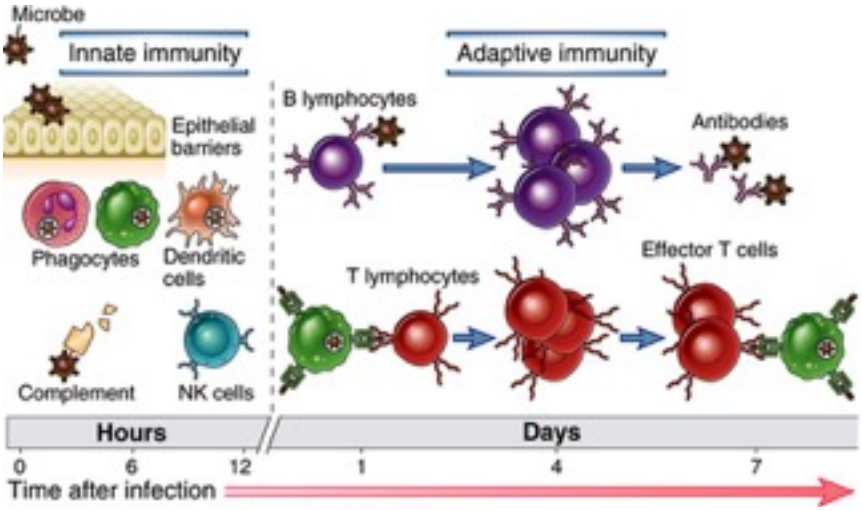

Fig. 2: Schematic diagram of the two types of immunity (innate and adaptive) and the cells involved in each of them. Image from [9]

As previously said, a person whose immune system overreacts to a substance that is tolerated by most people (an allergen), is said to be allergic. Taking the previous classification into account, hypersensitivity reactions are characterized as adaptive immunity responses because antibodies are involved in the detection of allergens. There are four types of hypersensitivity reactions; type I or anaphylactic; type II or cytotoxic; type III or immune-complex; and type IV or cell-mediated. The first three are antibody-mediated immune responses, while the last one is cell-mediated.

2.2.2. Fundamental Concepts

Antibodies (Abs) or Immunoglobulins (Igs)

Proteins synthesized and secreted by B cells whose role is to bind to a specific antigen to inactivate it. Different Ab types recognize different antigens. [8]

Immunoglobulin E (IgE)

Antibodies that account for less than a 0.1% of all the proteins of this type in blood and are characterized by ε heavy chains. They are located in mast cells and basophils and are involved in hypersensitivity reactions.[8]

Mast cells

Type of WBC, more concretely, a granulocyte arisen in bone marrow. It contains many secretory granules full of chemical mediators; such as histamine, heparin or cytokines; and neutral serine proteases, including tryptase and chymase. [7]

Basophils

Type of immune cell (WBC) that has granules containing enzymes to be released during an immune response. These enzymes are responsible of inflammation.[8]

Cytokines

Proteins secreted by cells, which have different and specific roles on the interactions between cells. In the case of allergic reactions, mast cells and basophils release several cytokines that contribute to allergic inflammation. [10]

Histamine

Vasoactive amine released by mast cells in connective tissue, and basophils and platelets in blood. It causes vasodilation and, as a result, an increase of vessel permeability and blood flow. [11]

2.2.3. Reactions of Immediate Hypersensitivity

In IgE-mediated reactions, IgE is released from B-cells. Right after, the immunoglobulin binds to high-affinity receptors on mast cells (FcεRI), coating their plasma membranes. As a result, mast cells become active when antigen cross-link IgE binds to them. A successive exposure to the same allergen cross-links the coated cell, causing its degranulation within seconds. in turn, inflammatory mediators such as histamine (most abundant), enzymes (chymase, tryptase, etc.), prostaglandins (especially prostaglandin D_2 (PGD_2)) and cytokines are released **(Fig. 3)**. In consequence, histamine binds to receptors on venular endothelial cells, which in turn synthesize and released nitric oxide, PGI_2 and platelet-activating factor (PAF). These mediators rapidly increase vascular permeability and dilation, causing vascular leak. Besides, PGD2 promotes neutrophil chemotaxis to the inflammation sites. These enzymes, in turn, cause the destruction of several proteins contained in tissue matrix, promoting the entrance of inflammatory leukocytes and lymphocytes into tissues within hours.[9][10]

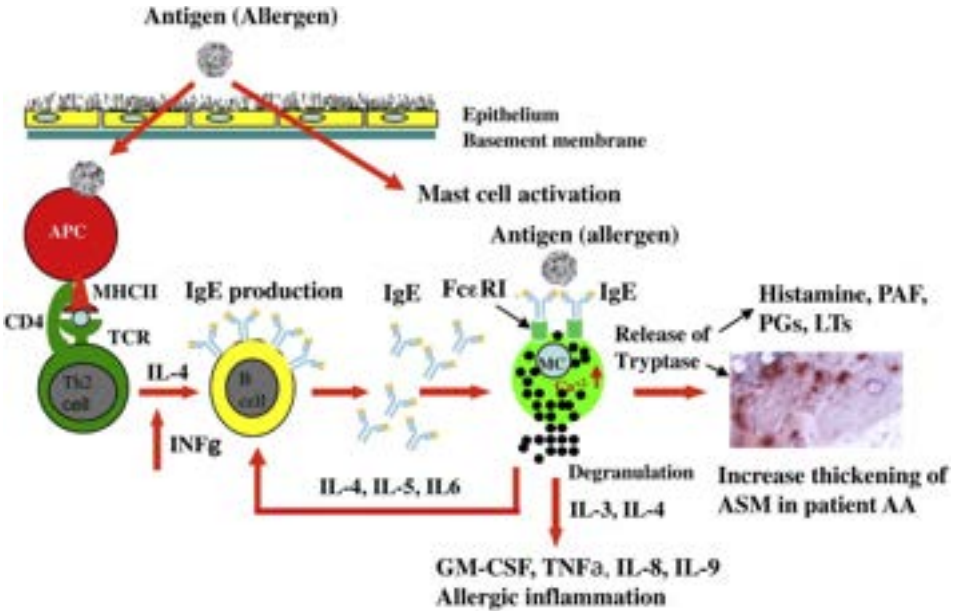

Fig. 3: Schematic diagram of immediate hypersensitivity reactions. Image from [10]

Therefore, when an individual receives an intra-epidermal injection of an allergen which which incited IgE antibody production previously, the previous processes take place. Subsequently, in allergy testing, local blood vessels dilate and the concentration of RBCs is increased. As a result, the injection site becomes red in skin appearance. Then, plasma from venules is leaked, causing the swelling of the site, which is called a wheal **(Fig. 4)**. Vessels surrounding the swelled area dilate, too, producing a red rim called a flare. This reactions appear within 5-10 minutes after the allergen injection, and may disappear in less than an hour. [9]

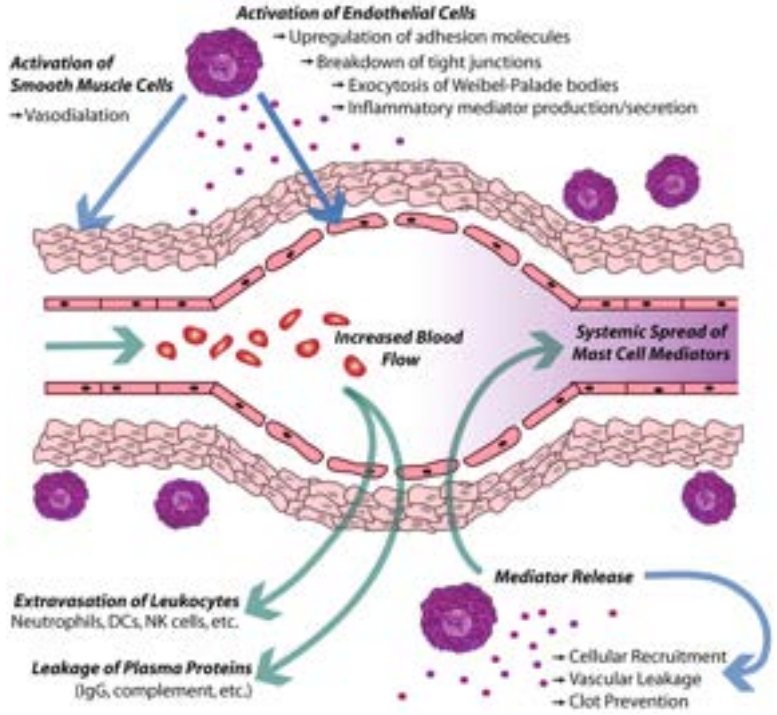

Fig. 4: Effect of mast cell's mediators release over venular musculature. Image extracted from [11]

2.2.4. Late-Phase Reactions of Hypersensitivity

As a consequence of the immediate reactions, the wheal and flare conditions follow from 2 to 4 hours later by the late-phase processes and reactions **(Fig. 5)**.

Once activated, mast cells synthesize and release products such as; chemokines; cytokines like IL-4 and IL-3; and lipid mediators such as leukotrienes. These mediators regulate endothelial expression of leukocyte adhesion molecules and recruitment of

leukocytes into affected tissues. This, in addition, allows other circulatory cells such as prostaglandins, thromboxanes and leukotrienes, to adhere to the endothelium, fulfilling an important role in inflammatory response. Some of the activated lymphocytes are T_H2. Following, basophils and eosinophils are attracted to the late-phase reaction inflammatory sites. The latter accumulate in large number and are believed to participate in tissue damage. [9][10][11]

This type of reaction can occur without proceeding the immediate hypersensitivity response. For example, in bronchial asthma disease, Th_2 cells and eosinophils can accumulate without vascular changes characteristic in inflammation [10].

2.3. Skin Optics

2.3.1. General Optics

Colors seen and measured in nature, and more concretely, in tissue, are the result of interactions between light and matter. These interactions consist of two processes; radiative, in which light wavelength is re-emitted after the interaction (scattering and emission); and non-radiative, by which the energy of the wavelength is absorbed (absorption). Light propagation within tissue is determined by the interaction of the incident light with the atoms constituting molecules and proteins [12]. Therefore, the contribution of radiative and non-radiative mechanisms depends on the atom's environment.

The Lorentz model is used to explain the process by which electromagnetic radiation interacts with an atom. First of all, a dipole moment is created when the incident light

transfers its energy to the atom, causing a displacement of charges that results in a dipole oscillating with the incident field. This may produce two different mechanisms;

1. Elastic scattering. The oscillating dipole can generate a second radiation at the same frequency as the incident field and with different propagation directions or phase, depending on the environment. This process is characterized by a conservation of the total energy and the total momentum of the initial radiation (**Fig.6**). [12][13]

2. Absorption. Another part of the transferred energy can be absorbed and delivered in form of vibrations. For this to occur, the photon's frequency and the frequency of the molecule's energy transition must be the same. This means that the absorption bands of a molecule or protein can identify its molecular composition. [12][14]

3. Emission. The atom might be displaces to an excited state as result of the transmission of enough energy. Then, the atom can re-radiate the light with a frequency and direction dependent on the transition state from ground to excited state of the dipole.[12]

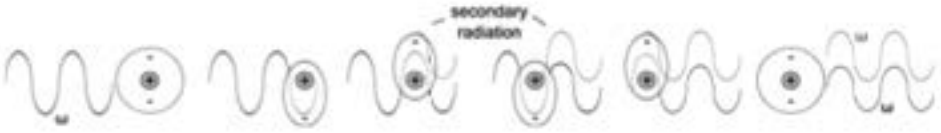

Fig. 6: Schematic of an electromagnetic wave interacting with matter though the Lorentz model. Re-radiation of the incident energy. Figure extracted from [12]

Distribution of light is determined by the tissue's optical properties, as well as the light source's characteristics. As explained in **Section 2.1.**, the skin is a layered structure composed of different molecules. Each of them contribute with their corresponding optical properties to explain the attributes of this tissue. These components are characterized by a high degree of randomness. Because of this, it is more convenient to use a statistical description on how the medium (on average) affects light propagation, instead of modeling it by means of the classical description [12]. For this purpose, the average shape, size, composition and spatial distribution of these objects need to be known. Three different statistical coefficients take all these parameters into account to

describe the properties of the tissue: scattering coefficient, absorption coefficient and scattering anisotropy.

- The scattering coefficient $\boldsymbol{\mu_S}$ (cm^{-1}), which describes a medium containing a concentration of scattering particles described as volume density ρ_s [cm^3]. Thus, it is the cross-sectional area of the scattering particle (σ_s [cm^2] = Q_sA_s [cm^2]) per unit volume of medium. Where Q_s is the scattering efficiency and A_s is the size of the particle. The coefficient is given by $\mu_S = \rho_s \sigma_s$. [14]

- The absorption coefficient $\boldsymbol{\mu_a}$ (cm^{-1}), is the cross-sectional area of the absorption particle per unit volume of medium (following the same idea as with $\boldsymbol{\mu_S}$). The coefficient is given by $\mu a = \rho_a \sigma_a$. [14]

- The scattering anisotropy **g** (dimensionless), which gives a description of the transparency of an object. After a scattering event, as seen in **Fig. 7**, the scattered photon is deflected from its original trajectory by an angle θ. This anisotropy measures the quantity of the forward direction that is kept after the event, which is given by $g = \langle \cos(\theta) \rangle$. Where cos(θ) represents the component of the new trajectory fixed at the forward direction. [14][15]

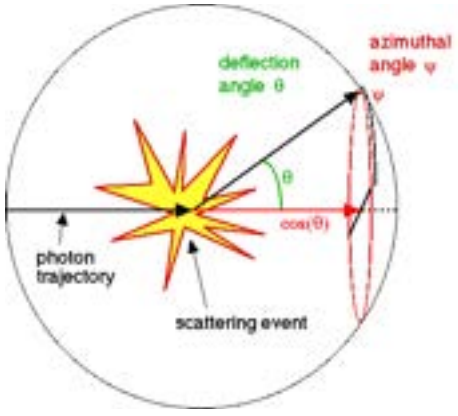

Fig.7: Schematic representation of a scattering event. The component cos(θ) represents the anisotropy. Extracted from [14]

These coefficients are used to model the spatial propagation of electromagnetic radiation statistically, which can be done using the equation of radiative transfer energy (RTE) [Eq. (2.1)]. This equation states that a beam of traveling radiation gains energy by emission, losses energy to absorption and redistributes energy by scattering.

Considering that cells have the same length or are even more than an order of magnitude larger than the incident wavelength; and that they are assumed to be particularly transparent spheres, scattering is highly forward-directed. Then, radiation becomes isotropic (diffusive); which results in a simplified situation of light propagation [16]. In this case, Mie theory is used to solve for the scattered intensity and absorption and scattering coefficients can be derived for diffuse radiation.

$$\frac{1}{c}\frac{\partial}{\partial t}I_\nu + \hat{\Omega}\cdot\nabla I_\nu + (k_{\nu,s}+k_{\nu,a})I_\nu = j_\nu + \frac{1}{4\pi}k_{\nu,s}\int_\Omega I_\nu d\Omega \qquad (2.1)$$

where:

I_v is radiance [$W\cdot sr^{-1}\cdot m^{-3}$]
j_v is the emission coefficient [cm^{-1}]
$k_{v,s}$ is the scattering coefficient [cm^{-1}]
$K_{v,a}$ is the absorption opacity [cm^{-1}]

As a result, in a medium dominated by scattering, the radiative transport theory, and thus optical transport, can be approximated into a simpler equation using Fick's 1st law of diffusion [Eq. (2.2)]. This gives rise to the Diffusion theory, based on modeling photon movement (related to flux) down its concentration gradients. [17][18]

$$J = -\chi\frac{\partial C}{\partial x} \quad [cm^{-2}s^{-1}] \qquad (2.2)$$

where:

J is the flux [$cm^{-2}\,s^{-1}$]
X is diffusivity [cm^2/s]

Visible and near-infrared light propagation through tissues is dominated by scattering events. To describe the diffusive movement of photons, it is useful to use the reduced scattering coefficient (μ_S'), which is a lumped parameter related to the scattering coefficient and the anisotropy of the tissue [Eq. 2.3]. The objective of μ_S' is to describe diffusion in terms or a random walk with "mean free path" steps representing isotropic scattering of photons. [19]

$$\mu_S' = \mu_S\,(1 - g)\ [cm^{-1}] \qquad (2.3)$$

As previously mentioned, photons' movement in a light-scattering medium can be modeled with the diffusion equations. This is explained by the relationship between the instantaneous fluence rate, F(r,t) [J s^{-1} cm^{-2}], and the concentration of optical energy, C(r,t) [J cm^{-3}], with the speed of light, c [cm/s] [Eq. 2.4]. [17]

$$F(r,t) = cC(r,t) \tag{2.4}$$

Then, for light, the diffusivity is proportional to the diffusion length D [cm] and the speed of light c [Eq. 2.5]. The diffusion length depends on the reduced scattering coefficient [Eq. 2.6]. [17]

$$\chi = cD\,[cm^2\,s^{-1}] \tag{2.5}$$

$$D = \frac{1}{(3\mu s\,(1\text{-}g))}\,[cm] \tag{2.6}$$

Using the previous relationships, for optical diffusion, flux from Fick's 1st law is finally described in terms of the negative fluence gradient and the diffusion constant (eq. 2.7) [17]. This approximation is achieved given a homogeneous isotropically scattering medium a a fluence rate at the origin. This theory gives a Gaussian distributed signal representing the energy loss of radiation when traveling through the medium; or the intensity of a cross section of the radiated sample. These concepts need to be applied specifically, to the skin tissue, to understand and model radiation propagation though skin.

$$J = -D\frac{\partial F}{\partial x}\ [W\,cm^{-2}] \tag{2.7}$$

2.3.2. Optical Pathways in Skin

Incident light follows different pathways when traveling through the different skin layers. An schematic of this light transport is shown un **Fig.2.3**. For this discussion, absorption and scattering centers are assumed to be uniformly distributed across each of the layers.

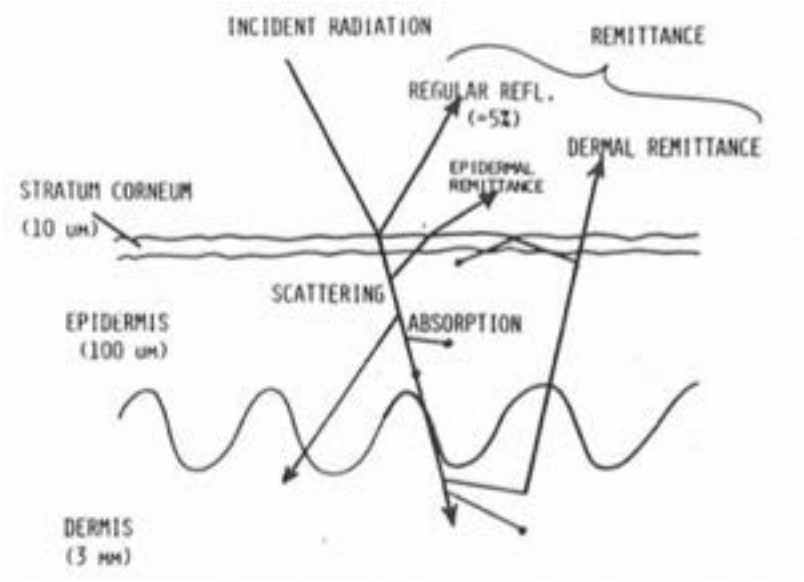

Fig.8: Schematic diagram of optical pathways in skin. [16]

First of all, around 4% to 7% of the incident light radiation is reflected at the surface [16]. This process is called regular reflectance [16] and is caused by the difference in the refractive indices of the air (approximately 1.0) and the stratum corneum (approximately 1.55 [20]). There exists an angular dependance of intensity regular reflection, which is proportional to the incident angle. Moreover, the roughness of skin also affects this relation; hairs, hair follicles and other superficial skin elements cause diffusion of the regular reflection and transmission [16].

Secondly, the remainder incident light enters the epidermal layer, which, as mentioned before, is composed of mainly cells that do not contribute in a significant scattering due to the distance between them. Densely-packed keratin fibers, on the other hand, could produce an appreciate scattering. However, due to the thin size of this layer, the effect is negligible. In relation to absorption, melanin acts as a strong light absorber. Thus, the degree of absorption depends on the volume of melanin. Melanin is one of the main chromophores of skin, which refers to light absorbing molecules.

Finally, as dermis is composed by a dense network of collagen fibers, a high amount of scattering takes place (this property is further developed in the following point). Taking into account that the scattering properties depend on the wavelength of the incident light, scattering is inversely proportional to wavelength increase [21]. Hence, a higher

amount of incident light corresponding to longer wavelengths is able to penetrate deeper into skin. Besides, the dermis layer is characterized by containing capillaries of both oxygenated and deoxygenated blood. Blood is mainly composed of a watery liquid extracellular matrix and formed elements. The first one is called blood plasma, accounting for ≈54% of the volume, from which around 90% of volume corresponds to water, and the rest to plasma proteins. Then, the formed elements conform a volume of ≈45%, while the rest (≈1%) is composed by white cells and platelets. From the formed elements, around the 99% are red blood cells (RBCs) [22]. These RBCs contain an oxygen-carrying protein called hemoglobin (Hb), which gives blood its red color and which is the skin chromophore that has a biggest impact on light absorption (both in its oxy and deoxy states). Furthermore, even though water does not absorb visible light significantly, it has a great impact on light absorption over larger wavelengths of the spectrum (from 900 nm and over). This fact of its spectral characteristics can be used to obtain information of tissue on its water content [1].

2.4. State-of-the-Art: In vivo Diagnostic Tests

2.4.1. Intra-epidermic testing (prick/puncture tests)

Skin tests are the main diagnostic procedure used with patients presenting indicative symptoms of allergic rhinitis/conjunctivitis and/or asthma, related to an IgE-mediated reaction. SPTs are highly used because they offer a high degree of correlation with symptoms, offering a high sensitivity and specificity for the diagnosis.

The methodology followed in these tests is based on placing a small quantity of antigen over the skin of the patient's forearm, so as to be introduced within the epidermis by means of a puncture using a lancet.

The test's reliability depends in a great manner on the quality of the allergen extracts. These must contain the appropriate allergenic components, be standardized and be stored under adequate conditions. The extracts are prepared using a solution of 50% glycerine or 0.3% albumin [23]. In addition to the allergen's extracts, positive and negative controls need to be tested, too. These are useful to detect false positives or negatives in the test results, thus, to make interpretations possible. The negative control used generally is either, the dissolvent employed in the extracts preparation, or a saline solution. The positive control is made up from histamine; a negative result for this solution indicates a weaker reactivity to histamine (which is the main substance that accounts for allergic symptoms).

First of all, it is necessary to verify that the cutaneous area is adequate; that it does not present any injury or alteration in skin, such as eczema, urticaria or tattoos. In addition, the patient must not be taking any medication that could interfere with the results of the test. Right after, marks are drawn on the patient's forearm with a marker to indicate where to place the different antigens. The separation between marks should be at least

2cm. Then, a lancet is used to puncture the skin through the deposited substance. This allows a small quantity to penetrate within the superficial layers of skin (epidermis). It is estimated that approximately $3.3*10^{-6}$ ml penetrate with this procedure [23]. If the substance penetrates too deep, even causing bleeding, a false positive can be encountered. On the other hand, if it is not infiltrated enough, a false negative may be recorded.

The interpretation of results is done after 15 to 20 minutes after injection, where there is a maximum reactivity for the antigen. For this diagnosis, the wheal and erythema are marked on the skin **(Fig.9a)** and are consecutively transposed to a piece of bandage. Then, the bandage is placed on a sheet of paper, so as to store the obtained test results for the future **(Fig.9b)**.

(a) **(b)**

Fig.9: Images from SPTs of real patients. (a) Marked wheals on skin. (b)Test results on paper.

This means that the only way to have a record of the patient's tests is paper based, which is problematic in terms of storage. The diagnosis is done by visually comparing the appearance of skin areas from the extracts and from the negative control. Even though the most correct diagnosis is made by measuring the wheals, the procedure generally followed only involves a subjective comparison. To certify that a patient is sensitized to an allergen, in terms of a positive test result, the diameter of the extract

tried needs to have a diameter at least 3mm larger than the one from the negative control. Besides the mentioned drawbacks, skin color can make even more difficult this interpretation; specially in black race patients.

Even if this test is considered highly reliable, it needs to be correlated to the medical history to confirm if a patient is allergic to that allergen, by demonstrating that the symptoms are caused by exposition to an specific allergen. However, the area of the wheal can provide enough information to consider a patient sensitized or not to a given extract [24]. An area of 31 mm^2 for perennial allergens and 32 m^2 for seasonal allergens can be used to distinguish between patines with clinical symptoms and the ones just presenting a sub clinic sensitivity.[24]

Over the years, a motivation for improving this procedure have lead to an increase in research in this area. Several approaches have been proposed in literature for the image detection of skin erythema [25][26][27]. Most of these cases are based on recording images of the affected areas using digital cameras, followed by image processing techniques. In spite of this boost, manual diagnosis is kept as the gold standard at hospitals.

2.4.2. Intra-dermic testing

Intra-dermic tests consist on injecting the desired allergen extract within the dermis; using an insulin needle, inserted over the capillary bed found under the epidermis. The region of the body used is the same one as with SPTs; the forearm (or the back, at given cases). Moreover, the diagnostic methodology is also very similar to the other test.

The substance is infused within the tissue until a wheal of 2-3 mm of diameter appears. Following, the immediate hypersensitivity reactions occurs 20 minutes after the injection. To be considered positive, a wheal's diameter must be larger than the negative control's diameter (or larger than 3mm, for some authors [28]). Besides, if erythema is not produced, the test might be invalid. These measurements rely on vision, different scales are employed for the test's interpretation; such as King and Norman scales (**Table**

1); or the quotient wheal/erythema in relation to histamine. The later is highly subjective and thus, can not be used in scientific research.

King and Norman criteria for intradermoreaction evaluation		
Grade	Erythema (mm)	Wheal (mm)
0	<5	<5
+/-	5-10	5-10
1+	11-20	5-10
2+	21-30	5-10
3+	31-40	10-15 or pseudopods
4+	>40	>15 or pseudopods

Table 1. King and Norman criteria for intra for intra-dermic testing diagnosis. Data obtained from [].

The drawbacks of intra-dermic tests are based on the probability of encountering false positive results. In addition, they are more adverse in terms of patient's comfort.

2.4.3. Epi-cutaneous testing

Epi-cutaneous tests are performed by exposing the patient's skin to direct contact with the suspected allergen. They consist of late-phase hypersensitivity reactions; the interpretation of results are generally done after 48 hours; and over several days. The methodology of diagnosis is the same as the previous cases; visual observation of the test areas. The diagnosis relies on the the criteria shown in **table 2. [alergia]**

GEIDAC clinic interpretation		
Inform	Results	Interpretation
+7	Weak erythema	Doubtful

+	erythema, infiltration and, maybe papula	Posible
++	erythema, infiltration, papula and blisters	Probably
+++	Intense erythema, infiltration and coalescent blisters	Very probably
-	Absence of reaction	Negative
RI		Irritating reactions
NP		Not proven

Table 2. GEIDAC clinic interpretation for epi-dermic testing diagnosis. Data extracted from[]

3. Materials and Methods

User specifications

In order to define the user specifications, several sessions of meetings with a doctor took place. In these, all the relevant information from SPTs was explained in detail; from the physiological characteristics of allergic reactions, including the measured parameters; to the clinical protocol followed. From these sessions, enough information and specifications were obtained for starting the project development.

As SPTs are carried in the forearm, one of the specification was that the device's structure had to include a specific location where to place this part of the body, so as to acquire images of the region of interest. The whole region of interest had to be recorded (so as to include all the allergens tested).

Moreover, another user specification was related to the detection of negative and positive controls, as these were used to correctly diagnose the allergic reactions. The location of these controls over the forearm was patient-dependent, as it depended on the number of allergens to be tested. A mark was done over the skin as an 'H' to point out positive control location, whereas an 'S' was marked as the negative control site. For the complete automatic diagnosis, detection of 'H' and 'S' was crucial.

The results for the diagnosis, as explained before, had to be in relation to the negative control, this meant, that a wheal to be considered as a sensitized component, its diameter had to be at least 3mm of length larger than the saline's diameter.

In addition, concerning the conditions for correct image acquisition, the lights of the room should be turned off to avoid signal contamination. Besides, the user's arm should be kept still to avoid motion artifacts and noise.

3.1. Photographic setup

To complete the first objective of the work; designing a suitable structure for the SPTs; an initial prototype was created to decide the best possible composition. In order to record the spectral reflectance of skin in the area of interest, the whole photographic set up had to be conformed by; a camera holder; light holders; and the location where to place the forearm. The accuracy of this process depended on several parameters, such as illumination, geometry, optics, etc. For this reason, different specifications were taken into account in the prototype design:

- Average length of a human's forearm: 20 cm
- Height distance for placing the camera (Related to field of focus, focal depth,)
- Type of illumination: LEDs (light-emitting diodes)
- Location of the illumination sources: obtain homogeneous illumination.
- Portability and size of the structure: thought to be used at the hospital.
- General diagram of the design (**Fig.10**)

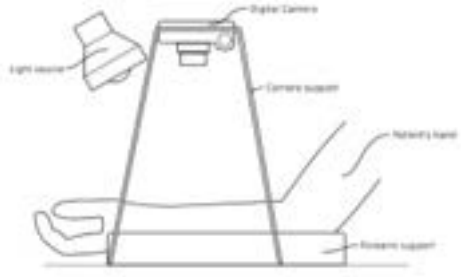

Fig.10 Diagram of the photographic setup for carrying SPTs. Image extracted from [26]

3.1.1. Prototype Structure

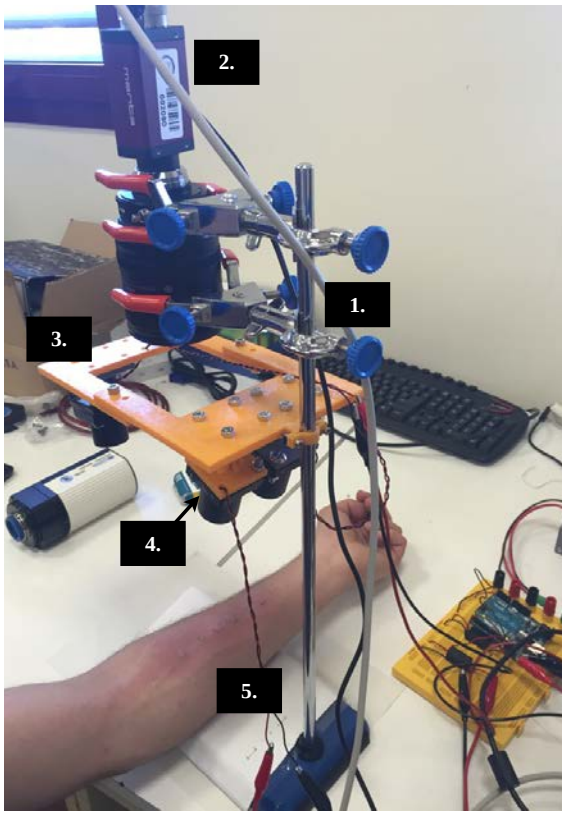

Fig.11 Picture of the prototype used as photographic setup for carrying SPTs.

1. Structure backbone/Supporter. (**Fig. 12**)

The height of the camera position was: 50 cm.

Fig. Picture of the prototype's structure backbone.

2. Camera (in this case, Manta GigE-145 NIR from Allied Vision).

3. Base for mounting the four LED structures. (**Fig. 12**)

3D printed structures from polymer PLA (Polylactic Acid) using a Prusia I3 printer (from BQ). This structure was attached to the the backbone structure, and parts **4.** were screwed to it. (CAD drawing dimensions attached at the end of the document as an appendix).

(a) **(b)**

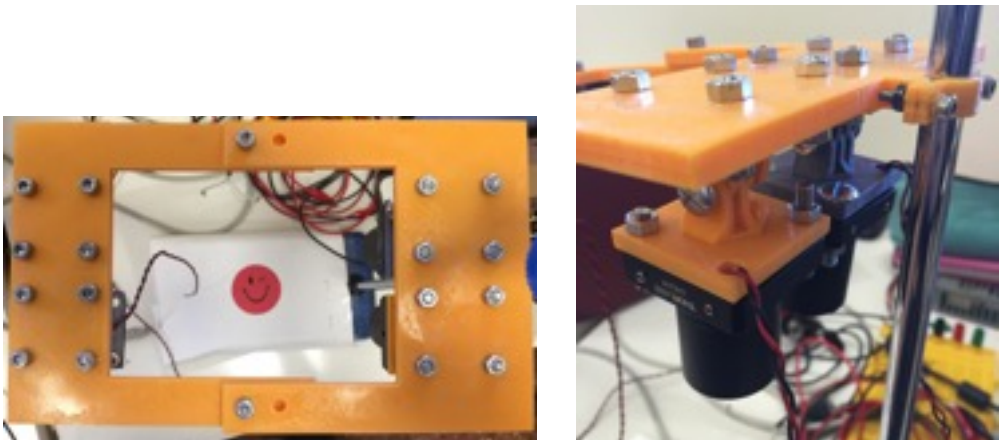

Fig. 12 Pictures of the prototype's base for mounting the LEDs., different views.

4. Single LED structure mount. (**Fig 13**)

3D printed structures from PLA (Polylactic Acid) using a Prusia I3 printer (from BQ). The structures containing the LEDs were screwed to this mount. (CAD drawing dimensions attached at the end of the document as an appendix).

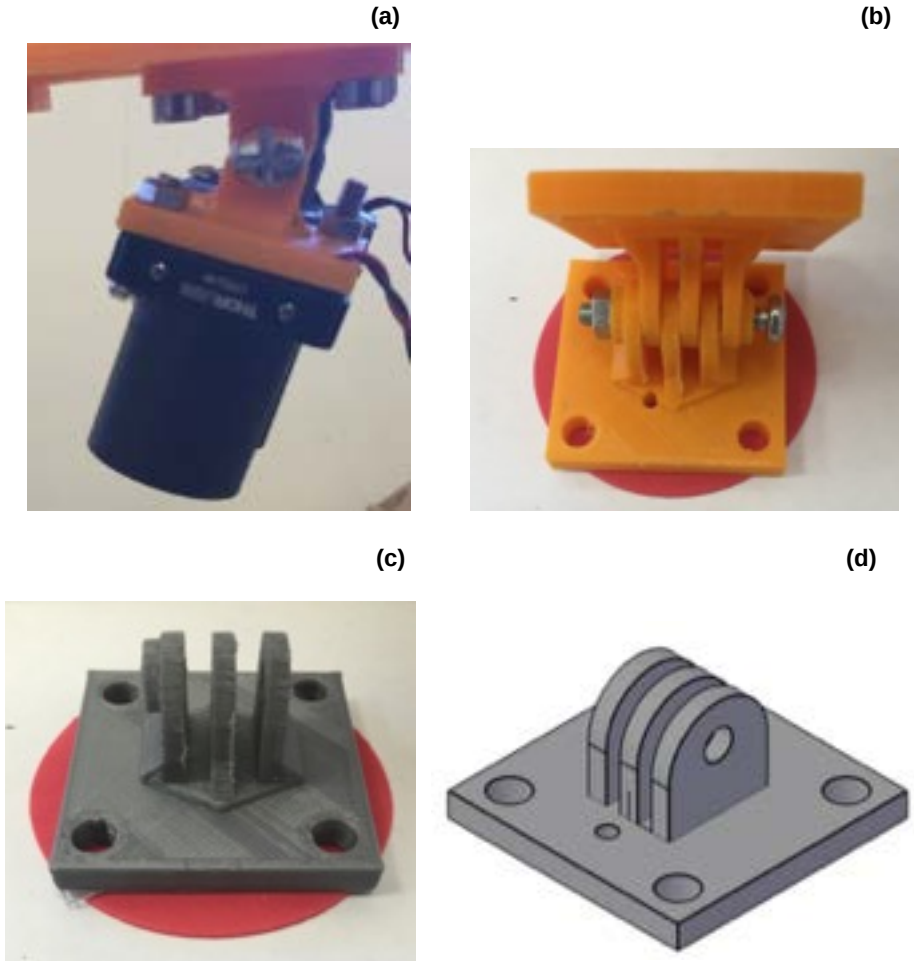

Fig.13 Mount structure for the LEDs to the base of the setup. (a) LED screwed to the structure. (b) The whole structure. (c) One of the parts that compose it. (d) CAD drawing of the figure

5. Arm's place

Relying on this prototype, an integrated structure was later designed, so as to build an official photographic setup that could be used at the hospital. The idea and measurements tested on the previous structure were used as reference. The final structure is shown in **Fig.14**. The CAD drawing of that pieces that conform it are attached as appendixes.

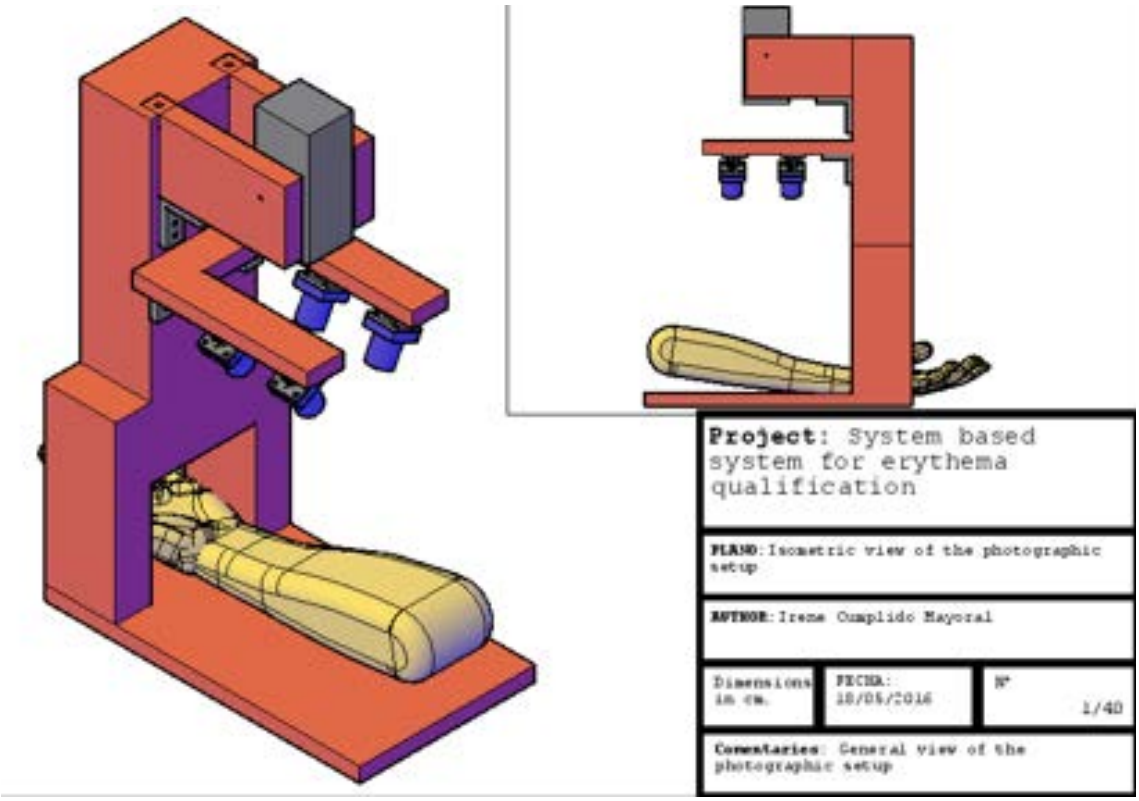

Fig. 14. Photographic setup prototype, CAD drawing.

3.1.2. Camera

For the images acquisition, two different CCD sensor cameras were used. A CCD sensor is composed of an array of p-doped metal-oxide-semiconductor (MOS) capacitors, which represent each of the pixels. [29]

MOS structures are characterized by growing a layer of silicon dioxide (SIO2) on top of a silicon substrate and the depositing a layer of metal or polycrystalline silicon. Due to the dielectric properties of the silicon, MOS structures work as planar capacitors. [29]

These p-doped MOS capacitors convert energy of incoming light photons into electron charges at the semiconductor-oxide interface. This occurs when they are biased above the threshold for inversion, thus, starting image acquisition. Then, electron charges are amplified and quantized by an analog-to-digital (AD) converter. Therefore, the CCD

device is able to measure the spectral intensity of arriving light; which means that only light intensity is measured in these devices. [29]

To distinguish color, the different pixels are covered by a color filter, so that each of them measures only intensity from photons corresponding to the allowed frequencies. This also represents a loss of light, as the photons of mismatching energies are absorbed. Taking into account that human visual system consists of three different types of color sensitive cells in the retina; which are sensitive to red, green and blue correspondingly; color imaging adopts an RGB system to simulate wavelengths detection by these human cells. Therefore, red, green and blue filters are used to represent the primary colors which can be combined to obtain more color possibilities. For this study, images were acquired both in chromatic and monochromatic conditions.

As previously mentioned, for the experimental sessions, two different cameras with their specific characteristics were used.

Q-Imaging Retiga-2000R

Important parameters:

CCD sensor	
Light-sensitive pixels (Resolution)	1,600 x 1,200
Pixel size	7.4 µm x 7.4 µm
Digital output (ADC)	12 bits
Spectral response	**Fig.15**
Established Acquisition Parameters	
Exposure Time	200,000µs
Gain	7

Table 3. Retiga 2000-R Characteristics [

The field of view of the taken images was 20cm x 15cm . As it can be seen in the spectral response (**Fig.15**), the sensitivity in the NIR spectral range is very low. Besides, the final image resolution was of 200mm/1600pix = 0.125 mm/pixel.

(a)

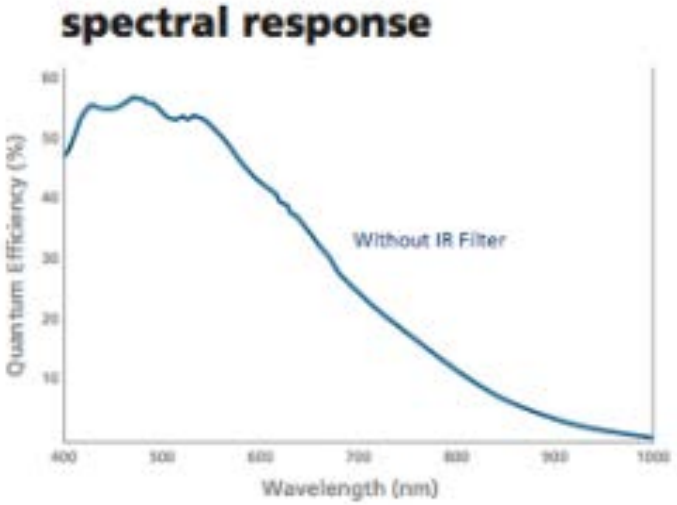

(b)

Fig. 15: Retiga-2000R. (a) Picture of the camera. (b) Spectral response of the sensor [30]

Allied Vision Manta G-145 NIR

Important parameters:

CCD sensor	
Light-sensitive pixels (Resolution)	1,388 x 1,038
Pixel size	6.45 µm x 6.45 µm
Digital output (ADC)	12 bits
Spectral response	**Fig. 16.**
Established Acquisition Parameters	

Exposure Time	200,000µs
Gain	7
Extra	
Computer connection	Ethernet cable

Table 2. Manta G-145 Characteristics

The field of view of the taken images is 20cm x 14.9cm . As it can be seen in the spectral response (**Fig. 16.**), the sensitivity in the NIR spectral range is higher than with the previous camera. The image resolution was of 0.19 mm/pixel.

(a) 

(b) 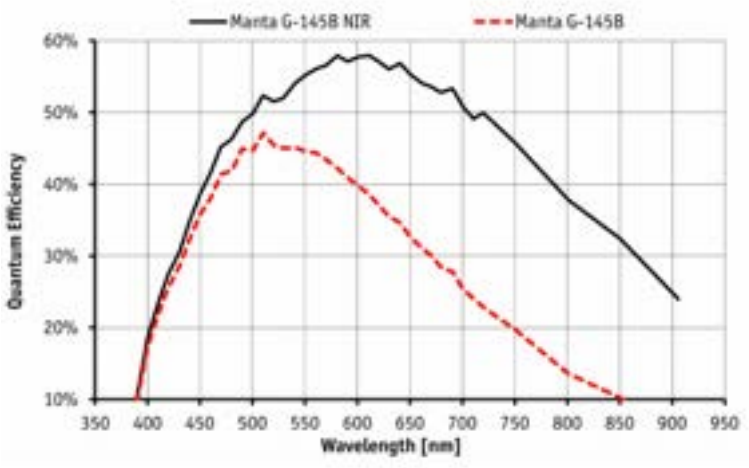

Fig. 16: Manta G-145B NIR. (a) Picture of the camera. (b) Spectral response of the sensor [31]

Objective Lens

Due to the set-up conditions (described in detail in **Section 3.1.4.**), the lens had to have a big ROI, because of that, a Nikon AF-S DX NIKKOR 16-85mm f/3.5-5.6G was used.

3.1.3. LEDs

The instruments used for the illumination set-up consisted on four LEDs (Light emission diodes) on Metal-Core Printed Circuit Boards (MCPCBs), two for each of the tested wavelengths. They offered a high-power output, in the need for obtaining an homogenous illumination of the ROI, the forearm.

Fig. 17: High-power output LED on MCPCB. From ThorLabs

This type of LEDs produce a large amount of heat. For this reason, a heatsink was required to avoid reduced lifetime and prevent unstable light output (a thermal adhesive was needed to attach the MCPCB to the heatsink, so as to distribute heat homogeneously over the MCPCB's cross section). The heatsink was purchased from ThorLabs.

Following, the LEDs were integrated into the optical assembly by using stackable lens tubes (Thorlabs SM1L10) (**Fig.18a**), which provided a good alignment. This structure was then mounted on a cage plate (Thorlabs CP06) (**Fig.18.b**), chosen due to the set of the four screw holes that could be used to mount the whole structure into the prototype.

(a) **(b)**

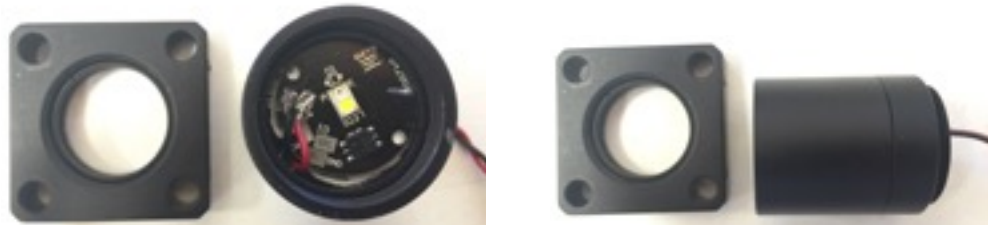

Fig. 18: Thorlabs Sm1L10 and CP06

3.1.4. Electronics

The electronics of the system were based on the control of the LEDs and the images acquisition. The device consisted on a camera connected to a computer, so as to control the acquisition of images and to store them for later processing. Moreover, images were taken under an alternating illumination; 1.No light - 2. Green light - 3. No light - 4. NIR light. Therefore, four images were taken in each of the series.

The turning of the LEDs on and off was controlled with an Arduino Uno microprocessor, which sent the corresponding pulses to modulate the setup illumination. As the LEDs required a constant current source, and taking into consideration their current input specifications (I_{input} = 2A), a LED driver was used to feed them. For this, a RECOM RCD-24 current LED Driver was purchased. Its output current goes up to 1200 mA, which was enough for feeding the LEDs. Two drivers were used in this case; one for the green LEDs, and another one for the NIR LEDs. Besides, their input voltage range needed to be 36V. Because of this, they were connected to an power supplier ADC converter, which in turn was connected with the 220V socket. A switch was also included in the design, so as avoid continuos feeding of the LEDs.

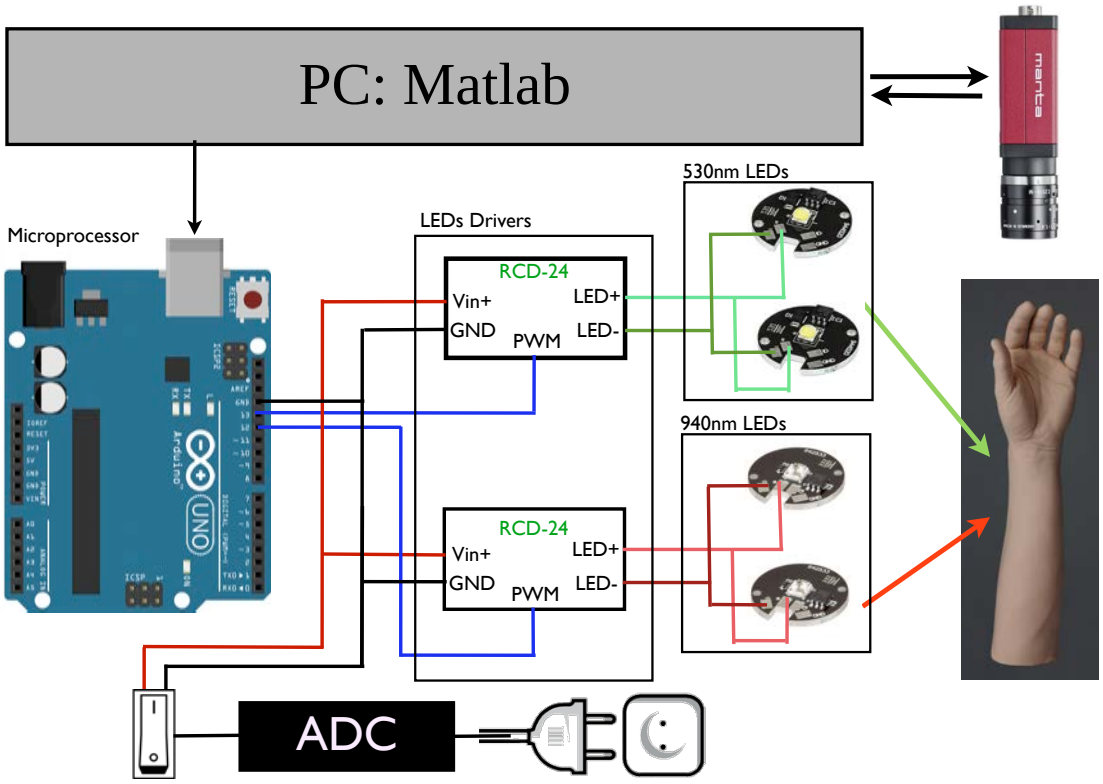

Fig. 19. Block diagram of Photographic setup

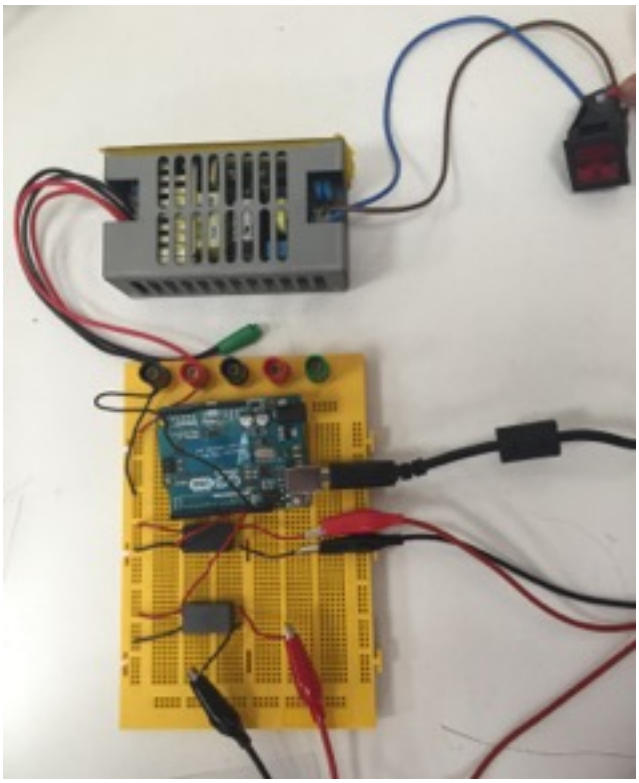

Fig. 20: Picture of the electronics

3.2. Optics and Illumination

3.2.1. Chromophores characterization

The illumination used in the project was chosen by studying the optical properties of skin; more concretely, its absorption spectrum (**Fig.21**).

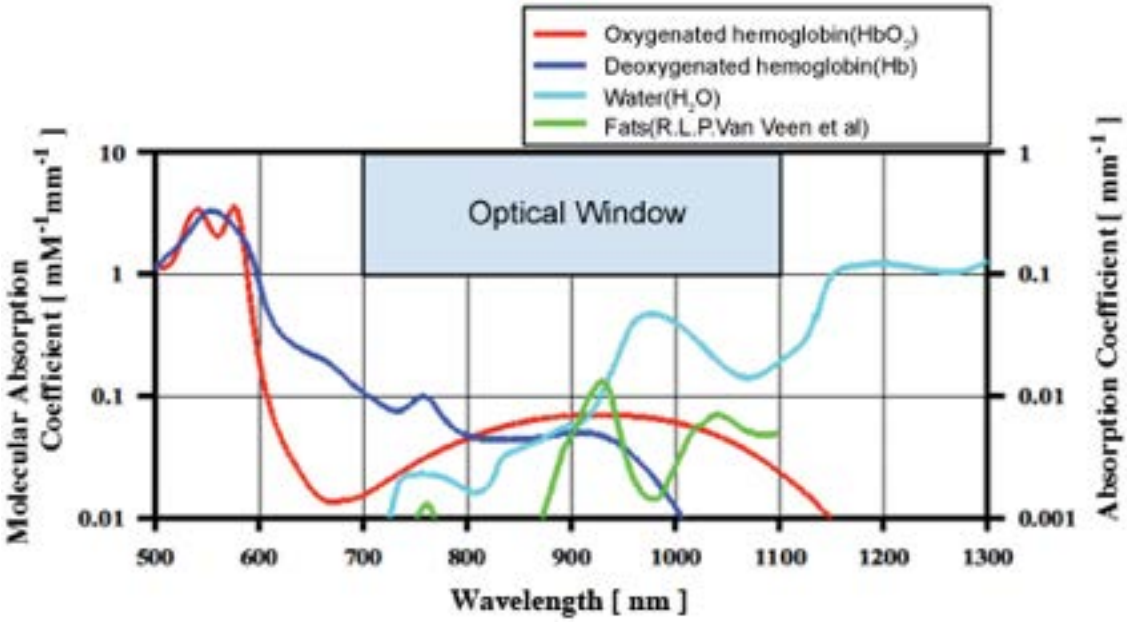

Fig. 21: Absorption spectrum of main substances in living tissue. [32]

Erythema refers to redness of the skin due to an increase of blood flow in the uppermost capillaries of the dermis (the sub-papillary plexus). This red appearance is a consequence of a dimmer reflectance of the green wavelengths. Taking into account the absorbance spectrum of the HbO_2 and the Hb (**Fig.21**), it can be seen that their absorption coefficient should be stronger in the blue and green regions than in the red one. Thus, light reemitted from the erythematous should have more energy related to red wavelength than to green and blue. That is the reason why erythematous skin area looks red in comparison to the surrounding skin.[33]

As a result, one of the illumination characteristics of the following set-up was related to enhancing erythema visual appearance, by considering the spectral absorbance of blood

(HbO2 and Hb). Some examples in literature describe the best parameters for erythema detection, which are around 500-565 nm [33][34][35]. This range corresponds to green color, whose penetration in skin is limited to a few hundred micrometers [36], being enough to reach the sub papillary plexus. In **Fig 22**. the relation of light reflectance from erythematous and white skin is shown; verifying the theoretical idea that for wavelengths below 600 nm, this optical property has less intensity for erythema.

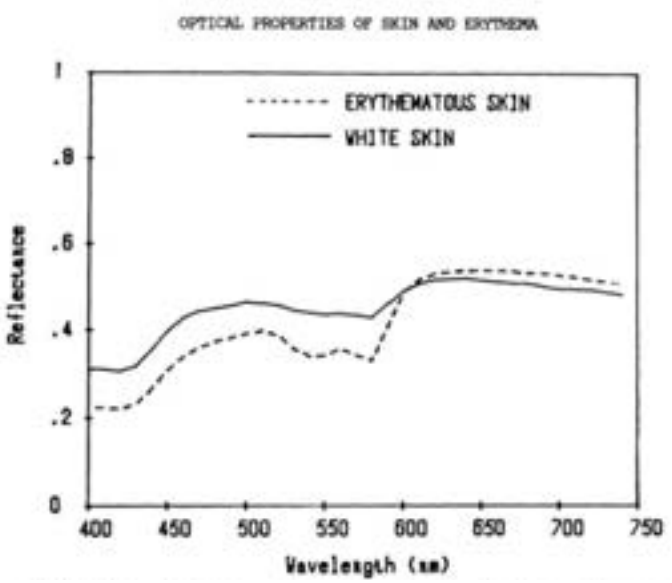

Fig. 22: Optical reflectance of skin in relation to the incident wavelength radiation. Comparison between erythematous skin (dashed line) and white skin (solid line). In the range smaller than 600 nm, erythematous skin absorbs more light, thus, the reflectance is smaller. [35]

Therefore, a wavelength peak of 565nm was chosen to illuminate the region of interest.

Moreover, as it can be seen in (**Fig**. **23**), the absorption coefficient of melanin, which is the main absorber chromophore in the epidermis, has lower values for longer wavelengths. By this, it could be assumed that absorption by melanin could be negligible for a light radiation of 550 nm and that the changes in reflectance depended mostly by blood absorption.

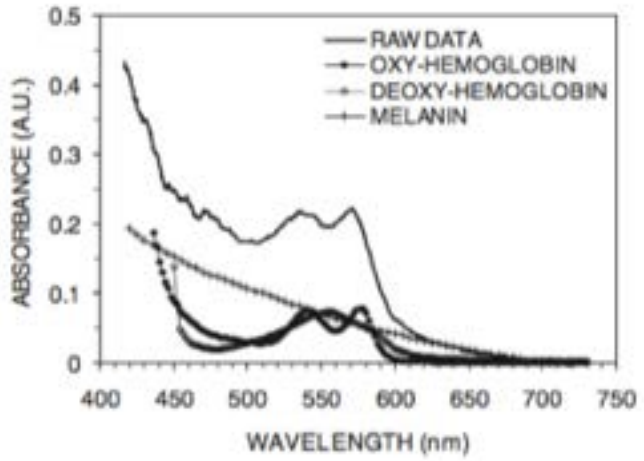

Fig. 23: Optical absorbance of skin chromophores in relation to the incident wavelength radiation. Comparison between HbO_2,Hb and Melanin; as well as the composition of the three of them (Raw data). [34]

Besides, another consequence of allergic reaction is the increase in vascular walls' permeability to blood plasma. This results in an increased concentration of extracellular fluid in the tissue, causing edema. As previously mentioned, blood plasma is mainly composed by water. Applying the same concepts of absorbance and reflectance properties as before, an illumination wavelength was chosen to enhance the visual distinction between the edematous area and the non-affected one. For this, water absorbance spectrum was studied (**Fig 21**); its absorbance coefficient increases for wavelengths over 800 nm [38]. This is due to the energy from the vibrational overtone of the O-H bonds [37].

Consequently, the second light wavelength chosen for illumination in the carried study was 940 nm, so as to enhance the visual observation of edema. Edematous regions would be characterized by a stronger absorption of NIR light than the rest of the skin chromophores; thus, it would be seen darker than the surrounding areas [34].

In addition, considering that the main goal of the project was to quantify skin erythema, the hypothesis of the light reflectance and absorbance could be used for completing this objective. For this, Beer's Law was used, which defines the relation between the absorbance and the concentration of the sample [Eq.(3.1)]. Relying on this law, the concentration of the substances should be found out (water and blood).

3.2.2. Optical Parameters

Even though the absorption coefficients of water and blood for those 565 and 940 nm wavelengths seemed suitable enough for diagnosing allergic reactions, the rest of the optical parameters of skin tissue had to be taken into account. With the purpose of modeling the light distribution of these wavelengths, tabulated optical parameters were looked in literature. The description of skin optics explained in [19] was chosen to characterize skin, which is found down below.

3.2.2.1.Epidermis

The absorption coefficient over epidermis depends on a smaller (almost negligible) baseline skin absorption coefficient ($\mu_{a,skin}$) and a dominant melanin absorption produced by melanosomes ($\mu_{a,mel}$) .

The baseline skin absorption coefficient is approximated for both epidermis and dermis, obtaining [eq. (2.8)]. This equation has been developed based on measurements of bloodless rat skin and expands from 350 nm to 1100 nm.

$$\mu_{a,skin} = 0.244 + 83.3\, e^{\frac{-(\lambda - 154)}{66.2}} \left[cm^{-1}\right] \tag{3.2}$$

As previously said, absorption in epidermis is dominated by melanin absorption. Melanin is a polymer that has a broad absorption spectrum, with stronger peaks at shorter wavelengths. This polymer is found in the internal membranes of melanosomes, which are membraneous particles of 1-2 μm in diameter. Thus, each melanosome absorbance is given by its interior, whose coefficient is approximated by [Eq.(2.9)] [19].

$$\mu_{a,mel} = (6.6\ x\ 10^{11})(\lambda^{-3.33}) \left[cm^{-1}\right] \tag{3.3}$$

To apply this coefficient, it is necessary to estimate the concentration of melanosomes in epidermis, which is given by the volume fraction of the epidermis that they occupy. Different estimations based on wavelength dependence can be found in literature [19].

The ones given in [19] are a descriptive convention for melanin in the range of 650-800 nm.

- Light-skinned adults: f_{mel} = 1.3 - 6.3%
- Moderately pigmented adults: f_{mel} = 11 - 16%
- Darkly pigmented adults: f_{mel} = 18 - 43%

Therefore, combining the previous parameters, the net absorption coefficient ($\mu_{a,epi}$) is presented in [Eq (2.10)].

$$\mu_{a,epi} = (f_{mel})\,(\mu_{a,mel}) + (1 - f_{mel})(\mu_{a,skin})\,[cm^{-1}] \tag{3.4}$$

The scattering coefficient of the epidermis ($\mu_{s,epi}$) is similar to the one from dermis, due to previous explanation, so it is assumed that $\mu_{s,epi} = \mu_{s,derm}$. Another property to be taken into account to calculate this coefficient is anisotropy (g). Typical values of g for skin tissue are between 0.7 and 0.95 (being 1 completely transparent) and are dependent on wavelength. However, for tissues, the rescued scattering coefficient ($\mu'_{s,epi}$) is more useful [Eq. (3.5)].

$$\mu'_{s,epi} = \mu_{s,epi}(1 - g_{epi})\ [cm^{-1}] \tag{3.5}$$

3.2.2.2. Dermis

The total absorption coefficient ($\mu_{a,derm}$) is specified by an average $\mu_{a,derm}$ that is independent of the blood's depth affecting the light optics. It is related to different parameters.

As said before, baseline absorption for epidermis and dermis is highly similar. Hence, they are treated by the same parameter $\mu_{a,skin}$. This gives one of the parameters.

Furthermore, hemoglobin contributes the most to absorption at dermis level. The absorption coefficient of blood (μ_{blood}) is defined in **Fig. 24** when it is composed of a

45% hematocrit (percentage of RBCs over volume). In order to know the exact absorption coefficient of blood for the wavelengths of interest, the molar extinction coefficient (ε) [cm^{-1}/(moles/liter)] for those wavelengths, the hemoglobin concentration [g/dl] and the molar concentration [mol/L], are used in [Eq.(3.6)]. Considering an average hemoglobin concentration of 150g/L of blood and the molar Hemoglobin concentration of 64,500 gHb/mole.

$$\mu_{a,blood}(\lambda) = \frac{2.303\,\epsilon(\lambda)\;\; 150\,\frac{g}{l}}{64,500\,\frac{gHb}{mol}} = 0.0054\,\epsilon(\lambda) \tag{3.6}$$

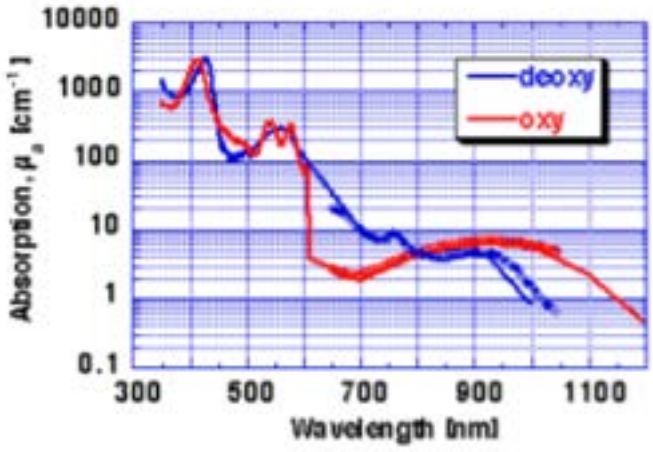

Fig. 24: Absorption coeffcient of blood (45%hematocrit).
Blue = deoxy-hemoglobin, Red= oxy-hemoglobin [7]

A conventional description of the average volume fraction (f_{blood}) can be adopted by assuming a uniformly distributed blood in the skin. Even though most of the cutaneous blood is concentrated in the venous plexus at 100-200 μm of depth (volume fraction around 2-5%), the approximation of homogeneously distributed blood with low f_{blood} appears appropriately equivalent to the values obtained for real superficial distribution and fraction volume. Following this equivalency, the net absorption of the dermis perfused with blood is calculated in eq. (2.12). [19]

$$\mu_{a,derm} = (f_{blood})(\mu_{a,blood}) + (1 - f_{blood})(\mu_{a,skin})\ [cm^{-1}] \tag{3.6}$$

Concerning the scattering coefficient of the dermis, both Mie scattering and Rayleigh scattering are taken into account. The first one is contributed by the large cylindrical collagen fibers that make up this layer. The latter one, on the contrary, is contributed by different small-scale structures associated with some cellular structures, including collagen fibers. Besides, the epidermis behaves in a way similar to the dermis due to its keratin fibers. Consequently, the coefficients of each layer are approximated.

Using Mie theory for cylinders and the average size (2.8 +/- 0.8 μm in diameter) and number density ($3*10^3$ [cm^3]) of collagen fibers in skin [14], the Mie scattering is calculated by [eq. (3.7)].

$$\mu'_{s,\,Mie\,fibers}(\lambda) = (2x10^5)(\lambda^{-1.5})\,[cm^{-1}] \tag{3.7}$$

In addition, due to the small structures found in collagen fibers, a Rayleigh scattering is present in dermis. To calculate its contribution, the collagen fiber volume is approximated by spheres of 100-nm diameter and a volume fraction os 22% collagen us used. This yields eq.3.8.

$$\mu'_{s,\,Rayleigh}(\lambda) = (2x10^{12})(\lambda^{-4})\,[cm^{-1}] \tag{3.8}$$

As a result, the scattering characteristics of dermis depend on Rayleigh scattering for small-scale structures in collagen fibers at short wavelengths (below 650 nm) and of Mie scattering from larger fibers at wavelengths over 650 nm. The sum of Eq.3.7 and Eq.3.8 gives the total reduced scattering coefficient found in dermis [Eq.3.9].

$$\mu'_s(\lambda) = \mu'_{s,\,Mie\,fibers}(\lambda) + \mu'_{s,\,Rayleigh}(\lambda) \tag{3.8}$$

Calculations for the skin optics for λ = 565 nm and for λ = 940 nm were done to understand the distribution of light in terms of absorption and scattering that would be seen in the experiments.

Assumptions: [1]

[1] Values for molar extinction coefficient ε extracted from [39]

- f_{mel} = 10%
- f_{blood} = 4%
- ε (565nm) = 39036.4 for Hb [cm^{-1}/(moles/liter)]
- ε (565nm) = 39956.8 for HbO_2 [cm^{-1}/(moles/liter)]
- ε (940nm) = 693.44 for Hb [cm^{-1}/(moles/liter)]
- ε (940nm) = 1214 for HbO_2 [cm^{-1}/(moles/liter)]

3.2.3. Light Propagation Characterization

Further, apart from the theoretical calculations and its corresponding assumptions, with the objective of visually studying light propagation in real cases, a tissue-mimicking phantom was used to test the chosen light wavelengths in a scattering medium.

The phantom used was a parallelepiped of sizes 8x6x1.5cm (**Fig. 25**), built from polyester resin. This material is purchased in its liquid state and then is solidified with application of the corresponding catalyzer. It is useful because its absorption and scattering coefficients are negligible, and the desired coefficients can be obtained by adding black ink and TiO_2 in the corresponding concentrations [40]. In this case, it was characterized by a μ_a= 0.3cm^{-1} and μ's = 10cm^{-1}, which correspond to average values found in literature [40].

(a) **(b)**

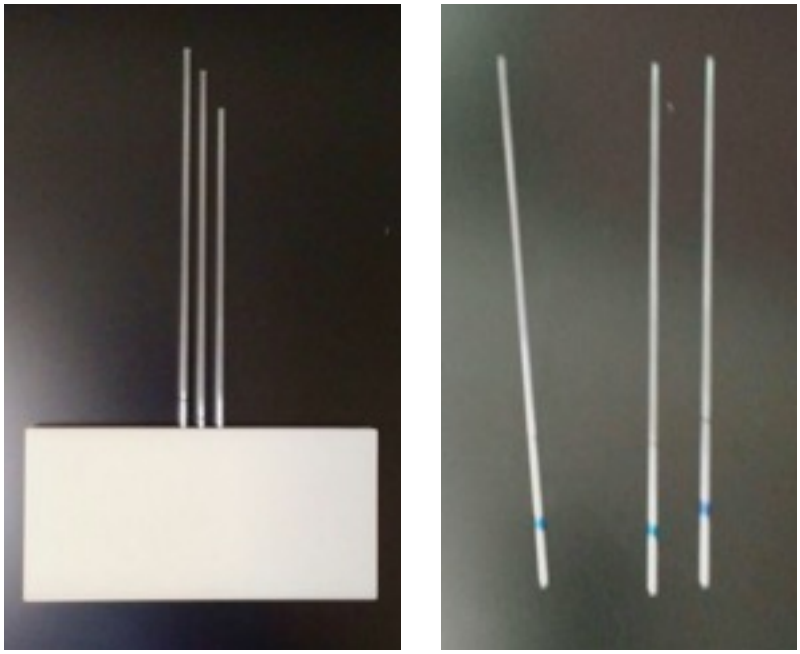

Fig. 25: Image of the tissue mimicking phantom. (a) Tissue phantom with the capillaries inside. (b) Crystal capillaries where liquid is introduced.

The tissue phantom had three holes to insert capillaries filled with the substances to be tested. In this case, oxygenated pig's blood, water and a reference substance of a μ's = 10 cm^{-1} were introduced.

3.3. Clinical Protocol

For the study, two different tests were carried out. In the first one, three volunteers's arms were used to do the analysis. In the second one, four volunteers participated (Out of those four, the three firsts were the same users that participated in the first test. All the participants had white skin.

The clinical protocols followed in the two tests was based on different steps, relying on the procedure carried at the hospital:

1. Drawing on the skin different lines with a separation between them, of, approximately, 2cm. These lines were used to tag the location for the different substances tested.
2. Delimiting in the forearm the region of interest for the test, by directly drawing two marks; in this case, the figure of a cross.
3. Placing a drop of each of the substances over the skin. The study was carried out with 4 different allergens, in addition to the negative and the positive control. These allergens were: **cat**; Dermatophagoides pteronyssinus (**Dpt.**); **Pbleum P**.; and **Olea**.
4. Puncturing with a lancet the different drops.
5. Taking pictures of the baseline, right after the puncture.
6. Taking pictures of the test results, after 15-20 minutes after injection.

3.4. Software

3.4.1. Image Acquisition

The image acquisition process makes use of both Arduino and Matlab softwares. The cameras used were provided with their corresponding drivers, that allowed them to be controlled through Matlab's Image Acquisition Toolbox. Therefore, processes of turning the LEDs and acquiring images were integrated in the Matlab workflow, which was presented to the user through a Matlab GUI (Graphical User Interface) (**Fig.26**).

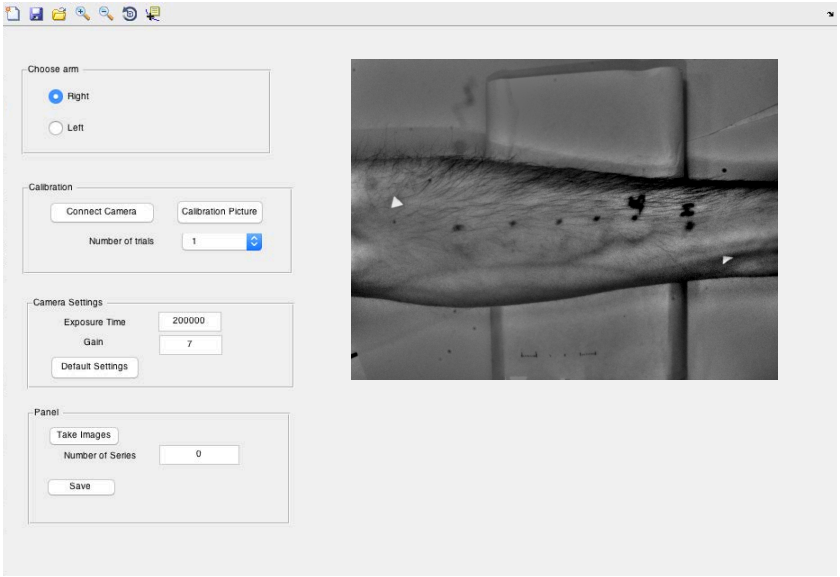

Fig. 26: Matlab GUI for images acquisition

First of all, the connections with the camera were stablished, and then the acquisition parameters were set up. The ones tested (exposure time and gain) to be good for the conditions where the tests took place were provided to the user as 'default' (inidicated in Section 3.1.). However, these could be changed according to different situations.

Then, parameters for future camera calibration (corresponding to the CCD sensor parameters) were obtained. For this, and for optimizing the acquisition, a pre-visualization of the field of view of the camera was shown. Additionally, the option to choose where to save the results was offered.

Matlab communicated with Arduino via serial port. The communication was used to determine the moment when Arduino had to turn on and off each of the LEDs. The pins used as Digital Output were pin 13 (connected to green LED) and pin 12 (connected to NIR LED). As this process was carried out through the LED drivers, and these had inverse logic, a positive pulse output from Arduino corresponded to LED off, while a 'no-pulse' corresponded to LED on (**Fig.27**).

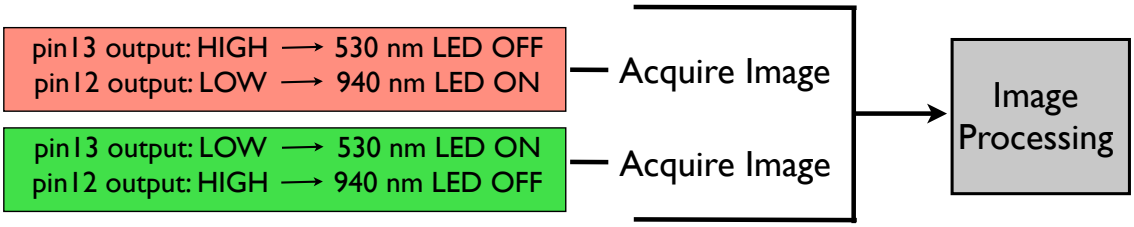

Fig.27: Display of Arduino Control and Matlab workflow

The images had to be taken when the green led was on and, consecutively, when the NIR led was on. Acquired images were then stored and processed.

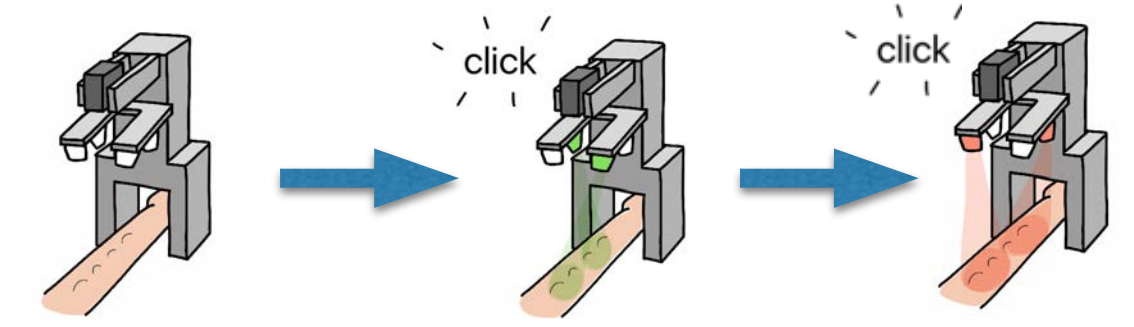

Fig.28: Schematic procedure of the test

3.4.2. Image Processing

To complete the objective of diagnosing allergy in an automated way, and making use of the previous methods, image processing was implemented. The general process is shown in **Fig**.**29** For both cameras, preprocessing steps were followed; the main difference was that for images acquired with the Retiga-2000R, preprocessing was done on channels red and green. While the output of the Manta 145B-NIR was already monochrome.

Moreover, as one of the objectives of the study was to show that specific energy photons were useful to distinguish and quantify physiological parameters (the chosen illumination was explained in **Section 3.1.2**.), independent component analysis (ICA) was performed on the RGB images acquired with the Retiga 2000R. This was because of the energy photons associated to the different color filters from the camera (red filter for IR light and green filter for green light). On the contrary, the analysis of the Manta 145B-NIR was based on one single channel.

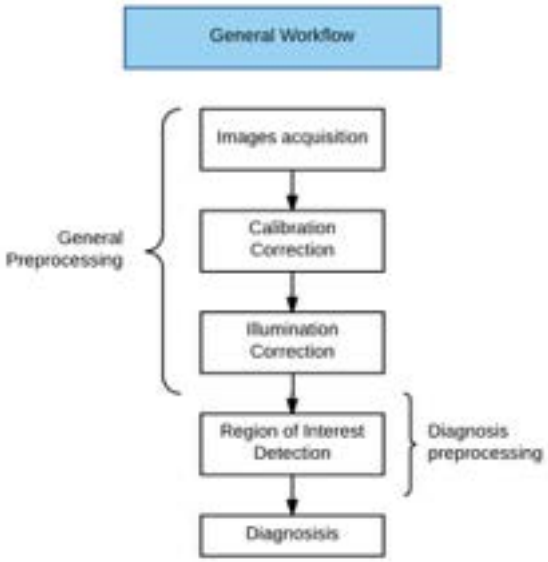

Fig.29 General Workflow of Image Processing

3.4.2.1. Image Preprocessing

Camera Calibration

First of all, noise corresponding to the CCD sensor and to the internal components of the camera had to be compensated; camera calibration was based on different reference images for achieving this. The whole process is schematically explained in **Fig.30**.

1. Average of the raw images acquired; images were acquired over intervals of 1 second. These were averaged to reduce noise. [39]
2. Bias correction (offset of the camera); this allowed to eliminate noise introduced by the internal components of the camera, such as electronics. For this, images were obtained establishing the minimum exposure time and with the lens closed. [39]
3. Thermal correction; dark images were recorded to obtain noise due to thermal changes. These images were obtained using the same exposure time as the one established in the scene acquisition, in dark conditions (not allowing the arrival of any light to the sensor). [39]
4. Gain correction; this allowed to correct darkness of the images due to different sensitivity between pixels, blemishes… For this, an image of a white homogeneous surface was used. [39]

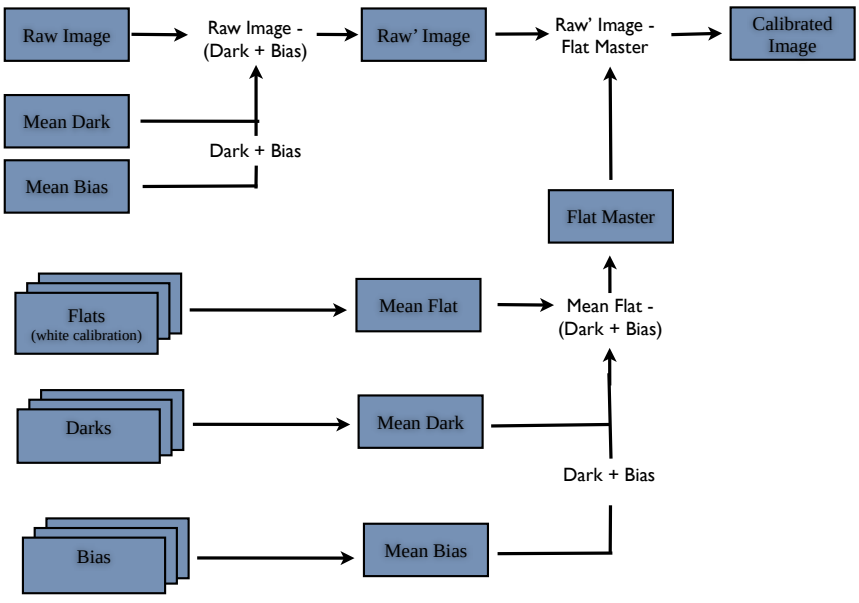

Fig.30: Schematics of camera calibration

An example of this calibration correction is shown in **Fig**.**31**.

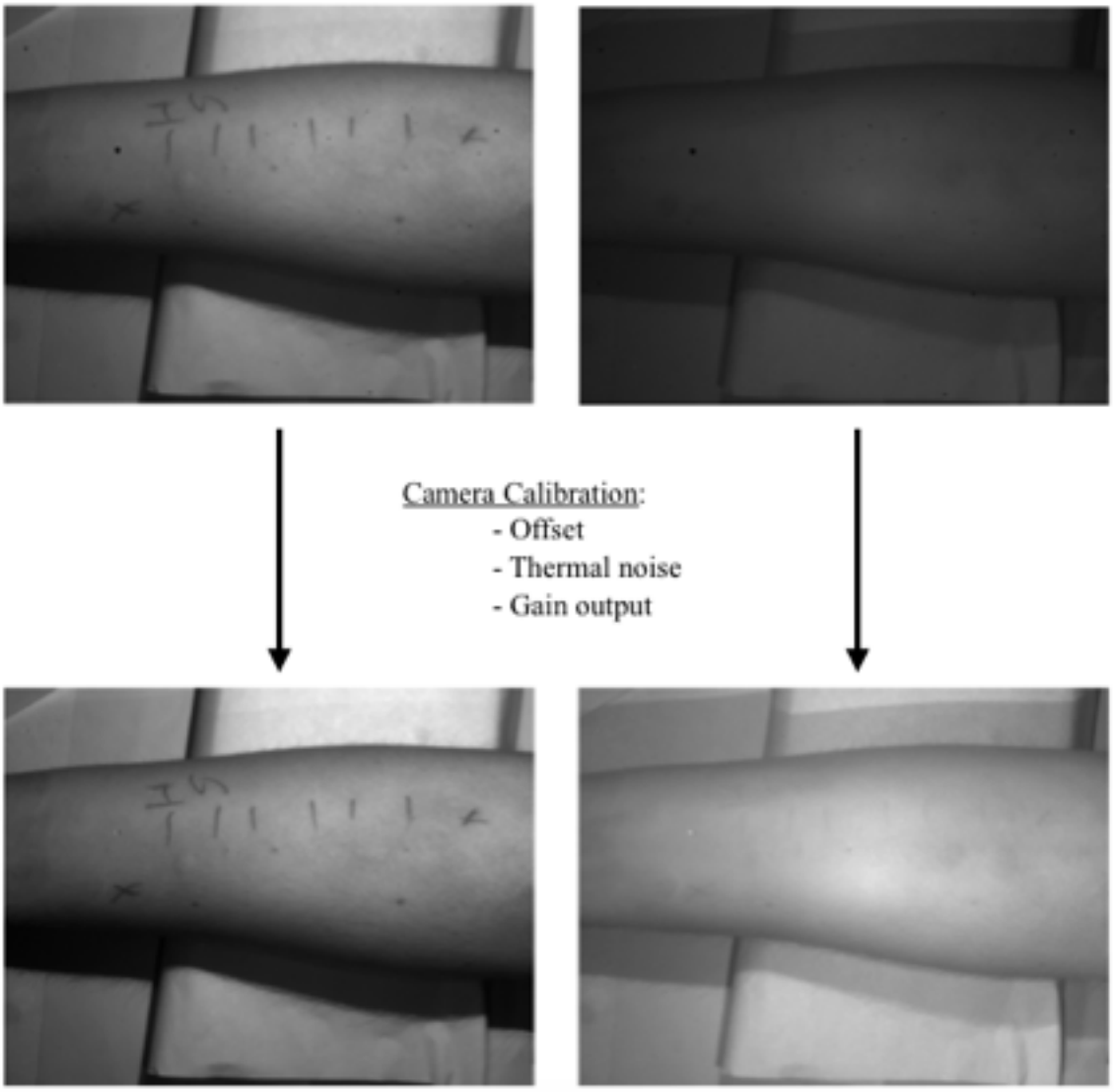

Fig.31: Volunteer 5. CCD calibration: before and after. a) Green light Image. b)NIR light image

Non-Uniform Illumination Correction

The second step was to obtain images independent from uneven illumination characteristics, so as to avoid changes in intensity contrast that could interfere with the desired result. Considering the obtained images **f(x,y)** as a 2-dimensional light intensity function resulted from the combination of the illumination and the reflection components, the desired element can be extracted. This function is given by **Eq. 3.9.** in

which I(x,y) is the amount of source light incident to the objects in the scene and R(x,y) is the amount of light reflected by the objects. [40]

$$f(x,y) = I(x,y) \cdot R(x,y) \tag{3.9}$$

Thus, the objective was to remove the illumination component, so as to keep only the object reflectance (this intensity would follow the behavior explained in **Section 3.2.1**). This illumination component could be found in the low frequencies of the image. Consequently, a low pass filter with a very low cut-off frequency was used to estimate this component (smoothed) and to remove it from the original image afterwards. The reflectance image was obtained by **Eq.3.10**. The cut-off frequency specified was 0.005, from which results such as **Fig**.**32** were obtained.

$$R(x,y) = \frac{f(x,y)}{I(x,y)} \tag{3.10}$$

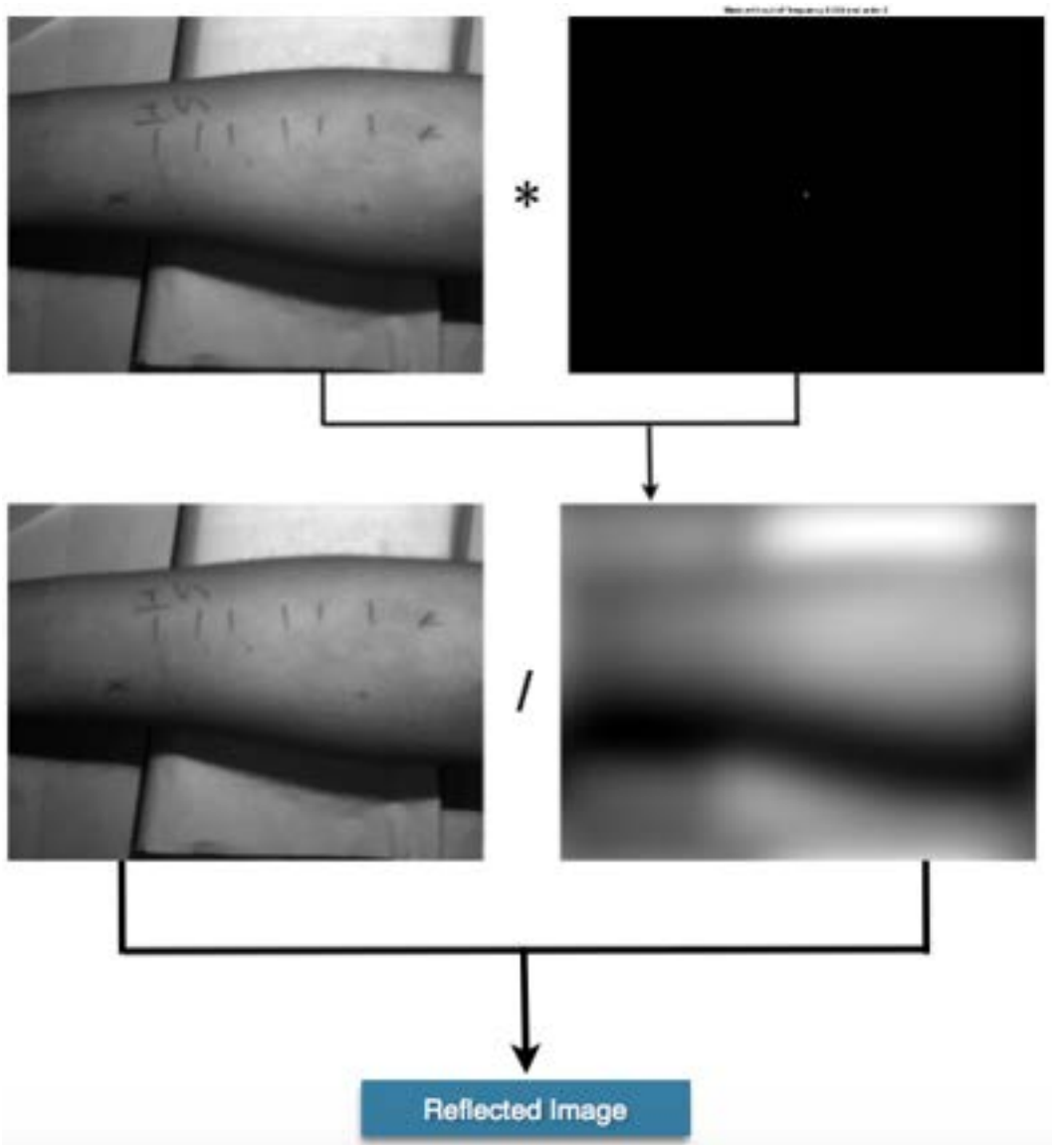

Fig.32: Volunteer 6. Illumination correction process

a)

b)

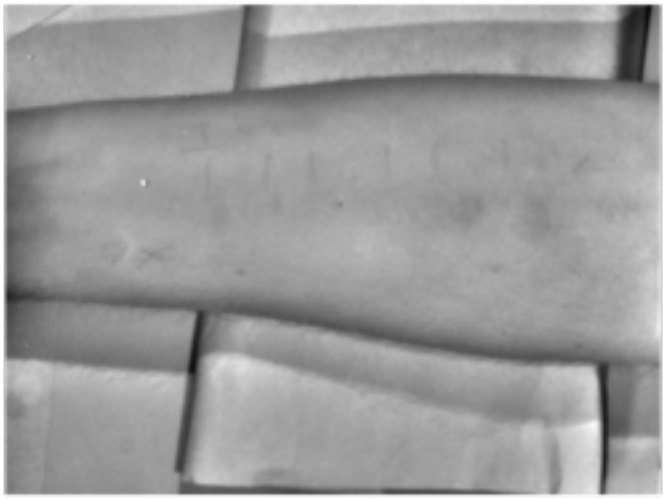

Fig.33: Volunteer 6. Illumination corrected images; reflectance. a) 565nm. b) 940 nm

Region of Interest Detection

The ROI was marked on the skin using two opposite crosses delimiting a rectangle. They were detected by shape characterization (**Fig**.**34**).

Fig.34: Example of detected shapes for ROI delimiting

Right after, lines delimiting the tested area in skin were also recognized. This processing was used to delimit the image analysis to local areas in order to diagnose reactivity of the different allergens. The whole process is shown in **Fig**.**35**.

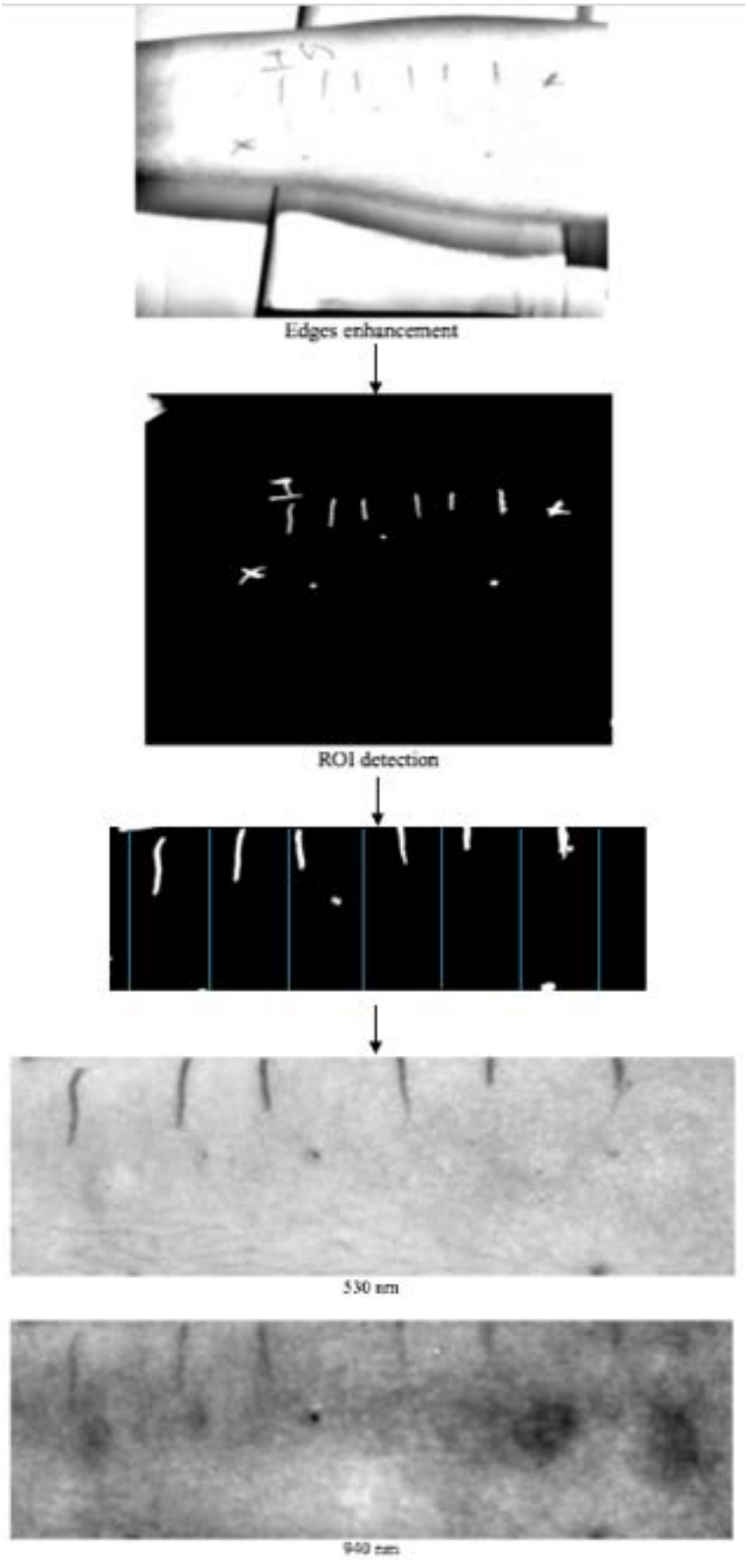

Fig.35: Volunteer 6. Region of interest separation.

Histamine and Saline Detection

One of the user specifications was the detection of the negative and positive controls used for measurements comparison in allergy diagnosis. Consequently, the automatic detection of the written ‘H’ and ’S’ on the skin was needed.

For this purpose, a neural network was trained and tested in Matlab, using the Neural Network toolbox. Three labels were introduced for the training: ‘H’,’S’ and *random noise; corresponding to 123 characters. Despite its training, the result was not reliable enough for detecting hand-written letters.

However, this fact did not affect the procedure of the experiments carried out, as the exact position of the histamine and the saline serine was previously known and, in addition, followed an easy distribution.

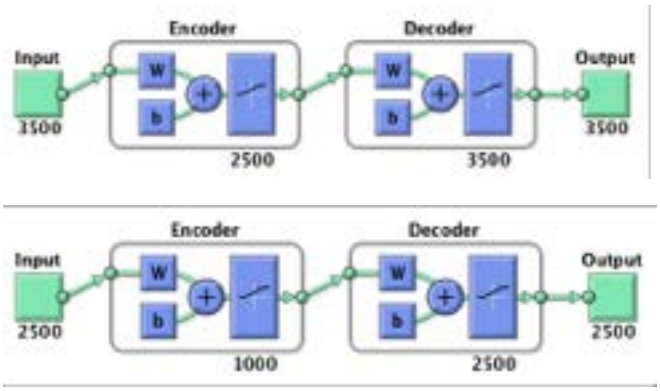

Fig.36: Training encoders for the Neural Network. a)First encoder. b) Second encoder

Diagnosis reference, manual procedure

The automatic diagnosis achieved was compared with the manual diagnosis given by the doctor. Hence, these measurements were used to determine if the automatic procedure was convincing and more trustworthy. An example of the segmentation procedure for obtaining the measurements of the doctor’s results is shown in **Fig.37** which consisted on applying a Canny filter to detect borders and segment the desired region.

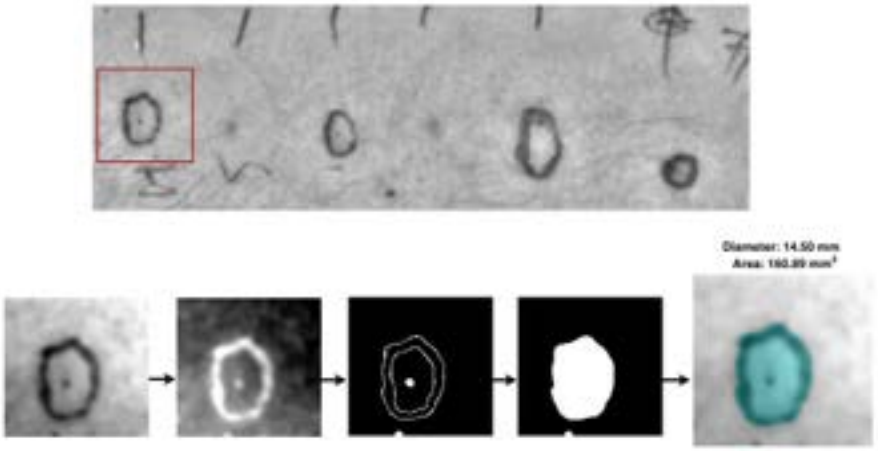

Fig.37: Volunteer 6. Doctor's control measurements for Histamine

3.4.2.2. Diagnosis

The image processing analysis was based on enhancing and detecting image features related to the physiological changes produced by allergic reactions. Therefore, the objective of this analysis was to:

- measuring the change in blood concentration in superficial blood vessels;
- measuring water concentration in the wheal produced by leakage of extracellular fluids;
- Making use of a simpler image processing than if no specific illumination was used.

Two images were obtained for the same object; one corresponding to illumination of 565nm and the other one corresponding to 940nm. Each of them represented the remittance spectrum, which contained information about the chromophores in an overlapped manner. Thus, to quantitatively describe the components of the skin and their concentrations, based on absorption and scattering parameters, the reflectance image needed to be converted to optical density absorbance maps.

Beer-Lambert's Law [Eq. 3.11] was used to figure out the the relation between absorbance and concentration of the chromophores (hemoglobin and water); describing

this possible absorbance in terms of the intensity of image pixels. Consequently, relative concentration of both chromophores was found and used for the diagnosis. As previously explained; reflectance of the object was given by Eq.3.10. [41]

$$T = \frac{P}{P_0} \tag{3.11}$$

where:

T= Transmittance
P= transmitted radiant power
P_0 = incident radiant power

Beer's law is also described in terms of the absorbance **A** [dimensionless] (Eq. 3.12).

$$A = \log\left(\frac{P}{P_0}\right) \tag{3.11}$$

Absorbance measures how much light is absorbed by a concentration for a given distance. This is shown in [Eq 3.13], given by length of the solution **l** [cm] and concentration of solution **c** [cm]. It is then related to Eq. 3.11 to yield the relation between absorbance and concentration used in this study. [41]

$$A = \epsilon l c \tag{3.11}$$

As a result, concentration maps of the chromophores were given in terms of their absorbance maps. Two types of absorbance maps were calculated; the hemoglobin one (for which green light was highly absorbed), and the water one (for which IR light was highly absorbed). The absorbance maps were calculated by the subtraction of the reflectance from the basal image to the reflectance from the reaction image. Consequently, registration algorithms were needed for calculating the absorbance in terms of the same region as the basal image.

Besides, using the mentioned concentration maps, quantitative information could be extracted. Hence, the relative quantification of the concentrations, based on intensity, could be used to calculate an average value for the apparent erythema (using the hemoglobin map); and an average value for the apparent edema (using the water map). [34]

Following, the processing was based on calculating the area and diameter of the segmented absorbance images. For this, segmentation methods based on automatic

processes were used. Segmentation of an image consists on dividing it into meaningful non-overlapping regions based on the idea that objects of the same region have the similar intensity values. Thus, from a gray image, a binary one is obtained by establishing a threshold over which pixels get white or black values. The methods of segmentation for data extraction used in this device were;

- Otsu's thresholding; finds a threshold that minimizes inter-class variance and maximizes inter-class variance.
- Texture classification;
- Watershed segmentation; in which the image is treated as a surface with high elevations (represented by light pixels); and low elevations (represented by dark pixels). Depending on the level of height used, some regions will get darker or others will get lighter.

Then, classification was based on the negative control’s measures and the extracted data.

The workflow of the diagnosis is shown in **Fig.38**.

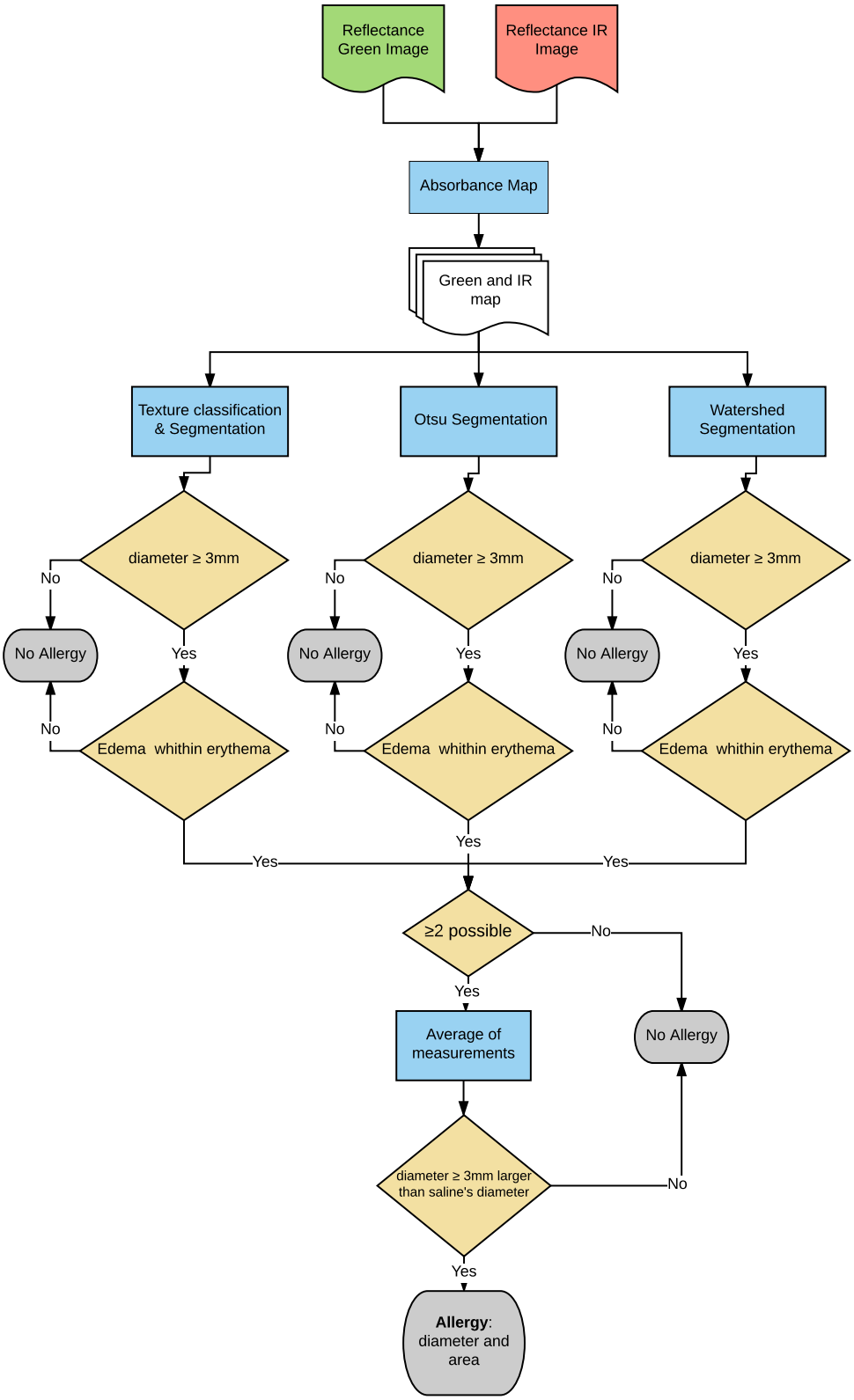

Fig.38: Wheal diagnosis Workflow

4. Results

4.1. Light Propagation

Light propagation within tissue for λ = 565 nm and for λ = 940 nm was studied using a tissue mimicking phantom. The objective was to show how the chromophores involved in allergic reactions (water and blood) behaved in terms of absorption for those wavelengths, studying this property in an intralipid scattering medium.

The images obtained when the phantom was illuminated are shown in **Fig**.**40** It could be seen that for the green light, only the blood capillary shows an intensity attenuation. This meant that it was the only substance tested out of the three that absorbed part of the incident light at that wavelength. While, for the IR, both blood and water capillaries described light absorption with different intensities.

Taking as reference literature absorption coefficients for blood and water (such as the one in **Fig.21**) and thus, the hypothesis for light absorption explained in **Section 3.2.2**, blood should not absorb as much light as water for wavelengths over 900nm. However, when illuminating blood vessels in a real human body using that spectral range, they are clearly seen. (Examples are shown in following **section, 4.2**). Therefore, the analysis of light propagation with the phantom was useful to understand that phenomenon and to test the reliability of the chromophore's maps concentrations.

a) **b)**

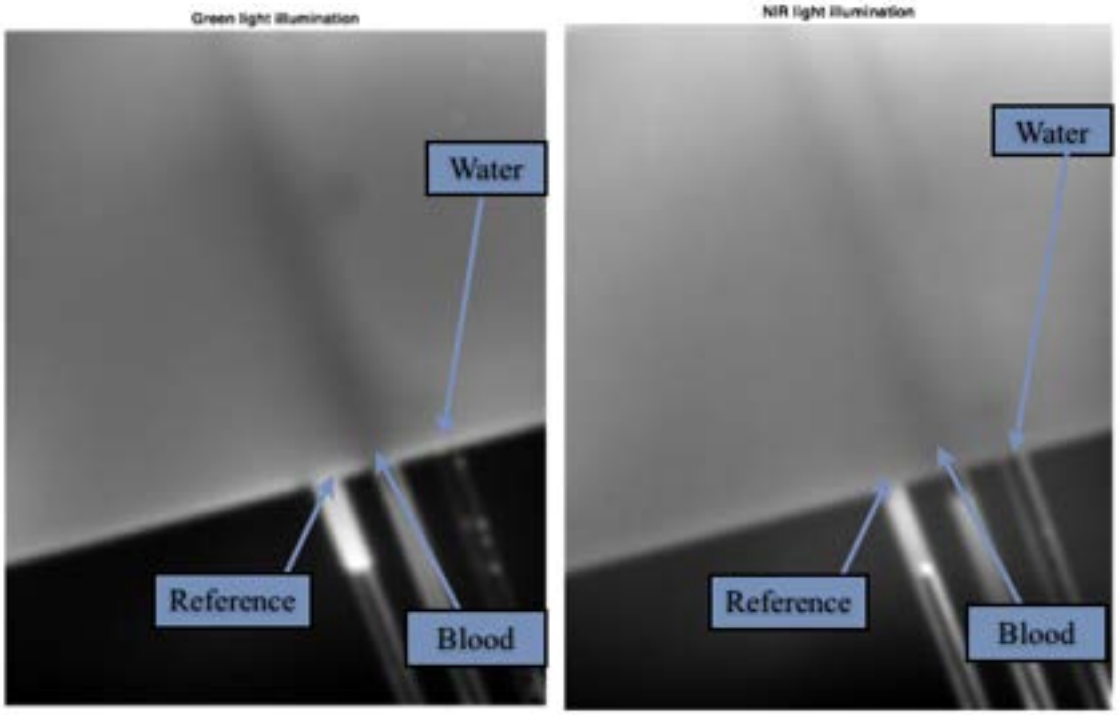

Fig.40: Phantom response to light. a) Illumination of 565nm. b) Illumination of

For the analysis, it could also be seen that, accounting for the blood filled capillary, the intensity changes related to green light absorption 'expanded' over a larger distance than the light expansion related to IR absorption. This means, the propagation of light produced locally when the light came in contact with the absorbing substance, seemed to diffuse faster when the incident light was in the IR spectrum. In order to see the intensity change differences more schematically, an intensity plot of the selected transversal section was done **(Fig.41)**. As a result, it could be determined that these differences could be explained by light diffusion propagation in an homogeneous isotropically scattering medium. Besides, the reference was a substance with the same μ'_s as the phantom's.

a) **b)**

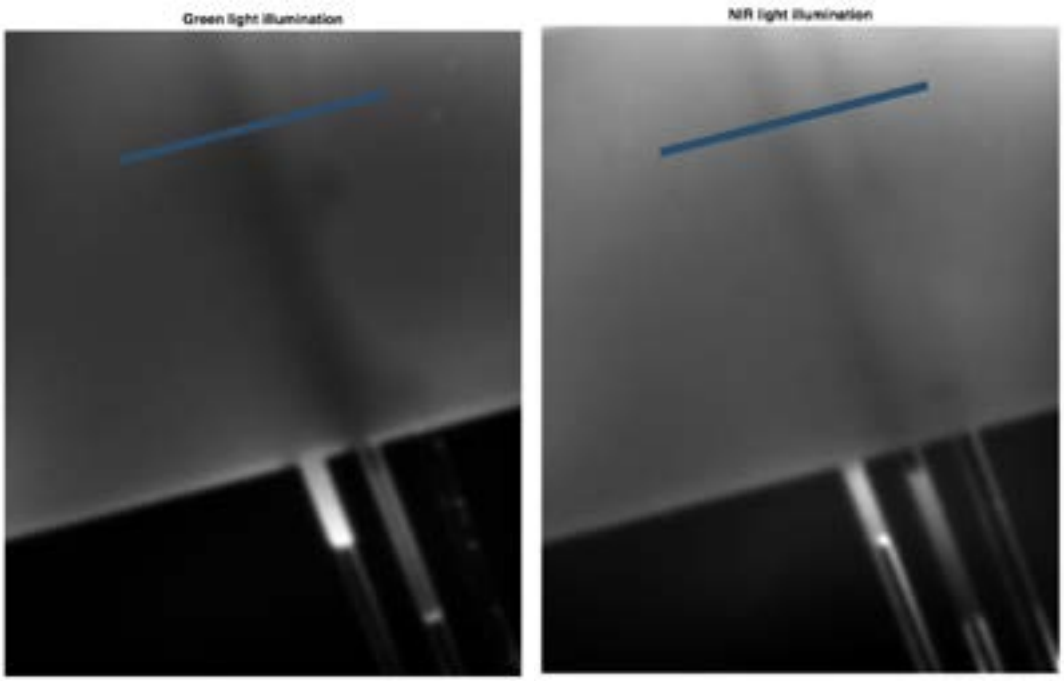

Fig.41: Transverse line for intensity profile of the phantom. a) Illumination of 565nm. b) Illumination of 940nm

The plots of the intensity profile are shown in **Fig**.**42** and **Fig**.**43**. In these figures, a Gaussian shaped light diffusion was obtained, in which the maximum peak represented the location for the absorption substance. It also explained how light propagated through the scattering medium after encountering that absorbing substance. Showing a difference in the diffusive propagation.

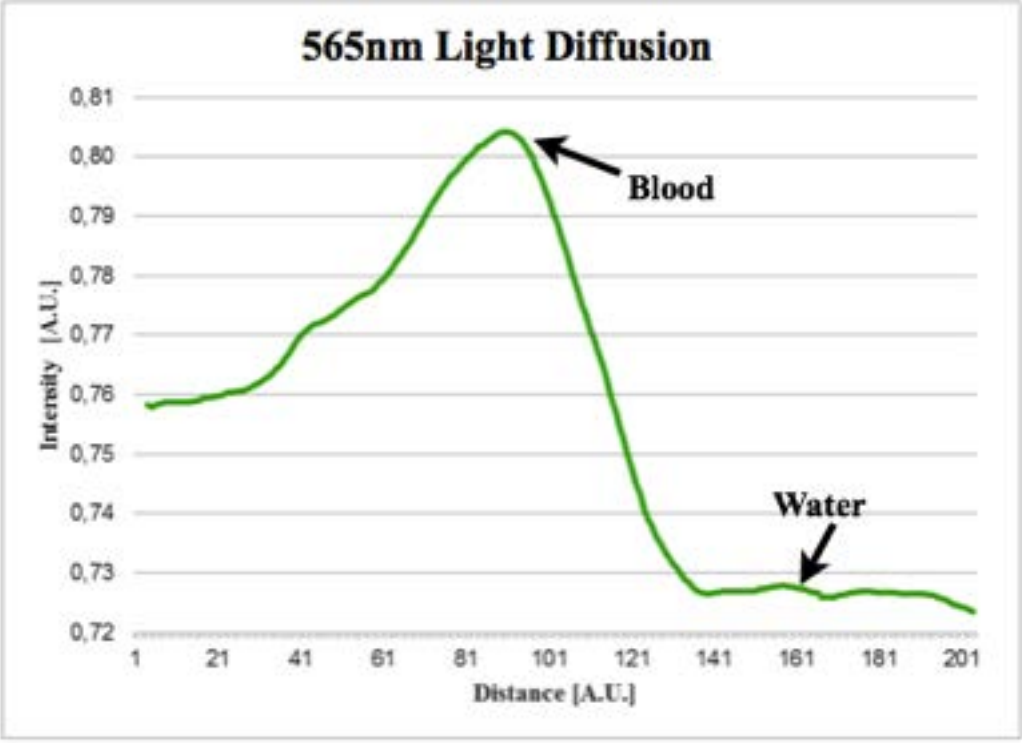

Fig.42: Transverse intensity profile for incident 565nm light.

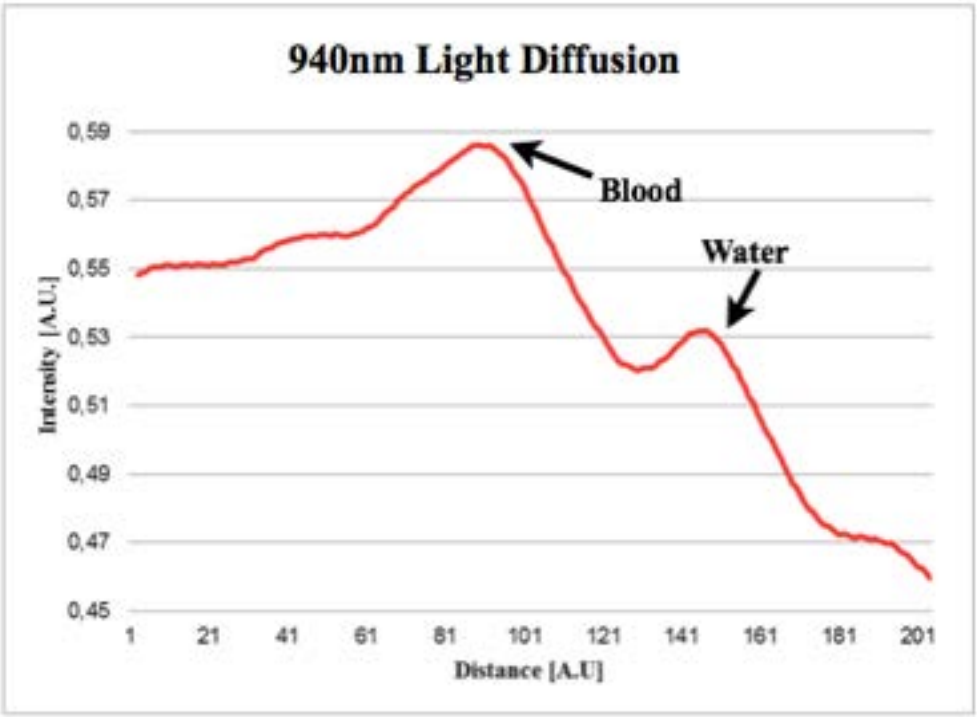

Fig.43: Transverse intensity profile for incident 565nm light.

As previously mentioned, light propagation in skin tissue was described by the diffusion theory, following Fick's law. Applying the explanations and demonstrations of **Section**

2.2.3, the value for the diffusivity constant dependent on the scattering coefficient was obtained; $D = \frac{1}{(3\mu s\,(1\text{-}g))}\,[cm]$, which is equivalent to $D = \frac{1}{3\mu'_s + \mu_a}$. [17]

For mediums in which the scattering coefficient of the volume surrounding the absorption substance was characterized as: $\mu_a << 3\mu_s'$, the effect of the absorption could be neglected, resulting in a diffusivity constant described by; $D = \frac{1}{3\mu'_s}$. Consequently, the diffusivity constant was inversely proportional to the reduced scattering coefficient, which in turn, determined diffusion by **Eq. 2.7**.

Considering the μ'_s values of intralipid over the whole spectrum, the ones related to 565nm and to 940 nm are obtained (**Fig.44**)

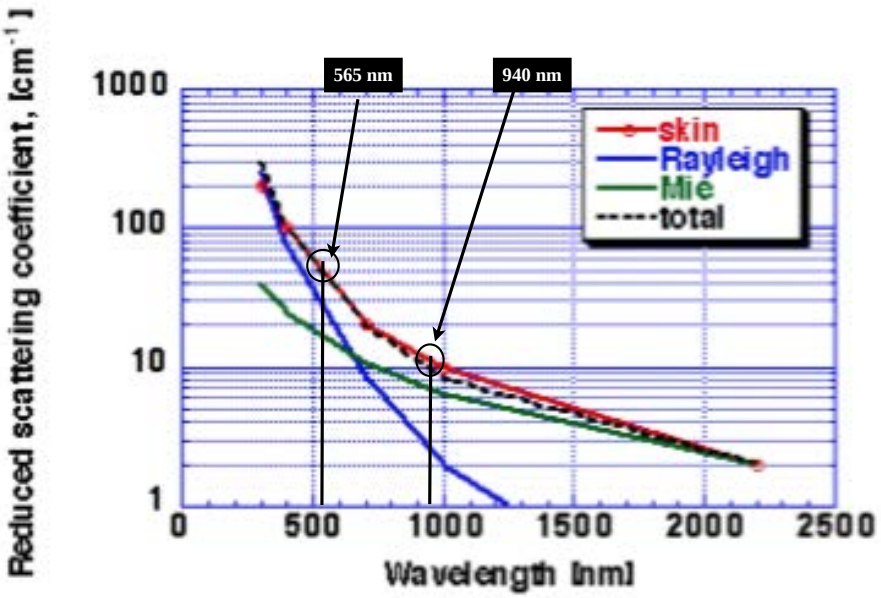

Fig.44: Reduced scattering coefficient of intralipids, pointing the μ'_s for 565 and 940 nm . Graph extracted from [19]

Given the relation, $\mu'_s(565) > \mu'_s(940)$, then D(565) < D(940). This meant that IR light diffused more than green light in the intralipid medium. This light propagation shape determined a stronger reflectance change for the IR light, even if the absorption coefficient for that wavelength spectra was not that high. As a consequence, absorption contrast would be lost within deep penetration, while scattering contrast would be maintained. In addition, as whole blood is composed of plasma, the absorbance

mechanisms due to water content would also affect the obtained reflectance change. Because of the low volume fraction of blood within tissues, light-tissue interactions are governed by local absorption. Besides, average absorption properties are ruled by global absorption. [14]

Calculating the scattering and absorption coefficient with the equations given in **Section 3.2.2.2**, and the assumptions made, the values for the coefficients are obtained. These are in concordance to the previous explanation; higher μ'_s and higher μ_a for the green light.

Theoretical skin optical parameters		
Wavelength (λ)	Absorption Coefficient **(μ_a)** [cm^{-1}]	Reduced Scattering Coefficient **($\mu s'$)** [cm^{-1}]
λ = 565 nm	73.97	41.74
λ = 940 nm	9.18	9.5

Table 3.: Table for the theoretical skin optical parameters for 565nm and 940 nm

4.2. Allergy diagnosis

Taking into account the hypothesis established and the results obtained from the light propagation experiment, the expected results for the tests on human arms where:

- 565nm light absorption for erythema; meaning darker intensities for the reflected light when erythema was encountered.
- 940 nm light absorption for edema; meaning darker intensities for the reflected light when edema was encountered.

The obtained results and the consequently discussions are shown in the section.

4.2.1. In-depth diagnosis

A representation of the diagnostic procedure and results obtained for Volunteer 4 is shown in this section.

First of all, after preprocessing and calibration correction for the images, the baseline image (taken right after allergen's injection) was used as reference for measuring the intensity changes produced by the allergic reactions. This baseline image was taken before any reaction occurred beneath the skin due to the injected substances. (**Fig**.**42**) The visual difference in reflectance representing the punctured areas could be seen, mostly for the visual light range.

a) b)

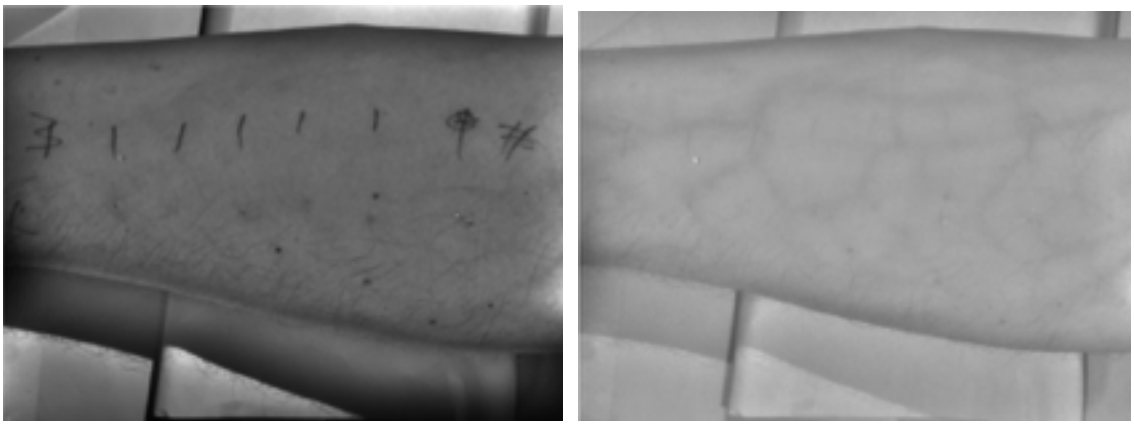

Fig.42: Images from the arm of volunteer 4, Basal (right after injection). a) 565 nm illumination. b) 940 nm

a) b)

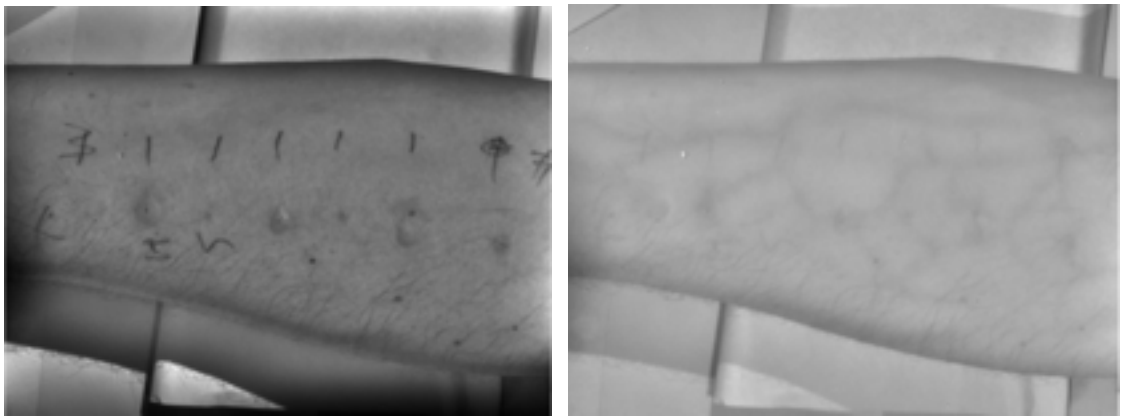

Fig.43: Images from the Volunteer 4's arm, SPTs done. a) 565 nm illumination. b) 940 nm

Additionally, for wavelengths above 600 nm (in this case for the 940 nm), the image looked brighter than the green illuminated one. This was because melanin and the two types of hemoglobin do not absorb strongly in that spectral region, thus, light penetrated deeper in the tissue without being attenuated. This obtained result was in concordance with literature [37].

Right after, ROI detection was done, as well as the region delimiting process. The results from this step is shown in **Fig.44**. For the NIR image, the regions with changes in intensity related to allergy were marked with different arrows.

a)

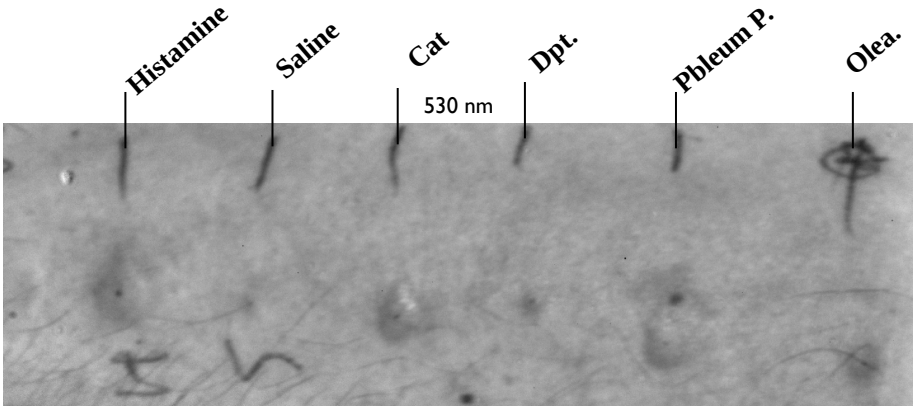

b)

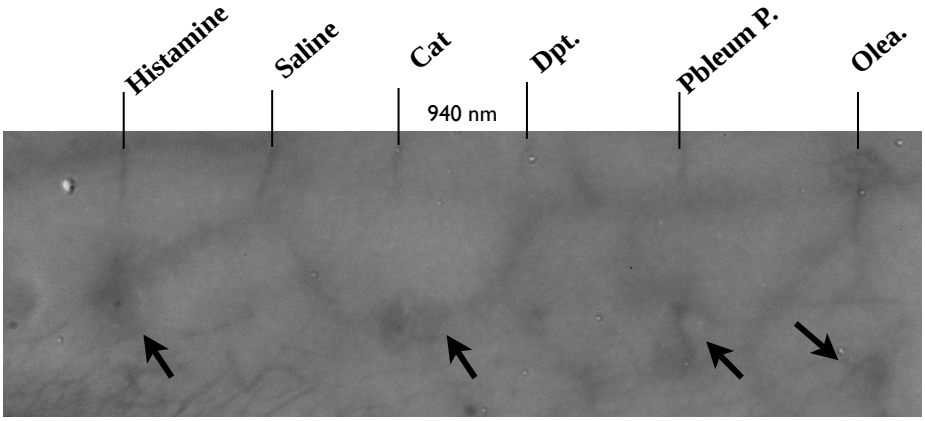

Fig.44.: Substances injected in volunteer 4, Basal (right after injection). a) 565 nm illumination. b) 940 nm

The expected results for the green-illuminated arm were images in which the affected areas where an increase of blood took place, had to be darker in terms of intensity in comparison to the surrounding non-affected regions. This change in intensity corresponded to erythema, due to the physiological changes explained before; as seen in **Section 2.2.1**., the release of mediators such as histamine and prostaglandins caused the relax of the smooth muscles forming the blood vessels and arterioles of the sub papillary plexus. This vasodilation resulted in an increase of blood volume in the affected area, which absorbed more green light than the non-affected regions. This was

due to hemoglobin concentration increase. This could visually be detected in **Fig. a)**., where histamine, cat, Pbleum P. and olea were darker than their surroundings, as the reflected light was less intense in that area due to the light absorption that took place.

The locations where the punctures took place could also be detected, due to the small injuries done to the skin. The absorbance related to skin injuries in the saline solution area were taken as the reference for determining the reactivity of the rest of the areas (negative control).

Concerning **Fig.44)**., under the incident light of 940nm, the superficial capillaries detected in the previous image were practically invisible in this spectral range. This occurred because of the deeper penetration of IR light within skin, it did not get much attenuated from the sub papillary plexus. On the other hand, deep large vessels' detection was visually enhanced. This was due to the high concentrations of hemoglobin and blood in local areas. In addition, an accumulation of water could also be seen in the affected areas (marked with arrows in the image **Fig. 44)**). Therefore, large blood vessels and edema were seen black due to am attenuation of the reflected light.

The described characteristics were used for the allergic reactions detection and further diagnosis. For this, changes in absorbance and reflectance were taken into account.

Following with the diagnosis characteristics; once the regions were delimited and extracted, the absorbance map for each of them was calculated. This map was done by calculating the absorbance at each of the image pixels in relation to the baseline image (baseline subtraction). An example of this absorbance map is shown in **Fig.45**, in which the different chromophores present showed the (approximate) expected results for intensity differences between tested allergens.

- Erythema → Under green light detection.

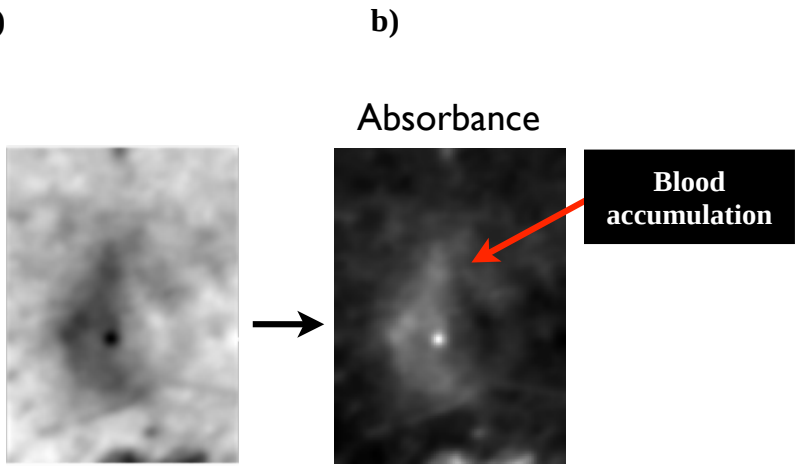

Fig..45: Histamine area of volunteer 4. under green illumination. a)Reflectance image. b)Absorbance image

In **Fig.46** the intensity related to the absorbance of superficial blood is shown. The intensity was higher for the sites where more light was absorbed. This could be interpreted as a map of the hemoglobin concentration.

- Wheal → Under IR light detection.

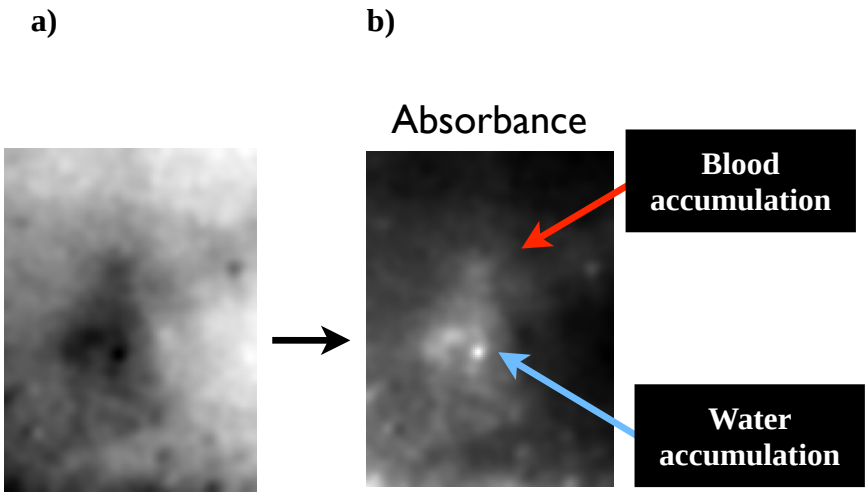

Fig.46.: Histamine area of volunteer 4. under IR illumination. a)Reflectance image. b)Absorbance image

In **Fig.46** the intensity related to the absorbance of water accumulation is shown. The intensity was higher for the sites where more light was absorbed, this was due to the absorption of energy by the increased concentrations of extracellular fluid in those edematous areas. As a result, this could be interpreted as a map of the water concentration.

In addition, a dimmer intensity could be found where blood flow was increased (containing lower concentrations of water). Consequently, for the analysis, the diameter that was taken into account for giving a diagnostic result was the water concentration map. In addition, the erythema area was used to make sure that the detected wheal was within the area of red skin. For this analysis, texture detection, Otsu segmentation and Watershed procedure were used to quantify the areas. The whole process was explained in **Section 3.4**.

Based on these results, the diagnosis for the whole ROI of volunteer 4 was done. The separated results are displayed on **Fig 47-50**. The segmentation showed are based on texture classification. However, for the whole diagnosis, the different methods are taken into account.

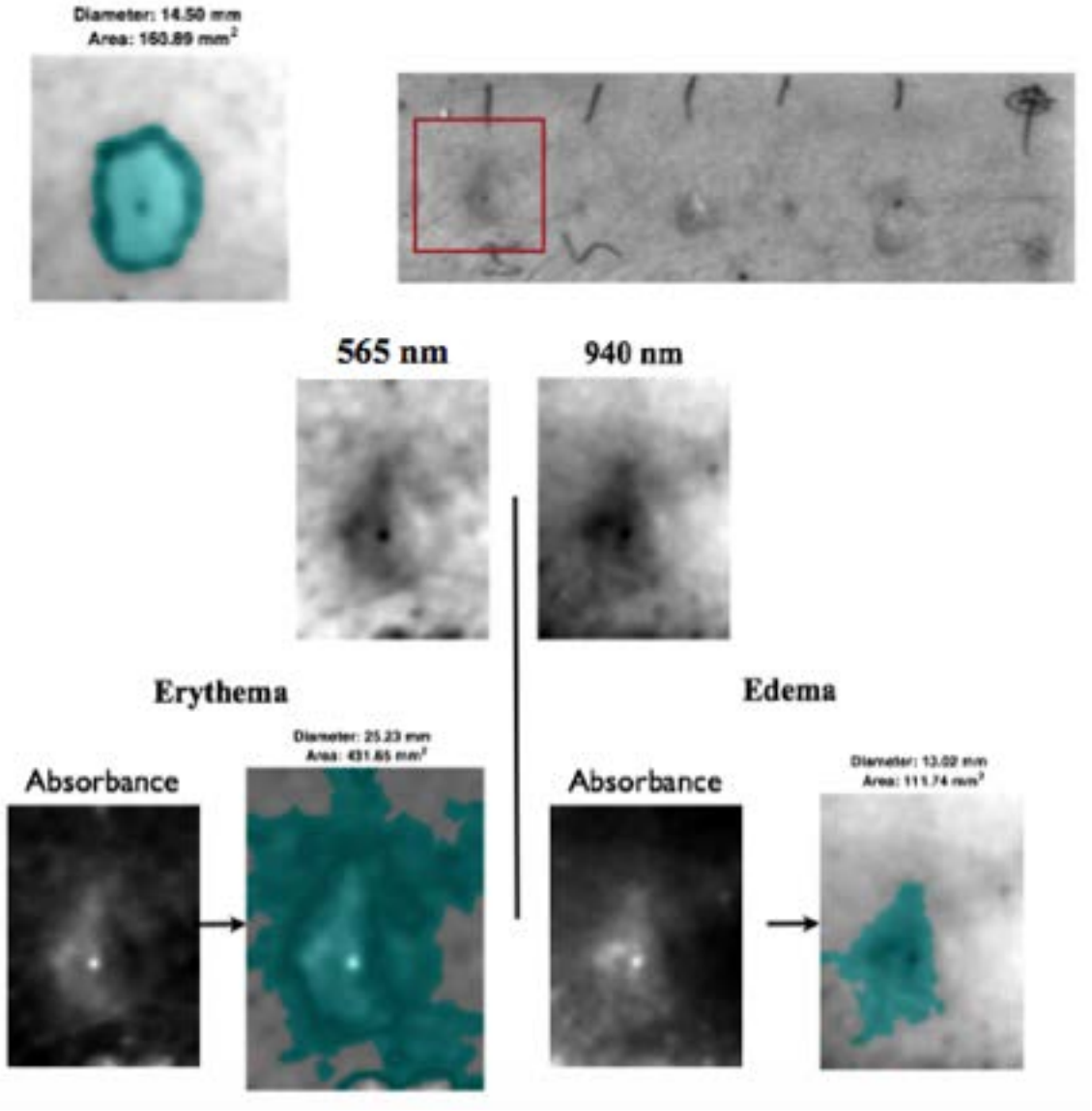

Fig 47: Histamine area of volunteer 4. under NIR illumination. a)Reflectance image. b)Absorbance image

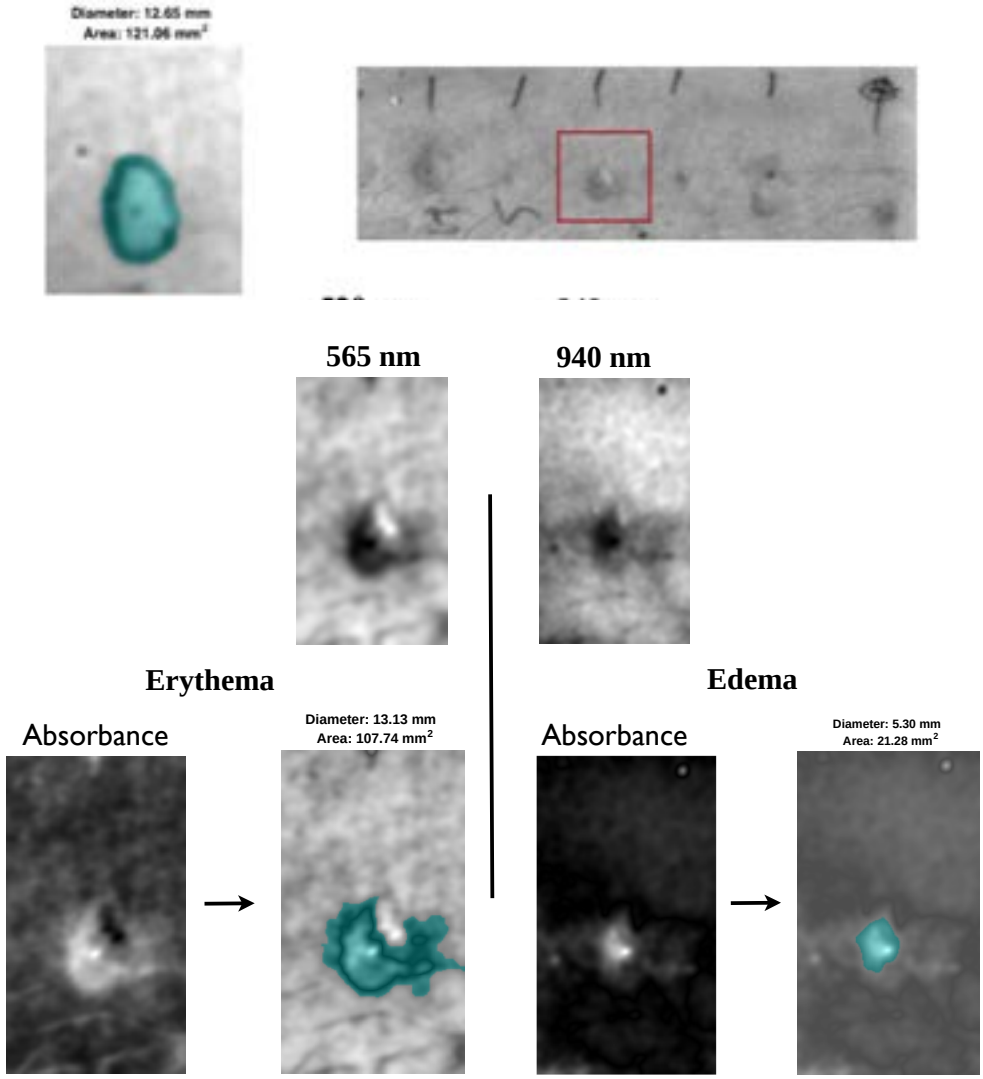

Fig 48: Analysis of Cat area of volunteer 4.

Analysis of the edema gave a different diameter and areas for the different techniques. Here, only texture detection is shown, however, the classification using the different methods was correct. The wheal was found within the erythema and had a diameter 3mm larger than the saline's one.

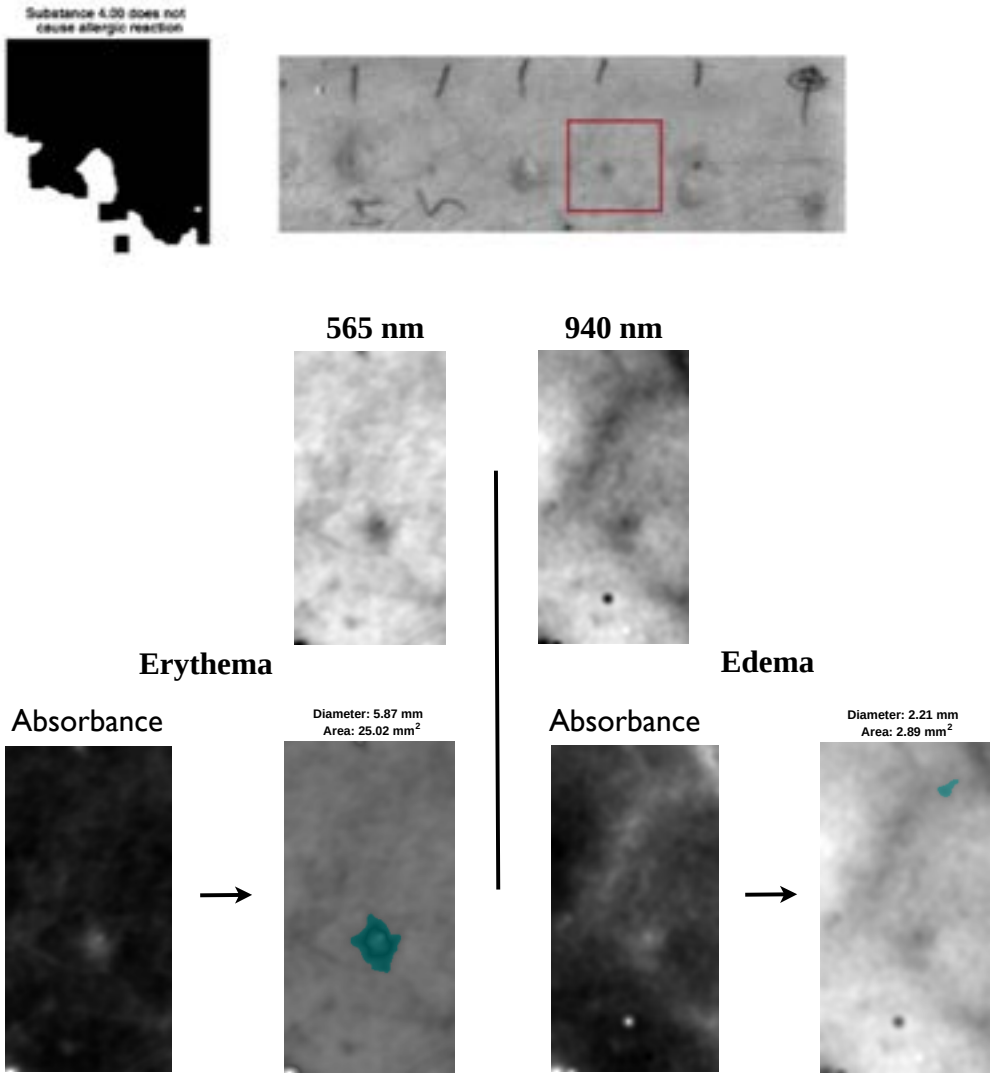

Fig 49: Analysis of Dpt. area of volunteer 4.

Even though the injection site got a small erythema, water accumulation was not enough for classifying the site as affected. However, this injection was done very close to a blood vessel, introducing unwanted signals. This fact was also a problem for volunteer 5, whose reaction sites where completely over a big large vessel.

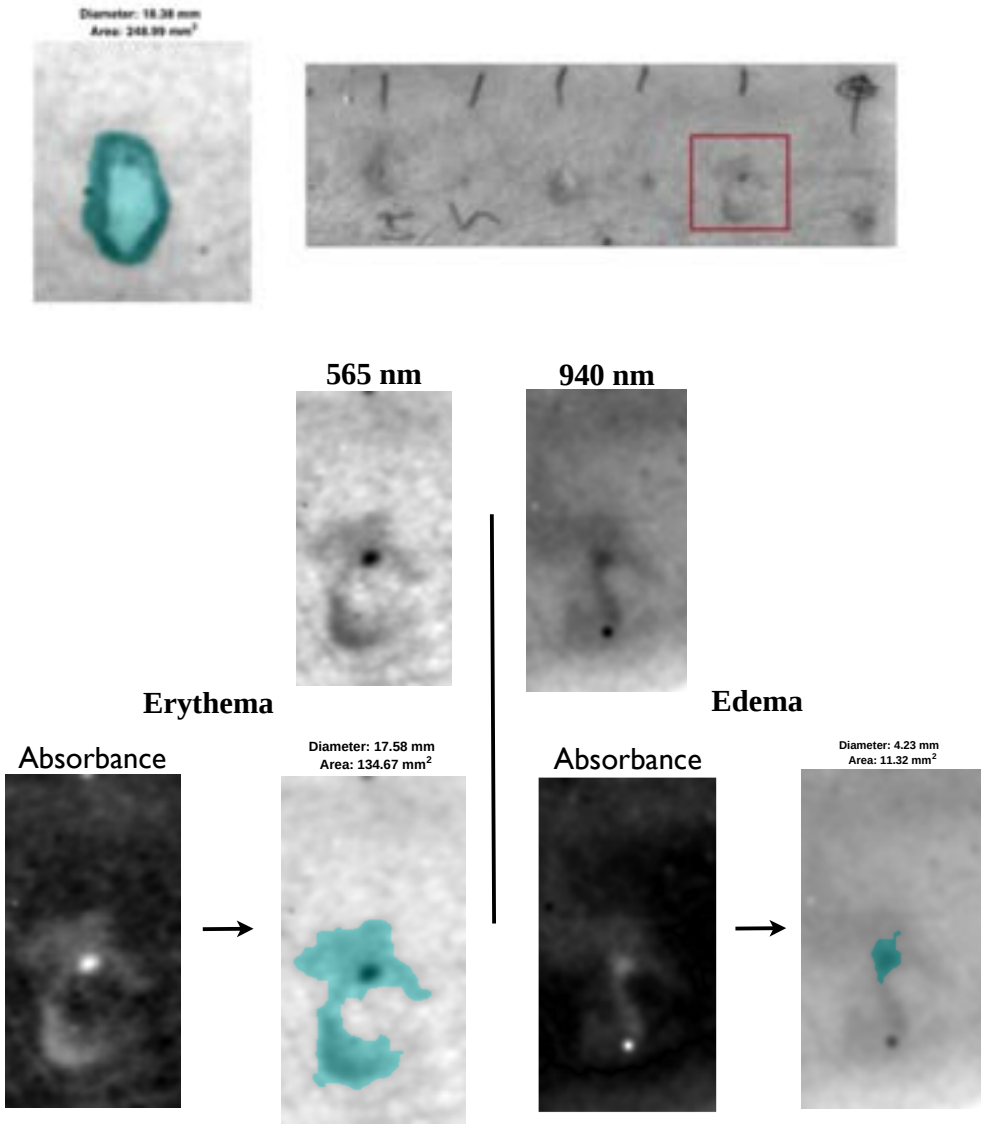

Fig 50: Analysis of Pbleum P. area of volunteer 4.

Artifacts on the skin affected the measurements. In area 5 of volunteer 4, segmentation was not done correctly. The reason for this was that there was a mole next to the injection site. The area surrounding the mole got red and inflamed, too. So the melanin found in the mole gave too much contrast of light absorbance, which in turn diminished light absorbed by water content. This gave an incorrect diagnosis measurement. On the other hand, for volunteer 4, the erythema was the same size as the wheal, for most of the cases. In this case, the erythematous area could be used for diagnosis measurements.

The comparison between the obtained results for volunteer 4 and the diagnosis performed by the doctor is shown in **Fig.51**.

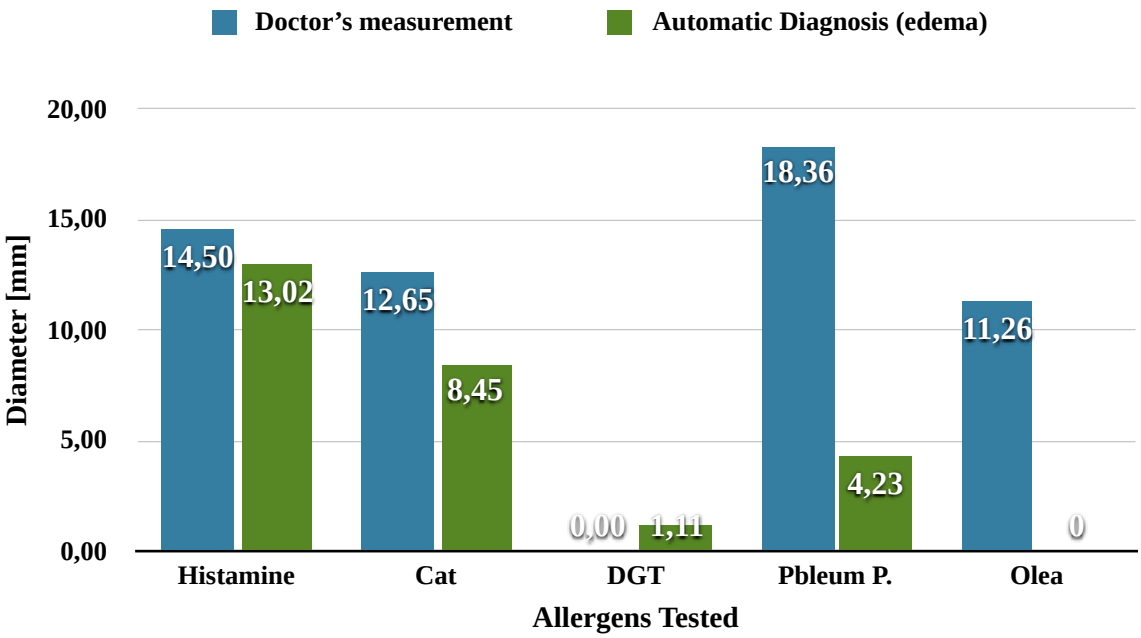

Fig 51: Comparison between doctor's measurement and automatic diagnostic performed.

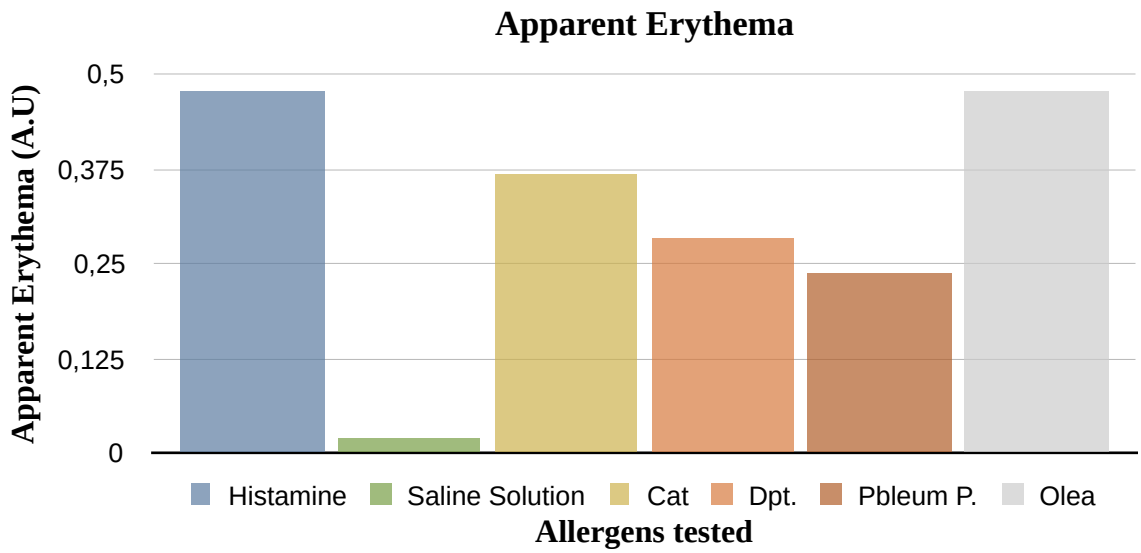

Fig 52: Apparent Erythema quantified from difference in intensity. Obtained from the hemoglobin concentration maps.

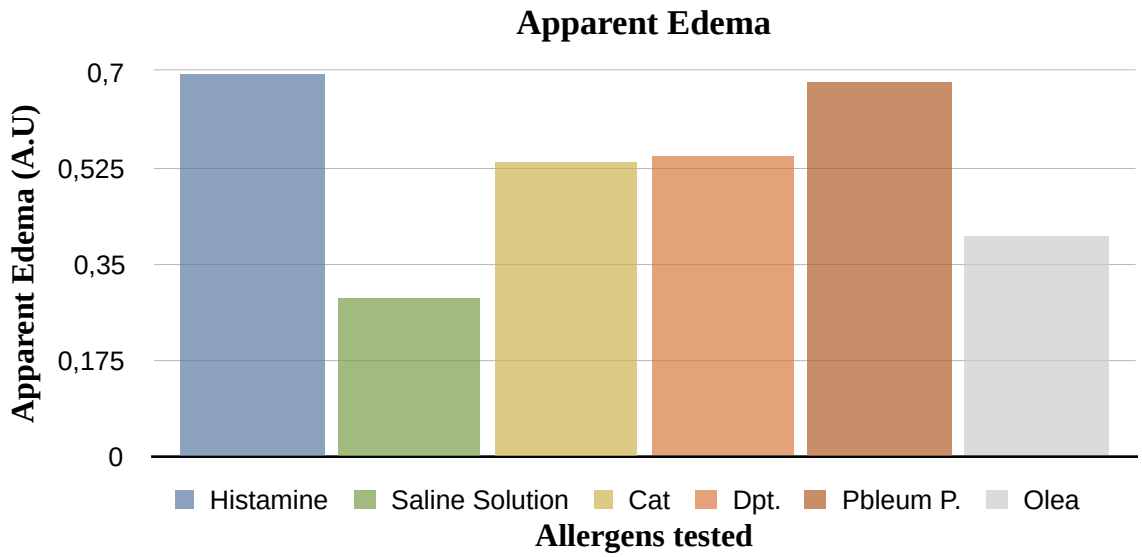

Fig 53: Apparent edema quantified from difference in intensity. Obtained from the water concentration maps.

The concentrations obtained (**Fig. 52** and **Fig. 53**) were an indication of the level of allergic reaction that took place. For the diagnosis, the level for the negative control was used as reference to determine the level of allergic reaction; fore example, histamine gave the biggest extracellular fluid concentration, very close to the Pbleum P. concentration.

Despite the applicability of this apparent edema measurement, the obtained results could be affected by blood veins. For substance 4 (Dpt), for which the volunteer 4 was not allergic, the apparent erythema obtained was higher than for Cat and Olea, which were positive results. The reason for this was the big blood vessel that crossed the averaged section, which influenced the light absorption.

In spite of the drawbacks related to artifacts, apparent erythema and edema were used to determine the allergic reactions, as a reinforcement for the area and diameter measured from the absorbance and reflectance maps.

4.2.2. RGB and Monochrome analysis comparison

Two different cameras were tested; the Retiga-2000R and the Manta G145-NIR. The first one had a much lower quantum sensitivity for the longer wavelengths (less than a 5% for the 940nm wavelength) and images with the RGB sensor were taken. On the contrary, the second one was monochrome for the whole range and had a higher sensitivity for that wavelength (around 20%). A comparison between the use of these two sensor possibilities was done, in order to see which one was the most reliable for allergy diagnosis.

For this comparison, two volunteers present at both tests were taken into account; **volunteer 1 (V1)** for first test was the same person as **volunteer 4** (**V4**) for second test; and **volunteer 3** (**V3**) for first test was the same person as **volunteer 6** (**V6**) for second test.

For the first test, independent component analysis was performed. The green illumination reflectance and absorbance was studied in the green channel, while the NIR illumination reflectance and absorbance was studied in the red channel. Results are shown for the analysis of histamine (the positive control).

a)

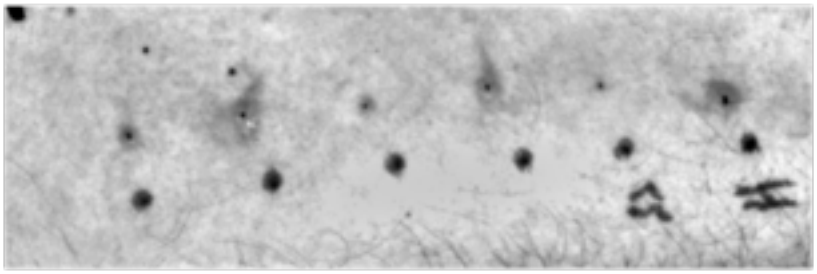

b)

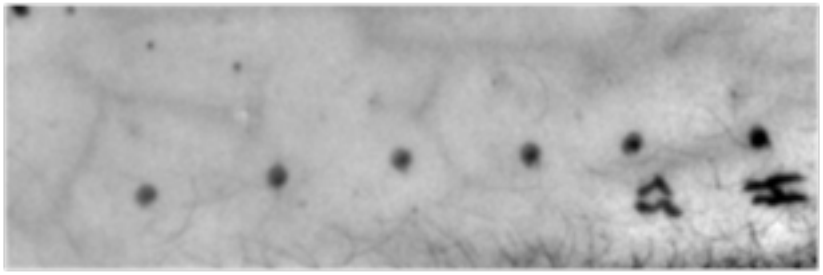

Fig 54: Volunteer 1. SPTs using the Retiga 200-R. a)Green channel for 565nm. b)Red channel for 940nm.

a)

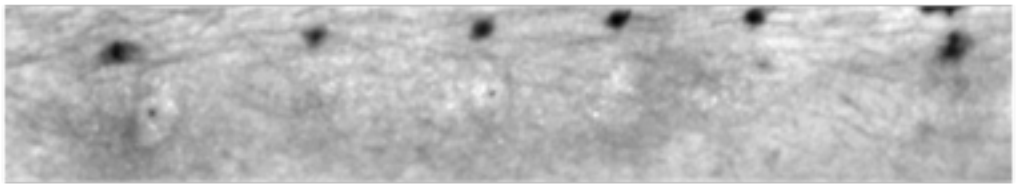

b)

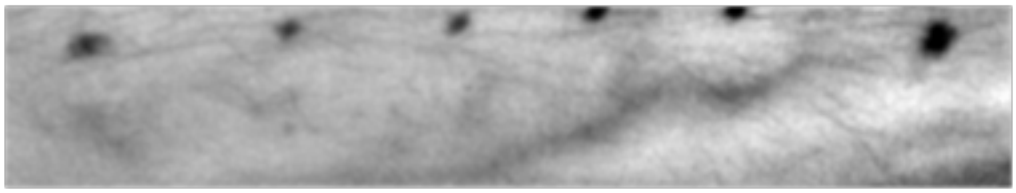

Fig 55: Volunteer 2. SPTs using the Retiga 200-R. a)Green channel for 565nm. b)Red channel for 940nm.

From **Fig .b** and **Fig .b** it could be deduced that the sensitivity for the 940 nm wavelengths was not enough to detect changes in water concentration or increased blood flow in the sub papillary plexus. However, this range of light could have other applications, both at this situation (it could be used to determine where the veins were, so as to avoid them when doing the test). These change in intensity due to veins was explained by the diffusion transport of light, as a result of a high accumulation of hemoglobin and water in blood vessels.

In relation to the diagnostic procedure, NIR images could not be used, as they were not relevant enough for determining allergic reactions. Because of this, the image processing for those images relied only on the green channel illuminated with the 565 nm light. This green light, in terms of the theoretical absorbance coefficients, was not sufficient to detect chromophores involved in the reactions, as no information for edemas was provided.

According to the diagnostic procedure, obtained images were not feasible to be correctly classified using the image processing simple and straightforward based on absorbance maps. As mentioned, one of the goals was to demonstrate than when using specific wavelengths for the illumination, the features were so highly enhanced that a simple processing was enough for the segmentation and further classification. This could not be concluded for the images acquired with the low-quantum sensitivity camera.

5. Discussions and Future Work

This project has studied the viability of making use of spectral absorbance and scattering characteristics related to the chromophores involved in allergic reaction symptoms. The use of these properties have also been used to indicate an automatic diagnosis for SPTs.

It has been demonstrated the capability of detecting blood flow increase in superficial capillaries by the use of a 565 nm light, and extracellular fluid accumulation by the use of a 940 nm one. As these parameters are the ones involved in hypersensitivity reactions induced by Ig-E antibodies, a reliable method for quantifying these symptoms has been developed.

This work could be improved and completed so as to obtain an objective and automatized diagnostic procedure for SPTs at the hospital. Even though the obtained results have not simulated completely the manual diagnosis; a method based on standardized measurements could be completely implemented.

In order to improve and fulfill the initial objectives, future work should improve several points.

Regarding the image processing;

- A pre-visualization of large blood vessels could be included, so as to avoid performing the test over those areas that can introduce unwanted noises.
- An improvement of the preprocessing techniques should be achieved; for getting rid of moles, hair, skin injuries, etc.
- An automatic ‘H’ and ’S’ detection should be implemented.

- A deeper study in image processing for classification would be useful to improve the diagnosis.

Regarding the applicability;

- Testing the system with people of different skin color, specially studying black people, would be needed to confirm the advantages of the system.
- A consequence of digitalization of the diagnosis would mean a digital storage for the results, so data base for allergy results would be useful in the future.

Regarding the photographic setup;

- The use of a laser pattern exposed over the arm could be used, determining a more standardized and controlled region of interest.

In conclusion, even though the results of the automated diagnosis for some of the reaction areas have not been valid, it could be said that the objectives of the study have been completed. These included: the study of light propagation within skin; the proof that chromophores‘ concentrations could be detected and quantified using two specific wavelengths; classification of allergic reactions based on the chromophores detected; the initial automation diagnosis using a simple image processing; and the implementation of a device to be used with these purposes.

6. Costs

Budget of the project				
1.-Author				
Irene Cumplido Mayoral				
2.- Department				
Biomedical Imaging and Instrumentation Group				
3.- Project Description				
-Title	Image based system for the qualification of skin erythema			
- Duration (months)	6			
4.- Project budget (€)				
46565				
5.- Budget breakdown				
Human Resources				

Category	Human-hou	Cost hour		Cost (€)
Project coordinator	150	35		5250
Technical engineer 1	480	20		9600
Biomedical Engineer	960	25		24000
			Total	33600

Materials				
Description	Supplier	Units	Unit price (€)	Cost (€)
Ilumination set up				
IR (940 nm) LED on Metal-Core PCB, 1000 mA, 800 mW (Min)	Thor Labs	2	51,03	102,06
Green (530 nm) LED on Metal-Core PCB, 1000 mA, 350 mW (Min)	Thor Labs	2	60,3	120,6
Post-Mountable Cage Plate with Ø1.0" Double Bore, M4 Tap	Thor Labs	4	15,08	60,32
SM1 Lens Tube, 1.00" Thread Depth, One Retaining Ring Included	Thor Labs	4	12,83	51,32
C-Mount (1.00"-32) Coupler, Internal Threads	Thor Labs	4	8,55	34,2
Capturing system				
Manta G145B Nir	Allied visio	1	2050	2050
Nikon AFS DX 16-85 mm	Nikon	1	699,95	699,95
Electronics				0
Driver RECOM RCD 24	RECOM	2	8,56	17,12
Arduino UNO	Arduino	1	15,16	15,16
Supply source	RS	1	9,99	9,99
Protoboard	Wisher	1	5	5
Other		1	11,95	11,95

Chasis				
Chasis		1	700	700
Experimental materials				
Phantom		1	10	10
Capilaris		3	0,15	0,45
			Total	3888,12

Other direct costs

Description	Company			Cost (€)
Internet	Telefónica			640
Personal computer (20% depreciation)	Apple			259,8
Matlab 2015 (academic use)	Matlab			500
Windows 7	Windows			99,95
Office 2013	Windows			79,99
			Total	1579,74

6.- General cost and industrial benefit

Description				Cost (€)
General cost (16%)				622
Industrial benefit (6%)				233
			Total	855

7.- Summary of costs

Description	Budget on total costs (€)
Personnel	33600
Materials	3888
Functioning costs	1580
Indirect costs	7498
Total without IVA	36787
IVA 21%	9779
Estimated total	46565

7. Appendices

7.1. Prototype Structure CAD

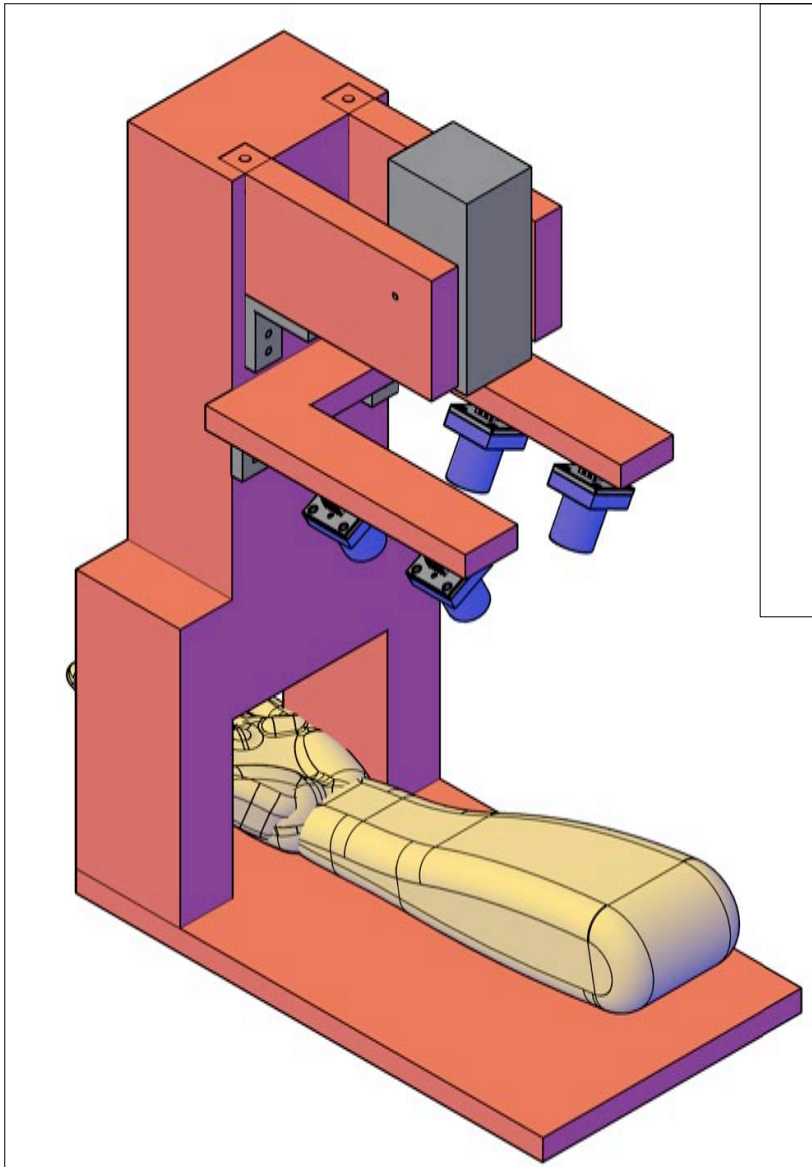

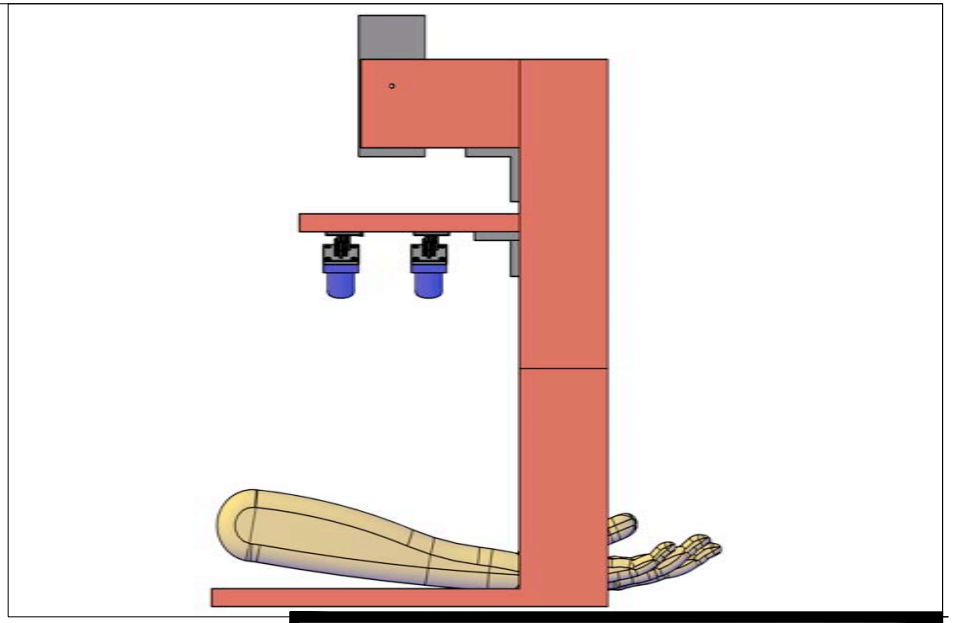

Project: Image Based System for the qualification of skin erythema

PLANE: Isometric view of the photographic setup

AUTHOR: Irene Cumplido Mayoral

.	**DATE:** 18/05/2016	**N°** 1/9

Comments: General view of the photographic setup

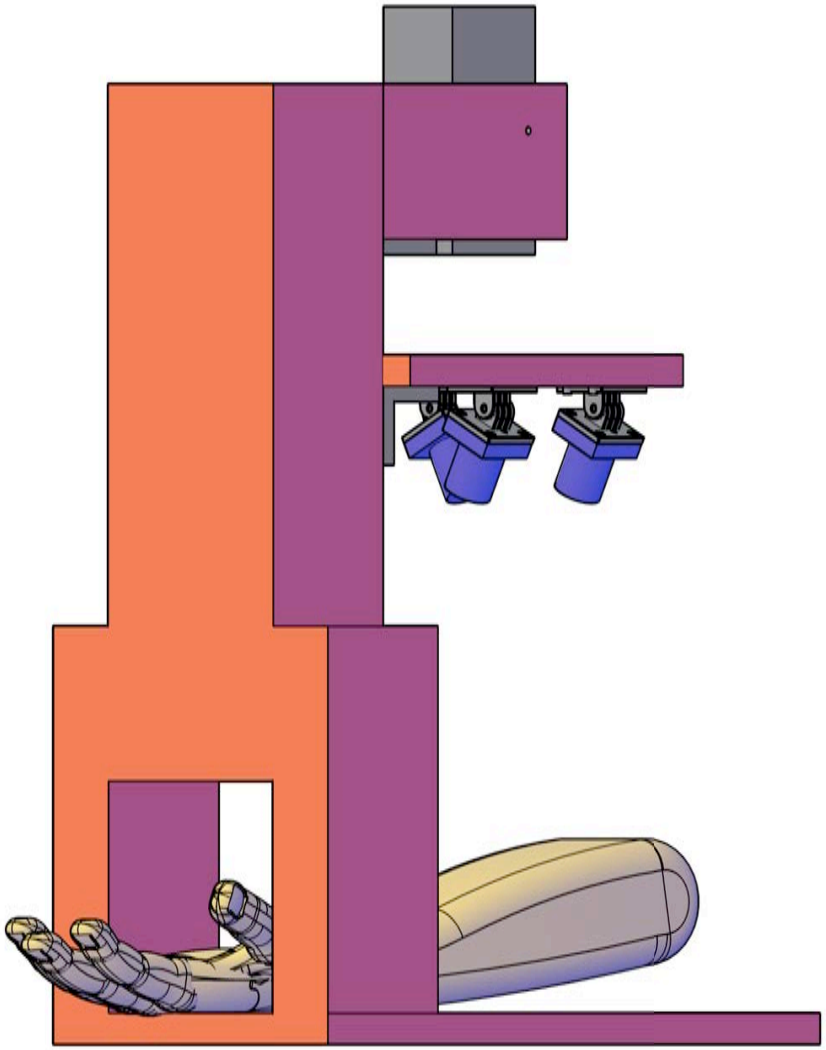

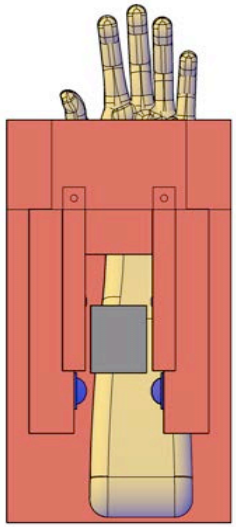

Project: Image Based System for the qualification of skin erythema

PLANE: Isometric view of the photographic setup

AUTHOR: Irene Cumplido Mayoral

DATE: 18/05/2016

N° 1/9

Comments: General view of the photographic setup

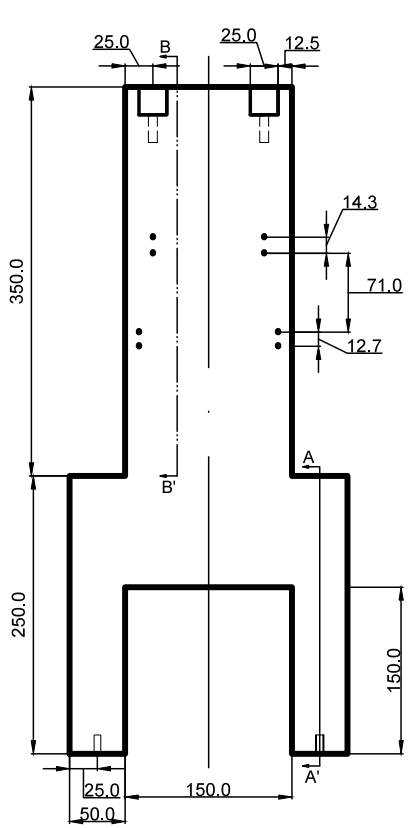

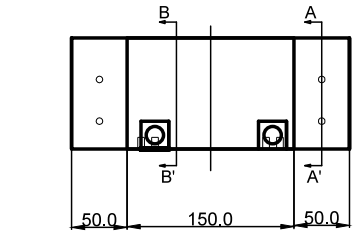

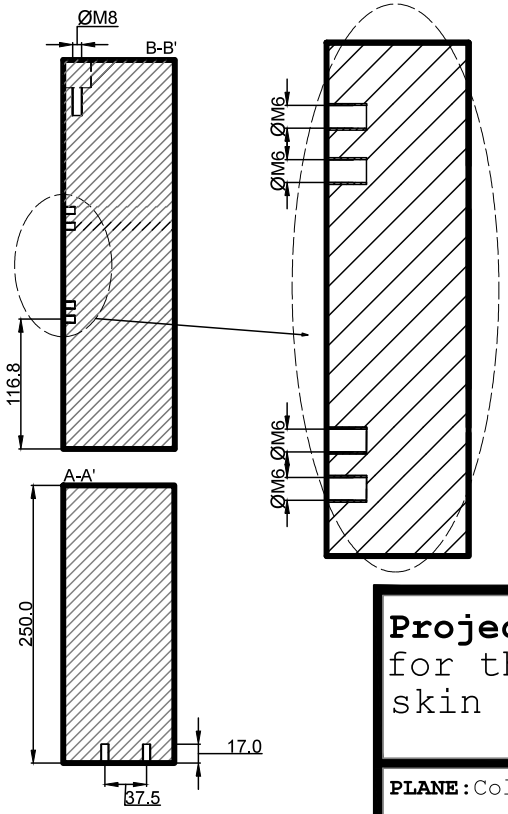

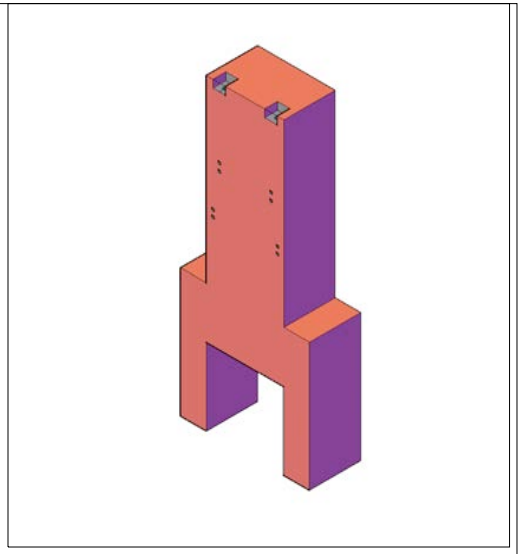

Project: Image Based System for the qualification of skin erythema

PLANE: Column (views)

AUTHOR: Irene Cumplido Mayoral

Dimensions in mm.	**DATE:** 18/05/2016	**N°** 3/9

Comments: Part 1. from the entire photographic setup:

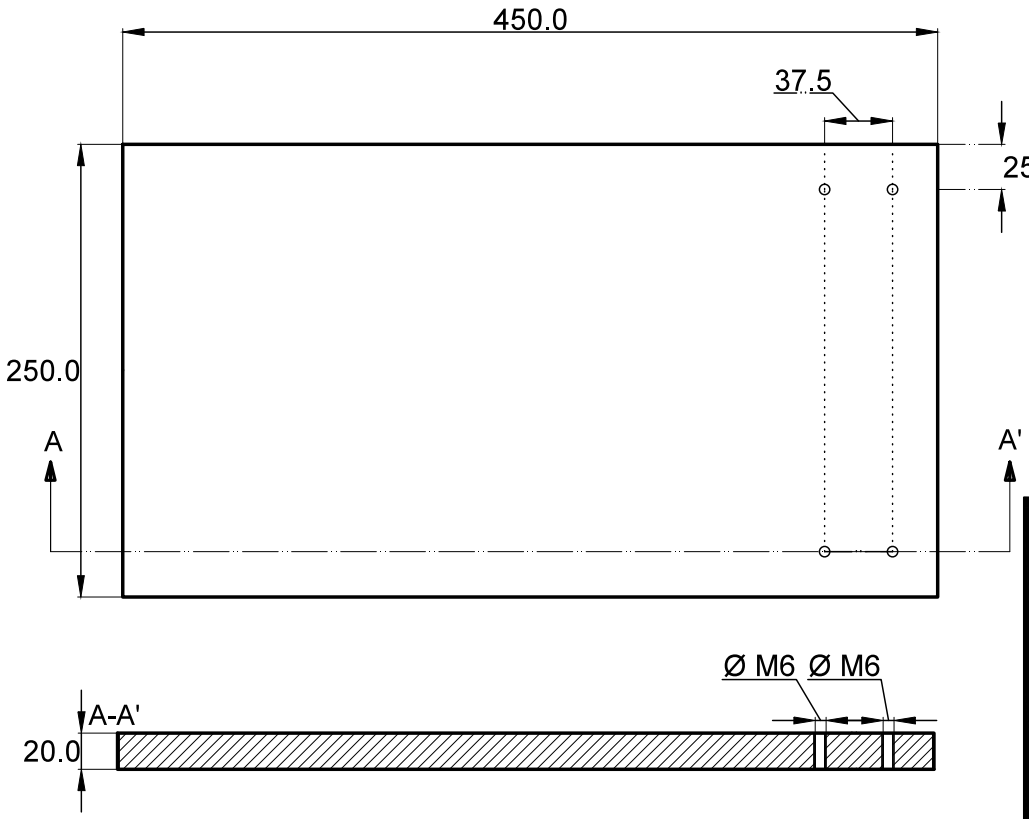

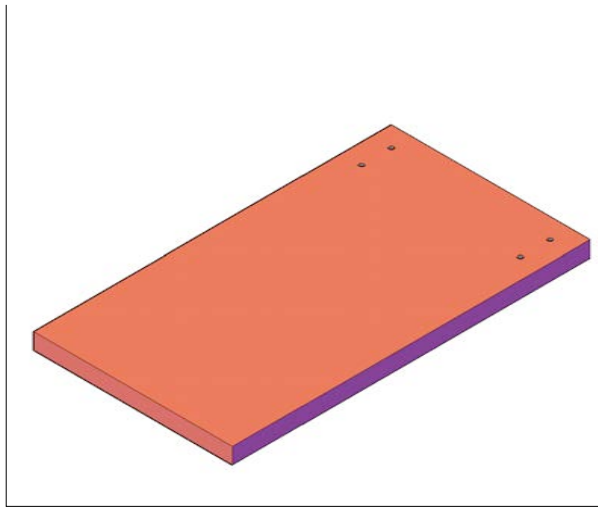

Project: Image Based System for the qualification of skin erythema		
PLANE: Base of the system (views)		
AUTHOR: Irene Cumplido Mayoral		
Dimensions in mm.	**DATE:** 18/05/2016	**N°** 4/9
Comments: Part 2. from the entire photographic setup:		

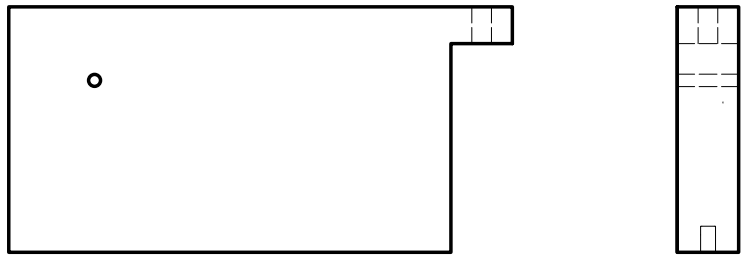

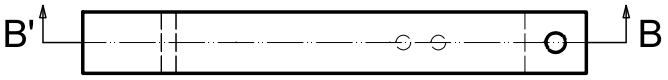

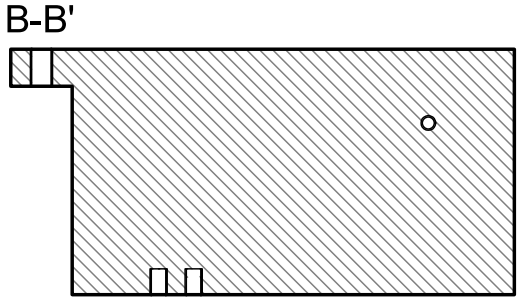

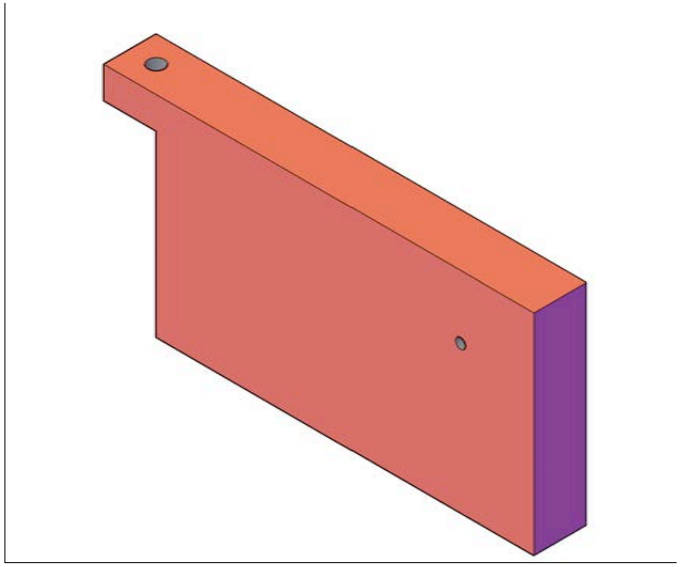

Project: Image Based System for the qualification of skin erythema		
PLANE: Camera Holder (views)		
AUTHOR: Irene Cumplido Mayoral		
Dimensions in mm.	**DATE:** 18/05/2016	**N°** 5/9
Comments: Part 3. from the entire photographic setup:		

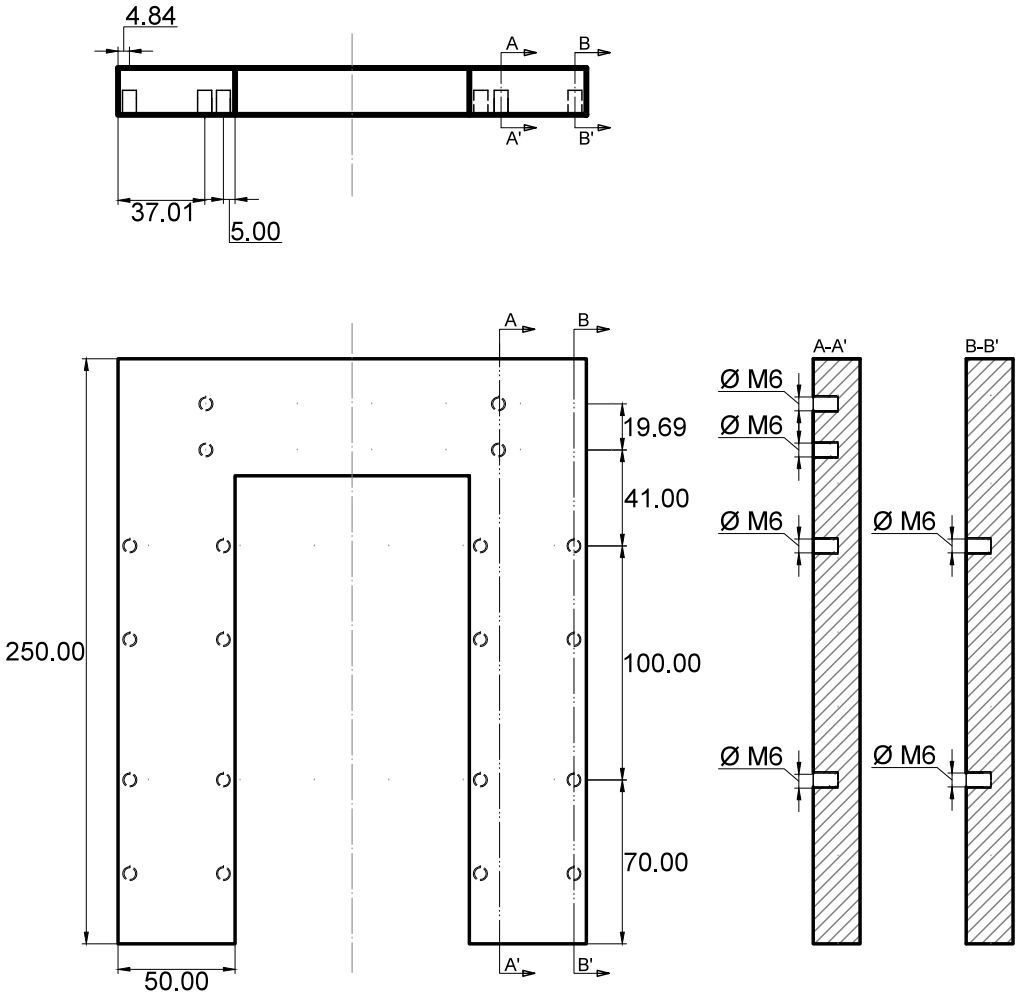

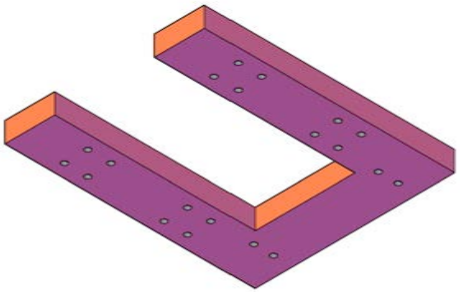

Project: Image Based System for the qualification of skin erythema		
PLANE: Strcuture for holding LEDs (views)		
AUTHOR: Irene Cumplido Mayoral		
Dimensions in mm.	**DATE:** 18/05/2016	**N°** 6/9
Comments: Part 4. from the entire photographic setup:		

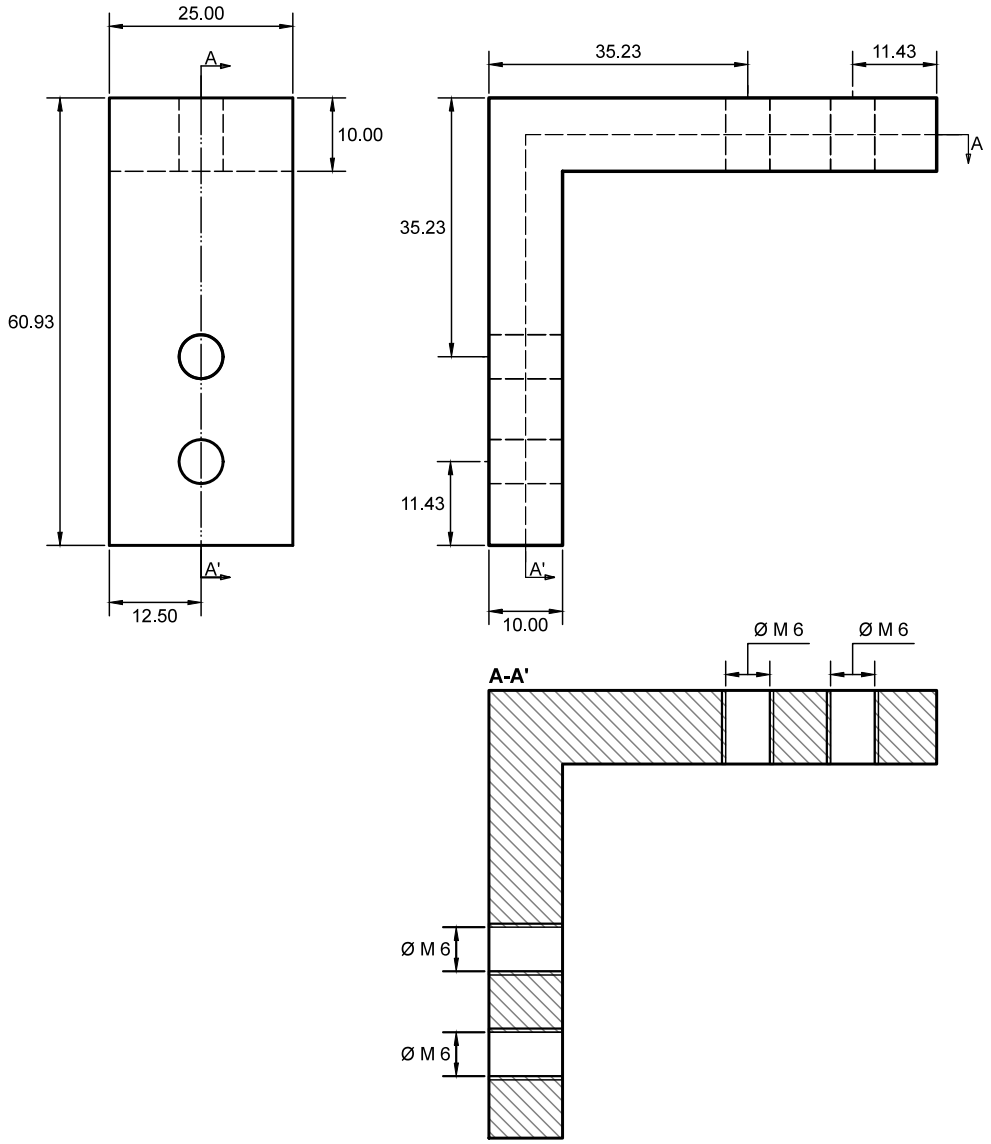

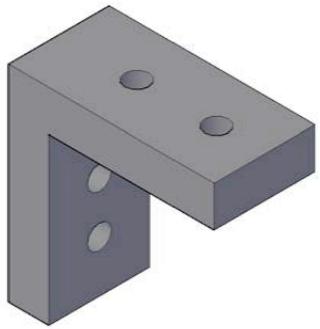

Project: Image Based System for the qualification of skin erythema

PLANE: Strcuture for holding the bases to the column (views)

AUTHOR: Irene Cumplido Mayoral

Dimensions in mm.	**DATE:** 18/05/2016	**N°** 7/9

Comments: Part 5. from the entire photographic setup:

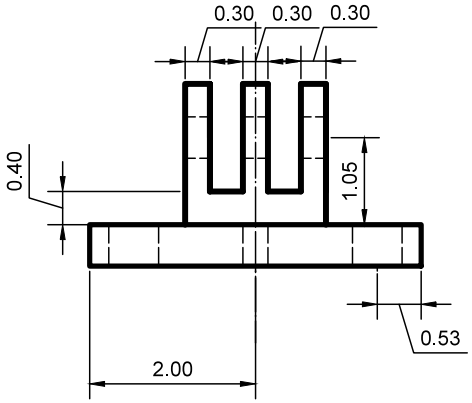

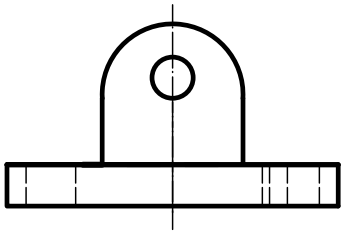

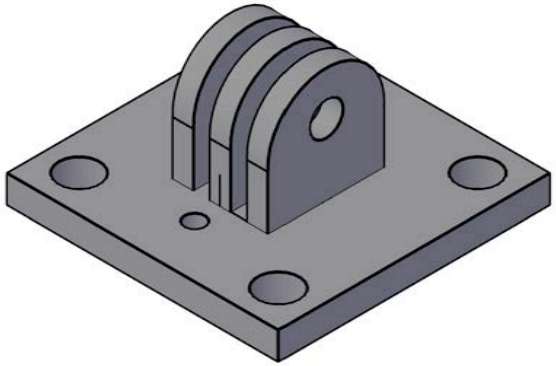

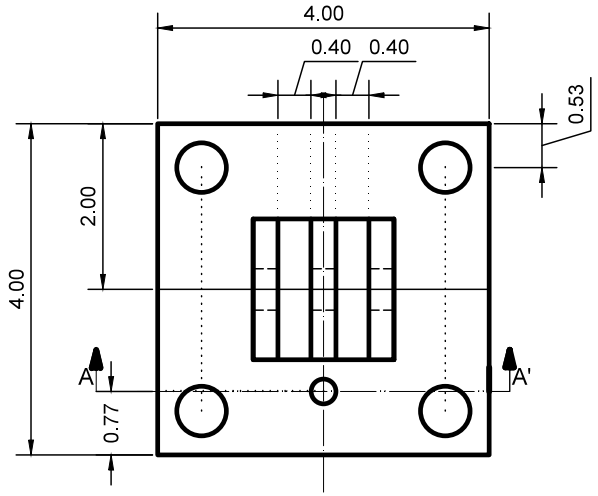

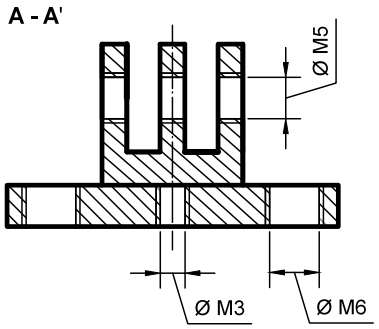

Project: Image Based System for the qualification of skin erythema

PLANE: Strcuture for mounting LEDs on the base(views)

AUTHOR: Irene Cumplido Mayoral

Dimensions in mm.	**DATE:** 18/05/2016	**N°** 9/9

Comments: Part 7. from the entire photographic setup:

7.2. 3D printed Pieces

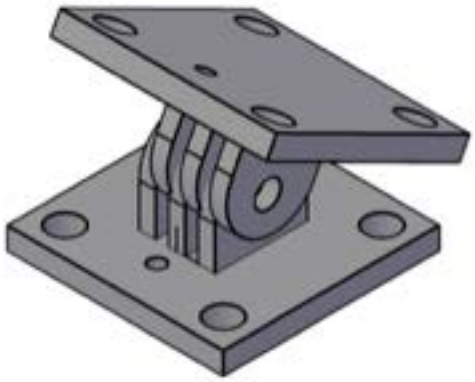

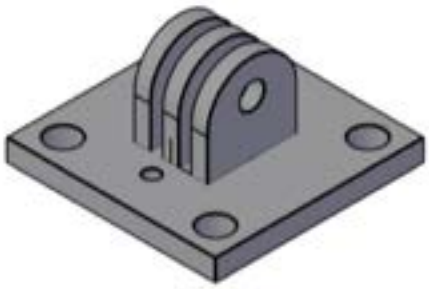

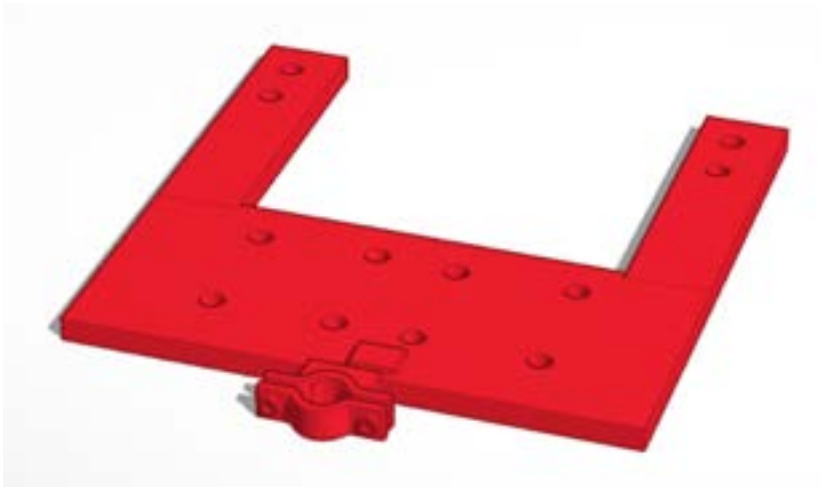

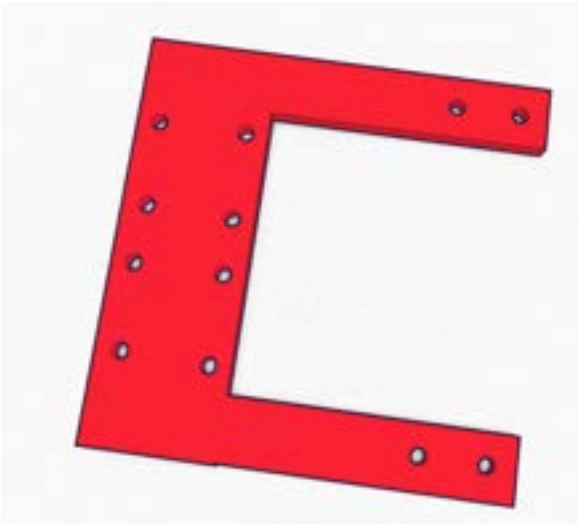

7.3. Matlab Script

Images Acquisition Function

```
function[imagesGood]=FotosFinalGigE(g)
%Cambiar properties de la Cámara
g = gigecam('169.254.73.194', 'PixelFormat', 'Mono12')
g.ExposureAutoAdjustTol = 50;
g.Gain = 7;
g.ExposureTimeAbs = 200000;

folder=input('Introduce the name of folder to save files: ')
        % If the folder doesn't exist, create it.
if ~exist(folder, 'dir')
   mkdir(folder);
end
cd='/Users/irucm/Documents/MATLAB/TFG2/';

delete(instrfind({'Port'},{'/dev/cu.usbmodem1411'}));
puerto_serial = serial('/dev/cu.usbmodem1411');
puerto_serial.BaudRate=9600;
warning('off','MATLAB:serial:fscanf:unsuccessfulRead');

fopen(puerto_serial);

    go=3;
    count=0;

    imagesGood=cell(100,1);
 for j=1:10
          for i=1:4
            if i==2
                g.ExposureAutoAdjustTol = 50;
                g.Gain = 7;
                g.ExposureTimeAbs = 200000;
            elseif i==4
                g.ExposureAutoAdjustTol = 50;
                g.Gain = 7;
                g.ExposureTimeAbs = 300000;
            end;

                in=int2str(i);
        fwrite(puerto_serial,in);
        count=count+1;
        img=snapshot(g);
        imagesGood{count,1}=img;
%         pause(1);
        end


%      end
end;
        save(fullfile(cd,folder,'RawImagesJJ.mat'),'imagesGood');
%        save(fullfile(cd,folder,'RawImages.mat'),'imagesGood');
```

```
       %[registered]=Registration(imagesGood);
       %save(cd,folder,'registration.mat','registered');
fwrite(puerto_serial,'4');

fclose(puerto_serial);
```

Calibration and Filtering

```
darkM=dark{1,1};
biasM=bias2Montura{1,1};
for i=2:16
darkM= darkM + (dark{i,1});
    if i<=10
        biasM =biasM +bias2Montura{i,1};
    end
end;

darkMean=darkM/16;
biasMean=biasM/16;

VerdeCalibrada=imagesGood{2,1};
IrCalibrada=imagesGood{4,1};

VerdeCalibradaControl = imagesGood{2,1};

% VerdeCalibradaControl=imagesGood{2,1};
VerdeBasal=imagesGood{2,1};
IrBasal=imagesGood{4,1};

for i= 5:4:16
    VerdeCalibrada=VerdeCalibrada+imagesGood{i+1,1};
    IrCalibrada= IrCalibrada+imagesGood{i+3,1};
end
    VerdeCalibrada=VerdeCalibrada/4;
    IrCalibrada = IrCalibrada/4;
    figure; imshow(VerdeCalibrada,[])
    figure; imshow(IrCalibrada,[])

    VerdeCalibradaControl=VerdeCalibradaControl - (darkMean+biasMean);

    VerdeBasalCalibrada=VerdeBasal-(darkMean+biasMean);
    IrBasalCalibrada =IrBasal -(darkMean+biasMean);

VerdeCalibrada=VerdeCalibrada - (darkMean+biasMean);
figure; imshow(VerdeCalibrada,[])

IrCalibrada=IrCalibrada - (darkMean+biasMean);
figure; imshow(IrCalibrada,[])


flatMM=flatLimpioBueno1000000{1,1} -darkMean-biasMean;
% flatMM=flatLimpioBueno{1,1} -darkMean-biasMean;
for i=2:16
    flatM=flatLimpioBueno1000000{i,1} -darkMean-biasMean;
%     flatM=flatLimpioBueno{i,1} -darkMean-biasMean;
```

```
    flatMM=flatMM+flatM;
end
flatMean=flatMM/16;

VerdeCalibradaControl=double(VerdeCalibradaControl)./double(flatMean);
VerdeCalibrada=double(VerdeCalibrada)./double(flatMean);
figure; imshow(VerdeCalibrada,[])

IrCalibrada=double(IrCalibrada)./double(flatMean);
figure; imshow(IrCalibrada,[])

IrBasalCalibrada=double(IrBasalCalibrada)./double(flatMean);
VerdeBasalCalibrada=double(VerdeBasalCalibrada)./double(flatMean);
IrBasalCalibrada2=filtering((IrBasalCalibrada),0.005,2);
figure; imshow(IrBasalCalibrada2,[])
IrBasalCalibrada3=imcrop();

VerdeBasalCalibrada2=filtering((VerdeBasalCalibrada),0.005,2);
figure; imshow(VerdeBasalCalibrada2,[])
VerdeBasalCalibrada3=imcrop();


VerdeCalibradaControl2=filtering((VerdeCalibradaControl),0.01,2);
VerdeCalibradaControl4=VerdeCalibradaControl2(ROIbuena{1,1},ROIbuena{2
,1});
figure; imshow(VerdeCalibradaControl4,[])
VerdeCalibradaControl3=imcrop();
VerdeCalibradaControl22=im2bw(imadjust(VerdeCalibradaControl2));

[VerdeCalibrada] = filtering((VerdeCalibrada),0.005,2);
[VerdeEnhanced] = filtering((VerdeCalibrada),0.01,2);

[IrCalibrada] = filtering((IrCalibrada),0.005,2);


%ROI detection
VerdeEnhanced=imadjust(VerdeEnhanced);
level=graythresh(VerdeEnhanced);
ve2=im2bw(VerdeEnhanced,0.9);
figure; imshow(ve2,[]) %Unsharp masking - enhance details
veIm=imcomplement(ve2);
figure; imshow(veIm,[]) %Unsharp masking - enhance details

[RegionsIrene,ROIzonaIrene]=ROI_detect(veIm,brazo,num);
IreneZOna=veIm(ROIzona{1,1},ROIzona{2,1},:);


 for i=1:6
         affect{i,1}=(newver(Regions{i,1},Regions{i,2},:));
        affectCalib{i,1}=(VerdePer(Regionsbueno{i,1},Regionsbueno{i,
2},:));
        affectCalib{i,2}=(IrIllumination(Regionsbueno{i,
1},Regionsbueno{i,2},:));
         affect{i,3}=(newnewIR(Regions{i,1},Regions{i,2},:));
         affectCalib{i,2}=(newnewVer(Regions{i,1},Regions{i,2},:));
         affect{i,2}=(ir(Regions{i,1},Regions{i,2},:));
         affectCalib{i,4}=(calibNew(Regions{i,1},Regions{i,2},:));
```

```
        affectControl{i,1}=(vve(RegionsControl{i,1},Regions{i,2},:));
    end;

    affectCalib{2,1}=affectCalib{2,1}(1:199,:);
    affectCalib{2,2}=affectCalib{2,2}(1:199,:);
```

Filtering Function

```
function [newnew] = filtering(ir,D0,n)
% Forward FT

[M,N,L] = size(ir);
if L>1
    ir=ir(:,:,1);
end;
% D0=0.01;
% n=2;
[mask] = Butterworth_mask(M,N,D0,n);
fslice = fftshift(fft2(ir)); % slice (spatial domain) transformed to
fslice (Fourier domain).
slice_fourier = fslice.*mask; % Multiplication of the image's FT with
the mask (Convolution of the image with the mask in the spatial
domain).
% Backwards FT
new_slice = abs(ifft2(ifftshift(slice_fourier))); % abs to work with
the real values from now on.
newnew=(double(ir)./new_slice);
```

Region of interest detection

```
function[Regions,ROIzona] = ROI_detect(veIm,brazo,num);

veIm=logical(veIm);
bord=regionprops(veIm,'MajorAxisLength',
'Extent','Area','PixelIdxList','BoundingBox','MinorAxisLength');
siIm=size(veIm);
di=[bord(:).MajorAxisLength];
di2=[bord(:).MinorAxisLength];
%eliminar los mayores de una size grande, y los mas peques que 2
pixels
 minDist=55/10;
good=find(di <= (siIm(1)/2) & di <= (siIm(2)/2) & di >=  3*minDist &
di2 >=  3);
borderSepar=zeros(siIm(1),siIm(2));

for i=1:length(good)
    %Eliminar zonas menores que el tamaño mínimo para el diámetro
mayor
    %para que se considere positivo (1 mm)
    pix=(bord(good(i)).PixelIdxList);
    %Eliminar zonas menores que el tamaño mínimo para el diámetro
menor
```

```
    borderSepar(pix)=1;

end;
figure; imshow(borderSepar,[])
newBord=bord(good);

% % % % % % % % Detectar ROI con cruces
locs=cell(2);
Cross=cell(length(newBord),1);
count=0;
chos=[];
xPos=[];
yPos=[];
for i=1:length(newBord)
    Extent(i)=newBord(i).Extent;
    bounding = floor(newBord(i).BoundingBox)+1;

    if Extent(i) < 0.49 && Extent(i) > 0.25 &&  bounding(3)>minDist*5
&& bounding(4)>minDist*5
        count=count+1;
        %Area divided by the area of the bounding box, for a cross,
large
        %bounding Box for the selected area
%         Cross{count,1}=newBord(i);
        chos(count)=i;
        locs{count,1} = floor(newBord(i).BoundingBox);
        figure;
imshow(borderSepar(bounding(2):bounding(2)+bounding(4),bounding(1):bou
nding(1)+bounding(3)),[]);
        xPos(count)=locs{count,1}(1,1);
        yPos(count)=locs{count,1}(1,2);
    end;
end;
maxXPoint=find(xPos==max(xPos));
minXPoint=find(xPos==min(xPos));
maxYPoint=find(yPos==max(yPos));
minYPoint=find(yPos==min(yPos));
Ypoint=locs{minYPoint,1}(2)%+locs{minYPoint,1}(4);
Xpoint=locs{minXPoint,1}(1)+locs{minXPoint,1}(3);
%ROI; area contained between the marks
ROI=borderSepar(Ypoint:locs{maxYPoint,1}(2)+locs{maxYPoint,1}
(4),Xpoint:locs{maxXPoint,1}(1),:);
% figure; imshow(ROI,[])
ROIzona=cell(2,1);
ROIzona{1,1}=(Ypoint:locs{maxYPoint,1}(2)+locs{maxYPoint,1}(4));
ROIzona{2,1}=(Xpoint:locs{maxXPoint,1}(1));


%Areas detection (points) in the ROI
% ROI=borderSepar;
 L = logical(ROI);
circles=regionprops(L,'MajorAxisLength','Extent','Perimeter','Area',..
.
    'Centroid','PixelIdxList','BoundingBox','MinorAxisLength');
meanArea= mean([circles(:).Area]);
 areaDist=floor((25*55/10)/2)-1;
Regions=cell(1,2);
count2=0;
```

```
Extent2=[circles(:).Extent];
        Perimeter=[circles(:).Perimeter];
    Area=[circles(:).Area];
    CircleMetric = (Perimeter.^2)./(4*pi*Area);  %circularity metric
    sorted=sort(CircleMetric);
    smaxis= [circles(:).MinorAxisLength]';
    bigaxis= [circles(:).MajorAxisLength]';


      circlesfound=find(Extent2(:) > 0.33 & Extent2(:) < 1 &
smaxis(:)>= minDist & bigaxis>4*smaxis);
    %If a selected area is much smaller than the rest, it is an
artifact
for i=4:length(circlesfound)
    if strcmp(brazo,'left')==1;

            bounding = floor(circles(circlesfound(i)).BoundingBox);
            figure;
        Ytop=floor(bounding(2)+bounding(4));
        Xcenter=floor(circles(circlesfound(i)).Centroid(1));
        count2=count2+1;
        Regions{count2,2}={};

       Regions{count2,1}=(Ytop:size(ROI,1)-10); %-Ytop

      Regions{count2,2}=(Xcenter-areaDist-5:Xcenter+areaDist+1+5);

    else

            bounding = round(circles(circlesfound(i)).BoundingBox);
            figure;
imshow(ROI(bounding(2):bounding(2)+bounding(4),bounding(1):bounding(1)
+bounding(3)));
        Ytop=floor(bounding(2));
        Xcenter=floor(circles(circlesfound(i)).Centroid(1));
        count2=count2+1;
        Regions{count2,2}={};
            Regiones=ROI(Ytop:Ytop+1+areaDist,Xcenter-areaDist:Xcenter
+areaDist+1);
            figure; imshow(Regiones,[])

            Regions{count2,1}=(Ytop:size(ROI,1)-Ytop-10);
            Regions{count2,2}=(Xcenter-areaDist-5:Xcenter+areaDist
+1+5);

     end

end;
```

Main diagnosis script

```
refDist=3*1388/200;
minDist=1*1388/200;
pixDist1=200/1388;
```

```
pixArea=pixDist1*pixDist1;
pixDistmax=20*1388/200;


%%
[affect,suero,histamina,affectControl,histaminaControl,sueroControl]=P
reprocessingImages2Nuevo(name,1,brazo,control,controlir,num);
[affect,sueroChannel,histaminaChannel,affectChannelControl,histaminaCh
annelControl,sueroChannelControl]=PreprocessingImages2Nuevo(name,
2,brazo,control,controlir,num);



%Control del médico
%ControlMeasures cell: 1. Diameter - 2.Area - 3.Position
[controlMeasures,histHistamineControl,histmaskControl]=ControlRegion(a
ffectControl,minDist,pixDist1,pixArea,num);
%%

Absorbance=cell(6,2);
%SUERO
        %GREEN
   suero=double(affectCalib{2,1});
   suero = (suero - min(suero(:)))*(1 - 0)/(max(suero(:)) -
min(suero(:))) + 0;
  suero2=imgaussfilt(suero,2);
  figure; imshow(suero2,[])

        %NIR
   sueroNir=double(affectCalib{2,2});
   sueroNir = (sueroNir - min(sueroNir(:)))*(1 - 0)/(max(sueroNir(:))
- min(sueroNir(:))) + 0;
  sueroNir=imgaussfilt(sueroNir,2);
  figure; imshow(sueroNir,[])

    %Basal
    figure; imshow(sueroNir,[])
    sueroNirBasal=imcrop();
   sueroNirBasal=double(sueroNirBasal);
   sueroNirBasal = (sueroNirBasal - min(sueroNirBasal(:)))*(1 - 0)/
(max(sueroNirBasal(:)) - min(sueroNirBasal(:))) + 0;
  sueroNirBasal=imgaussfilt(sueroNirBasal,2);
  figure; imshow(sueroNirBasal,[])

     %Basal
    figure; imshow(suero2,[])
    sueroverBasal=imcrop();
   sueroverBasal=double(sueroverBasal);
   sueroverBasal = (sueroverBasal - min(sueroverBasal(:)))*(1 - 0)/
(max(sueroverBasal(:)) - min(sueroverBasal(:))) + 0;
  sueroNirBasal=imgaussfilt(sueroverBasal,2);
  figure; imshow(sueroverBasal,[])


  %ABSORBANCE
  for i=1:6
Hgreen=-log(affectCalib{i,1}/mean(sueroverBasal(:)));
Absorbance{i,1}=Hgreen;
```

```
figure; imshow(Hgreen,[])
Hir=-log(affectCalib{i,2}/mean(sueroNirBasal(:)));
Absorbance{i,2}=Hir;
figure; imshow(Hir,[])
  end;
H2=-log(affectCalib{1,2}/mean(sueroNir(:)));
figure; imshow(H2,[])


%GREEN - ERITEMA

    %Suero
    Hsuero=-log(affectCalib{2,1}/mean(sueroverBasal(:)));
    Hsuero=imgaussfilt(Hsuero,2);
    figure; imshow(abs(Hsuero),[])

  %Detection of center point using the green-  enhanced features
[sueroC,diamSuero,areaSuero,sueroMask]=PointsDetection(affect{2,2},
0.3,minDist,pixDist1,pixArea,suero2,2);

      %AFFECTED AREA
affectMeasuresEry=cell(6,2,6); %1.Diameter - 2.Area
affectMeasuresEdema=cell(4,2,6); %1.Diameter - 2.Area

count=0;
for i=5:num
   count=count+1;

%1388 pix - 200 mm
%Green Channel
   affectCalib{i,1}=double(affectCalib{i,1});
   affectCalib{i,1} = (affectCalib{i,1} - min(affectCalib{i,1}(:)))*(1
- 0)/(max(affectCalib{i,1}(:)) - min(affectCalib{i,1}(:))) + 0;
   affectCalib{i,1}=imgaussfilt(affectCalib{i,1},2);
  figure; imshow(affectCalib{i,1},[])

    %Absorbance
  Hgreen=-log(affectCalib{i,1}/mean(sueroverBasal(:)));
    figure; imshow(abs(Hgreen),[])
    title('Absorbance')

             %Center
    [centr,centerDiam,centerArea,ne2]=PointsDetection(affectCalib{i,
1},0.5,minDist,pixDist1,pixArea,affectCalib{i,1},1,'green');

              %Otsu from absorbance
[OtsuEry,affectMeasuresEry{1,1,i},affectMeasuresEry{1,2,i},ne2]=Points
Detection(abs(Hgreen),0.5,minDist,pixDist1,pixArea,affectCalib{i,1},
2,'green');
    ne2=imfill(ne2);

        %Texture
[SIgreen,statsgreen,GreenTexture,affectMeasuresEry{2,1,i},affectMeasur
esEry{2,2,i},GreenTextureIm]=Texture2(abs(Hgreen),n,pixDist1,pixArea,m
inDist,centr,'green');

          %Watershed
```

```
    [Ar,Final]=Morphological_Watershed_Mitad(affectCalib{i,
1},minDist,pixDist1,pixArea,200,0.5,centr);

[affectMeasuresEry{3,1,i},affectMeasuresEry{3,2,i}]=SavingPlottingResu
lts(Ar,Final,affect{i,1},pixDist1,pixArea)

        %Division
[Ar,affectMeasuresEry{5,1,i},affectMeasuresEry{5,2,i}]=OneChannelRefer
ence_2(suero2,abs(Hgreen),minDist,pixDist1,pixArea,centr);
        %External Force

[EextI2,affectMeasuresEry{6,1,i},affectMeasuresEry{6,2,i}]=extForce(do
uble(abs(Hgreen)),1, 10, 2,10,pixDist1,pixArea,minDist,centr);

end;

for i=2:num
    %NIR Channel
   affectCalib{i,2}=double(affectCalib{i,2});
   affectCalib{i,2} = (affectCalib{i,2} - min(affectCalib{i,2}(:)))*(1
- 0)/(max(affectCalib{i,2}(:)) - min(affectCalib{i,2}(:))) + 0;
   affectCalib{i,2}=imgaussfilt(affectCalib{i,2},2);
  figure; imshow(affectCalib{i,2},[])

    %Absorbance
  HIr=-log(affectCalib{i,2}/mean(sueroNirBasal(:)));
    figure; imshow((HIr),[])
    title('Absorbance')

   level=graythresh(abs(HIr));
    HIrbw=im2bw(abs(HIr),0.8);
      figure; imshow(HIrbw,[])

    %NIR image
            %Otsu
[OtsuIr,affectMeasuresEdema{1,1,i},affectMeasuresEdema{1,2,i},ne2Ir]=P
ointsDetection(abs(HIr),0.4,minDist,pixDist1,pixArea,affectCalib{i,2},
1,'ir');
        EdemaOtsu=ne2Ir;
        EdemaOtsu(ne2==0)=0;
        figure; imshow(EdemaOtsu,[])

[imFinal,diamSuero,areaSuero,EdemaOtsu2]=comparedPoints(centr,EdemaOts
u,minDist,pixDist1,pixArea,affectCalib{i,2})

        %Texture
[SItodo,statsTodo,IRtexture,affectMeasuresEdema{2,1,i},affectMeasuresE
dema{2,2,i},IRtextureIm]=Texture2(abs(HIr),n,pixDist1,pixArea,minDist,
centr,'nir');

          %Watershed
       [Ar,Final]=Morphological_Watershed_Mitad(affectCalib{i,
2},minDist,pixDist1,pixArea,200,0.2,centr);

[affectMeasuresEdema{3,1,i},affectMeasuresEdema{3,2,i}]=SavingPlotting
Results(Ar,Final,affect{i,2},pixDist1,pixArea);
```

```
[ne2,imFinal,affectMeasuresEdema{4,1,i},affectMeasuresEdema{4,2,i}]=Mo
rphological_Watershed_Mitad(affectCalib{i,2},minDist,pixDist1,pixArea,
200,0.2,centr);
                %Division
[Ar,affectMeasuresEdema{5,1,i},affectMeasuresEdema{5,2,1}]=OneChannelR
eference_2(suero,abs(HIr),minDist,pixDist1,pixArea,centr);
        %External Force
    [EextI2,affectMeasuresEdema{i,1},affectMeasuresEdema{i,
2}]=extForce(double(abs(HIr)),1, 10,
2,10,pixDist1,pixArea,minDist,centr);

end
```

Points detection function

```
function[centr,diamSuero,areaSuero,ne]=PointsDetection(im,level,minDis
t,pixDist1,pixArea,suero,n,led)
sueroVer=im;
  if n==1
      sueroVer2=im2bw(im,level);
      figure; imshow(sueroVer2,[])
      if strcmp(led,'green')
          sueroVer2=imcomplement(sueroVer2);
      end;
      figure; imshow(sueroVer2,[])

     elseif n==2
      bw=graythresh(im);
      sueroVer2=im2bw(sueroVer,bw);
      if strcmp(led,'green')
                sueroVer2=imcomplement(sueroVer2);
      end;
      figure; imshow(sueroVer2,[])
  end

  point=regionprops(sueroVer2,'Area','Centroid','MajorAxisLength',...
'BoundingBox','MinorAxisLength','PixelIdxList','PixelList');
axis=[point(:).MajorAxisLength];
axisSmall=[point(:).MinorAxisLength];

diameters = (axis+axisSmall)/2;
si=size(sueroVer2);
sir(1)=si(2);
sir(2)=si(1);
center=[point(:).Centroid];
%El centro va a estar un poco alejado de los bordes (10 pixels)
dist1=abs(sir(:)-10);
dist2=abs([1 1]+10);

l=length(point);
distL=[];
distH=[];
number=[];
```

```
for i=1:l
    distH=[distH dist1'];
    distL=[distL dist2];
    H=point(i).Centroid <=dist1' ;
    L=point(i).Centroid >= dist2;
    if isempty(find(H==0)) && isempty(find(L==0))
         number=[number i]
    end
end
centr=point(number);
num2=find([centr(:).Area]==max([centr(:).Area]));
centr=centr(num2);
ne=zeros(size(im));
ne([centr(:).PixelIdxList])=1;
%morphological improvement
[fil] = MorphoProcess(10,ne);
[diamSuero,areaSuero]=SavingPlottingResults(fil,centr,suero,pixDist1,p
ixArea)
```

8. References

[1] J. Zubeldia, L. Baeza, I. Jáuregui y C. J. Senent, Libro de las enfermedades alérgicas de la fundación BBVA. Bilbao: Fundación BBVA, 2012.

[2] R. Pawankar, G. Canonica, S. Holgate and R. Lockey, World Allergy Organization (WAO) white book on allergy. United Kingdom: WAO, 2011.

[3] J. Charles A Janeway, P. Travers, M. Walport and M. Shlomchik, "Allergy and Hypersensitivity", *Garland Science,* 2001.

[4] J.C. García, E.Rodriguez, G. Hernández, E. Díaz, "Técnicas diagnósticas in vivo."

[5] American College of Allergy Asthma & Immunology, "Allergy Diagnostic Testing:

An Updated Practice Parameter", *Annals of allergy, asthma, & immunology*. vol. 10, no. 3, 2008.

[6] W. James, T. Berger, D. Elston and G. Andrews, *Andrews' Diseases of the Skin: Clinical Dermatology,* 10th ed., p. 1, Philadelphia: Elsevier Saunders, 2006.

[7] P. Kolarsick, M. Kolarsick and C. Goodwin, "Anatomy and Physiology of the Skin", Journal of the Dermatology Nurses' Association, vol. 3, no. 4, pp. 203-213, 2011.

[8] G. Tortora and B. Derrickson, *Principles of anatomy & physiology*, 13th ed. Hoboken, N.J.: Wiley, 2011, pp. 875-908.

[9] A. Abbas, A. Lichtman MD PhD and S. Pillai MBBS PhD, *Cellular and molecular immunology*, 7th ed. Philadelphia: Saunders, 2003.

[10] K. Amin, "The role of mast cells in allergic inflammation", Respiratory Medicine, vol. 106, no. 1, pp. 9-14, 2012.

[11] C. Kunder, A. St John and S. Abraham, "Mast cell modulation of the vascular and lymphatic endothelium", Blood, vol. 118, no. 20, pp. 5383-5393, 2011.

[12] J. Ripoll, "Light Absorbers, Emitters and Scatterers: The Origins of Color in Nature", in *Principles of Diffuse Light Propagation*, 1st ed., J. Ripoll, Ed. 2012.

[13] R.R. Anderson and J.A. Parrish, The science of photomedicine Chapter 6: Optical properties of human skin. Plenum Press, 1982.

[14] S. L. Jacques and S. A. Prahl, "ECE 532, 3. Optical Properties", Omlc.org, 1998. [Online]. Available: http://omlc.org/education/ece532/class3/. [Accessed: 26- May- 2016].

[15] S. Jacques, "Optical properties of biological tissues: a review", Physics in Medicine and Biology, vol. 58, no. 11, pp. R37-R61, 2013.

[16] R. Anderson and J. Parrish, "The Optics of Human Skin", Journal of Investigative Dermatology, vol. 77, no. 1, pp. 13-19, 1981.

[17] S. L. Jacques and S. A. Prahl, "Diffusion Theory: Fick's 1st Law", Omlc.org, 2016. [Online]. Available: http://omlc.org/classroom/ece532/class5/ficks1.html. [Accessed: 03- Jun- 2016].

[18] T. Durduran, A. Yodh, B. Chance and D. Boas, "Does the photon-diffusion coefficient depend on absorption?", Journal of the Optical Society of America A, vol. 14, no. 12, p. 3358, 1997.

[19] S. L. Jacques and S. A.Prahl, "Skin Optics Summary", Omlc.org, 2016. [Online]. Available: http://omlc.org/news/jan98/skinoptics.html. [Accessed: 07- Jun- 2016].

[20] R.J. Scheuplein, "A survey of some fundamental aspects of the absorption and reflection of light by tissue", Journal of Society of Cosmetic Chemists, vol. 15, no.2, p.p. 111–122, 1964

[21] J.D. Hardy, H.T. Hammell, and D. Murgatroyd. "Spectral transmittance and reflectance of excised human skin". Journal of Applied Physiology, no. 9, p.p. 257–264, 1956.

[22] G. Tortora and B. Derrickson, *Principles of anatomy & physiology*, 13th ed. Hoboken, N.J.: Wiley, 2011, pp. 728-752.

[23] Paper de alergia

[24] E. Pastorello, C. Incorvaia, C. Ortolani, S. Bonini, G. Canonica, S. Romagnani, A. Tursi and C. Zanussi, "Studies on the relationship between the level of specific IgE antibodies and the clinical expression of allergy: I. Definition of levels distinguishing patients with symptomatic from patients with asymptomatic allergy to common aeroallergens", Journal of Allergy and Clinical Immunology, vol. 96, no. 5, pp. 580-587, 1995.

[25] V. Voipio, H. Huttunen and H. Forsvik, "Practical Imaging in Dermatology", Digital Image Processing, 2012.

[26] O. Bulan, "Improved wheal detection from skin prick test images", Image Processing: Machine Vision Applications VII, 2014.

[27] E. Roullot, J. Autegarden, P. Devriendt and F. Leynadier, "Segmentation of Erythema from Skin Photographs for Assisted Diagnosis in Allergology", Pattern Recognition and Image Analysis, pp. 754-763, 2005.

[28] K. Turjanmaa, T. Palosuo, H. Alenius, F. Leynadier, J. Autegarden, C. André, H. Sicard, M. Hrabina and T. Tran, "Latex allergy diagnosis: in vivo and in vitro standardization of a natural rubber latex extract", Allergy, vol. 52, no. 1, pp. 41-50, 1997.

[29] S. Taylor, "CCD and CMOS Imaging Array Technologies: Technology Review", 1998.

[30] “QImaging Scientific Cameras”. [Online]. Available: http://www.qimaging.com/products/cameras/scientific/retiga_2000r.php [Accessed: 20-Feb-2016].

[31] “Digital Industrial Camera Solutions,”. [Online]. Available: https://www.alliedvision.com/en/digital-industrial-camera-solutions.html. [Accessed: 5-Mar-2016].

[32] H. K.K, "Time-resolved spectrophotometry — Bioimaging using light:Fundamental research & Applied research | Hamamatsu Photonics", *Hamamatsu.com*, 2016. [Online]. Available: http://www.hamamatsu.com/us/en/technology/innovation/trs/index.html. [Accessed: 18- Feb- 2016].

[33] A. Bekina, I. Diebele, U. Rubins, J. Zaharans, A. Derjabo and J. Spigulis, "Multispectral assessment of skin malformations using a modified video-microscope", Latvian Journal of Physics and Technical Sciences, vol. 49, no. 5, 2012.

[34] N. Kollias and G. Stamatas, "Optical Non-Invasive Approaches to Diagnosis of Skin Diseases", Journal of Investigative Dermatology Symposium Proceedings, vol. 7, no. 1, pp. 64-75, 2002.

[35] B. Diffey, "Optical properties of skin: measurement of erythema", The Physical Nature of the Skin, pp. 179-189, 1988.

[36] G. Stamatas and N. Kollias, "In vivo documentation of cutaneous inflammation using spectral imaging", J. Biomed. Opt., vol. 12, no. 5, p. 051603, 2007.

[37] G. Stamatas, M. Southall and N. Kollias, "In Vivo Monitoring of Cutaneous Edema using Spectral Imaging in the Visible and Near Infrared", Journal of Investigative Dermatology, vol. 126, no. 8, pp. 1753-1760, 2006.

[38] "Tabulated Molar Extinction Coefficient for Hemoglobin in Water", Omlc.org, 2016. [Online]. Available: http://omlc.org/spectra/hemoglobin/summary.html. [Accessed: 08- Jun- 2016].

[39] P. A. Mansouri, "Development of a protocol for CCD calibration: Application to a multispectral imaging system", Int. J. Robot. Autom. 2005, 2016.

[40] D. Lymperis, A. Diamantis, G. Syrcos, S. Karagiannis, ”Image processing algorithms for a computer assisted allergy testing system”

[41] D. F. Swinehart, "The Beer-Lambert law," Journal of Chemical Education, vol. 39, no. 7, p. 333, Jul. 1962.